Diplomarbeit

Towards process intensification: Enhancing growth, production and robustness of *Corynebacterium glutamicum* on spent sulfite liquor

ausgeführt zum Zwecke der Erlangung des akademischen Grades eines Master of Science (MSc) unter der Leitung von

Associate Prof. Dipl.-Ing. Dr. nat. tech. Oliver Spadiut

betreut durch

Projektass. Dipl.-Ing. Daniel Waldschitz

Institut für Verfahrenstechnik, Umwelttechnik und Technische Biowissenschaften

Technischen Universität Wien
Fakultät für Technische Chemie

von

Mark-Richard Neudert, BSc. BSc.
[redacted]

Wien, am	Unterschrift des Betreuers	eigenhändige Unterschrift

Eidesstattliche Erklärung

Hiermit erkläre ich, dass ich diese Diplomarbeit selbstständig verfasst habe, dass ich die verwendeten Quellen vollständig angegeben habe und dass ich Zitate die anderen Publikationen im Wortlaut oder dem Sinn nach entnommen sind, unter Angabe der Herkunft als Entlehnung kenntlich gemacht habe.

Wien, am	eigenhändige Unterschrift

Abstract

Bioprocesses that efficiently utilize sustainable resources for manufacturing of high-value products are an important enabler for the urgently needed transition towards a bio-based circular economy. To achieve economic feasibility of such a process, intensification strategies have to be considered in the development stage. A previously established SSL-based fed-batch process utilizing *C. glutamicum* for the production of the antimicrobial peptide pediocin PA-1 was analyzed for a potential bioprocess intensification. Several problems in this bioprocess were identified that reduced the efficiency and hindered the envisioned intensification towards a repetitive fed-batch. Problems in the batch phase such a long unpredictable lag-phase, low biomass yield and incomplete substrate utilization were attributed to inhibitors present in SSL and the necessary detoxification by cells. Further, problems in the fed-batch of the original process such as overfeeding were hypothesed to be directly related to the aforementioned issues of the batch-phase and the consequent poor starting conditions. To resolve these problems, increase the reliability of the process and provide comparable starting conditions for subsequent investigations in the fed-batch phase, the inoculum amount was adapted. By increasing the inoculum size, the detoxification load per cell is reduced, resulting in less variability, shorter lag-phases and higher achieved biomass concentrations. The fed-batch pH value and carbon-phosphorous ratio were identified as promising factors influencing the pediocin production and investigated using a three level full-factorial experimental design. Both the pH value and the C:P-ratio as well as their interaction were shown to have a significant influence on the maximum achieved pediocin titre. The obtained data was further checked for consistency by elemental balancing and utilized to establish a mechanistic model. The substrate utilization was modelled sucessfully with monod-like equations and a NRMSE of below 10% for all considered substrates (glucose, xylose, mannose, acetate). Modeling the biomass concentration failed to meet the set acceptance critereon (10%) with a 15% NMRSE. Analytical challenges associated with SSL matrix and the consequent inability to determine important factors such as the phosphate and product concentration prevented a successful modeling of the pediocin formation. After process intensification the developed biorefinery concept has potential for integration into existing pulp and paper mills for production of high value products.

Deutsche Zusammenfassung

Die Verwendung nachhaltiger Ressourcen für Bioprozesse zur Herstellung hochprofitabler Produkte ist ein wesentlicher Schritt hin zu einer biologisch basierten Kreislaufwirtschaft. Um die ökonomische Machbarkeit eines solchen Prozesses zu gewährleisten, sollten Intensivierungsstrategien bereits in der Entwicklung berücksichtigt werden. Ein zuvor entwickeltes Zulaufverfahren mit SSL als Substrat zur Herstellung des antimikrobiellen Peptids PA-1 wurde auf die Möglichkeit der Bioprozessintensifizierung untersucht. Im Verlauf des Prozesses wurden Probleme identifiziert, die die Effizienz mindern und die geplante Intensivierung in ein wiederholtes Zulaufverfahren behindern. In der Satzverfahrensphase des Prozesses wurden eine lange unvorhersehbare Lagphase, niedrige Biomassausbeuten und unvollständige Substrataufnahme den in SSL vorhandenen Inhibitoren zugeschrieben. Des Weiteren wurden Probleme im Zulaufverfahren als Konsequenz der Probleme in der ersten Phase und daraus resultierenden schlechten Startbedingungen angenommen. Um diese Probleme zu beheben und vergleichbare Startbedingungen für folgende Untersuchungen in der Zulaufphase zu gewährleisten, wurde die Inokulumgröße angepasst. Durch Erhöhung der Menge des Inokulums wird die Detoxifizierungslast pro Zelle reduziert, was zu verkürzten Lagphasen, geringerer Variabilität und höherer Biomasskonzentration führt. Der pH-Wert und das Kohlenstoff-zu-Phosphor-Verhältnis wurden als wichtige Faktoren zur Verbesserung der Produktivität identifiziert und mithilfe eines voll faktoriellen Experimentplans untersucht. Es wurde ein signifikanter Effekt sowohl des pH-Werts als auch des C:P-Verhältnisses und ihrer Interaktion auf den maximal erzielten Pediocin-Titer festgestellt. Die gesammelten Daten wurden mittels elementarer Bilanzierung überprüft und für die Erstellung eines mechanistischen Modells verwendet. Der Substratverbrauch der Substrate (Glukose, Xylose, Mannose, Acetat) konnte erfolgreich mit Monod-artigen Gleichungen mit einem NMRSE unter 10% modelliert werden. Die Modellierung der Biomasse innerhalb der gesetzten Grenzen (10%) scheiterte jedoch mit einem NRMSE von 15Analytische Herausforderungen im Zusammenhang mit der SSL-Matrix haben die präzise Bestimmung wichtiger Faktoren wie der Phosphat- und Produktkonzentration verhindert, was eine erfolgreiche Modellierung der Pediocin-Produktion verhinderte. Nach der Intensivierung des Prozesses hat das konzipierte Bioraffineriekonzept das Potenzial, in bestehende Zellstoff- und Papierfabriken integriert zu werden, um höherpreisigen Produkte zu erzeugen.

List of Abbreviations

Ace	Acetate
ANOVA	Analysis of variance
BPI	Bioprocess intensification
CAPEX	Capital Expenditures
CER	Carbon evolution rate
CM	Chloramphenicol
DCW	Dry cell weight
DO	Dissolved oxygen
DoE	Design of Experiment
DoR	Degree of reduction
EU	European Union
FDA	US Food and Drug Administration
Glc	Glucose
GRAS	Generally recognised as safe
HMF	5-hydroxymethylfurfural
HPLC	High performance liquid chromatography
IPTG	Isopropyl-β-D-1-thiogalactopyranoside
LAB	Lactic acid bacteria
LoD	Limit of detection
LoQ	Limit of quantification

Man	Mannose
MOPS	3-(N-morpholino)propanesulfonic acid
NP	Nitrogen and phosphate feed
NRMSE	Normalized root mean square error
OD_{600}	Optical density at 600 nm
OPEX	Operational Expenditures
OUR	Oxygen uptake rate
Q2	Predictability
P	Product / Pediocin PA-1
R2	Model fit
RFU	Relative fluorescence unit
RMSE	Root mean square error
RQ	Respiratory quotient
SSL	Spent sulfite liquor
StDev	Standard deviation
vvm	Volume air per volume liquid per minute
X	Biomass
Xyl	Xylose

List of Variables

c_i	$[\frac{g}{L}]$	Concentration of component i
K_{Si}	$[\frac{g}{L}]$	Half-velocity constant of component i
l	[-]	Log likelihood
M_V	$[\frac{L}{mol}]$	Molar gas volume ≈ 22.41
n	[-]	Sample size
$r_{C/P}$	[-]	Ratio of carbon moles to phosphorus moles
$r_{C/P,max}$	[-]	ratio of carbon to phosphorus at maximum product titre
$n_{product}$	$[mol;\ e^-]$	Measured molar/electron quantities
n_{educt}	$[mol;\ e^-]$	Molar/electron quantities provided to the system
q_{dO}	$[\frac{BU}{BUh}]$	Degradation/Oxidation rate at 15 % DO
q_P	$[\frac{BU}{g_X h}]$	Specific pediocin formation rate
$q_{P,max}$	$[\frac{BU}{gh}]$	Maximal specific pediocin formation rate
q_{S_i}	$[\frac{g_i}{g_X h}]$	Specific uptake rate of component i
$q_{S_i,max}$	$[\frac{g_i}{g_X h}]$	Maximal specific uptake rate of component i
$r_{balance}$	[-]	Balance ratio
r_i	$[\frac{g_i}{Lh}]$	Volumetric rate of component i
r_{inert}	[-]	Inert gas ratio
S_i	$[\frac{g}{L}]$	Substrate concentration of component i
t	[h]	Time

$\dot{V}_{in}$	$[\frac{L}{h}]$	Substrate inflow
V_R	[L]	Reactor volume
V_{sample}	[L]	Sample volume
$x_{CO_2,Air}$	[%]	Carbon dioxide fraction air
$x_{CO_2,Offgas}$	[%]	Carbon dioxide in offgas
$x_{O_2,Air}$	[%]	Oxygen fraction air
$x_{O_2,Offgas}$	[%]	Oxygen in offgas
$\hat{y}$	[-]	Predicted y value
y_i	[-]	ith observation
$\overline{y_i}$	[-]	Mean of measurements at the ith observation
y_i	[-]	Predicted value of the component i
$Y_{i/j}$	$[\frac{g_i}{g_j}]$	Yield of component i over j
γ_K	[-]	Collinearity index
$\hat{\Theta}$	[-]	Optimization criterion
μ	$[\frac{g_X}{g_X h}]$	Specific growth rate
$\overline{\mu}$	$[\frac{g_X}{g_X h}]$	Mean of the specific growth rate
μ_{max}	$[\frac{g_X}{g_X h}]$	Maximum specific growth rate
π	[-]	Circular number ≈ 3.14
σ	[-]	Variance

Contents

1 Introduction

1.1 General field of research

Climate change can be seen as the defining problem of the 21st century. The concentration of CO_2 and other greenhouse gases in the atmosphere has significantly risen as a result of human activities since the pre-industrial era. The associated changes in climate, such as rising temperatures, sea levels and the accumulation of extreme weather events, pose major challenges for current and future generations. Despite extensive scientific research on the links between greenhouse gases and the global warming, as well as the potential implications for humanity over the past 150 years, broader awareness only emerged relatively recently [1, 2, 3]. The increased public attention and the subsequent socio-economic pressure on policymakers and industry have led to several initiatives and agreements to combat climate change and its consequences. For example, the member states of the United Nations Framework Convention on Climate Change (UNFCCC) meet annually at the Conference of Parties (COP) [4]. At the 21st COP in 2015, the Paris Agreement was negotiated with the aim of limiting global warming to ideally 1.5 °C but no more than 2.0 °C compared to pre-industrial times [5]. It is estimated that this will require global greenhouse gas emissions to be reduced by 30 and 45 percent respectively by 2030 compared to projected emissions [6]. The industrial sector accounts for the largest proportion of net anthropogenic greenhouse gas emissions, contributing 34 % of direct and indirect emissions [7].

The UN sustainable development goals require further replacement of fossil resources with renewable alternatives [8]. To lessen industrial emissions and reduce dependence on fossil materials without jeopardising economic growth, significant transformation in the current economic system and technological advancements are necessary. The transition to a circular and bioeconomy, encompassing concepts that strive to lessen waste generation and resource consumption while prioritising renewable biological resources, is commonly viewed as a means to achieve sustainable growth and development [9]. Biotechnology offers the possibility to manufacture a wide range of products such as platform chemicals, pharmaceuticals and fuels from renewable feedstocks and is therefor often regarded as a key enabler in this transition.

1.1.1 Biorefineries

The concept of biorefineries is inspired by that of petroleum refineries in the chemical industry, which extract and refine a wide range of different products, for example chemicals, fuels or energy from crude oil. However, instead of relying on fossil resources like crude oil, biorefineries rely on biomass. Therefore, biorefineries can be defined as the sustainable conversion of biomass into a range of marketable products such as food, feed, materials, chemicals, and energy such as fuels, power, and heat (IEA definition) [10]. While the definition is rather broad, biorefineries can further be classified depending on the used feedstocks, the involved processes and plattforms as well as the obtained products.

It has to be mentioned that classification of biorefineries is subject to change due to the huge diversity of biomass and the ongoing development of new technologies that enable a broader spectrum of feedstocks, plattforms and products. Several different classification mehtods have been reported [11, 10, 12, 13]; the following section is mainly based on the system established by the international energy agency (IEA) Bioenergy Technology Collaboration Program [10]. Products can generally be divided into energy, chemicals, materials, food and feed. Biorefineries can involve a variety of processes that can be categorised into chemical, biotechnological, thermochemical and mechanical processes. Platforms serve as intermediaries between the raw materials and the end products of the refining process. Depending on the utilized processes and desired products, different platforms are obtained.

The origin of the biomass raw material is another important categorisation criterion for biorefineries. Examples of different biorefineries based on their feedstocks include lignocellulosic biorefineries, starch crop biorefineries or oil crop biorefineries. Feedstocks are often further grouped into generations. First-generation feedstocks are edible sugar-, starch-, or oil-based crops like sugar beet, corn or rapeseed respectively [14]. Although these are renewable biomass resources, their utilization competes with their use for food and feed purposes, leading to concerns about food supply and safety. Furthermore, extensive exploitation of first-generation biomass negatively impacts land and water usage, and poses a threat to biodiversity and ground water due to mono-cultures and excessive fertilizer usage [15, 16, 17]. Hence, they cannot be regarded as socially and environmentally sustainable, therefore prompting a need for second-generation feedstocks. The feedstocks are derived from lignocellulosic biomass like agricultural and forestry residues, woody biomass, industrial and urban waste, providing a sustainable alternative to the use of dedicated food crops [18, 19].

1.1.2 Lignocellulose

Lignocellulose is the most abundant form of biomass on the planet, with an estimated annual production of 181.5 billion tonnes [20]. However, with less than 10 billion tonnes per year [20], only a small portion of this quantity is utilised, indicating a significant renewable resource potential remains untapped. While there undoubtedly are enormous amounts of lignocellulosic biomass, not all of them are accessible and allow sustainable utilization. Uncontrolled use, for example over-exploitation of forests

poses a threat to biodiversity and elevates greenhouse gas levels in the atmosphere as a result of the elimination of carbon sinks [21]. Consequently the harvesting of certain lignocellulose resources is limited by regional policies to avoid deforestation and other unsustainable utilization [22, 23]. Another source of lignocellulose feedstocks is lignocellulose from agricultural and forestry residues and from industrial waste streams. Most of this biomass is currently not used and ends up in landfills or is incinerated. Lignocellulose describes plant biomass, primarily consisting of cellulose, hemicellulose, and lignin, with compositional variations depending on the source [24]. The main component is cellulose, a linear polysaccharide of β-D-glucose linked through β-(1→4) glycosidic bonds, with the repeating unit being the disaccharide cellulobiose. By means of inter- and intramolecular interactions, cellulose molecules arrange to form elementary fibrils featuring both crystalline and amorphous structures [24]. Hemicellulose is a branched heteropolysaccharide comprising diverse hexoses and pentoses. Between different plants like hardwoods and softwoods, hemicelluloses show significant variations [24]. Lignin, the third component, is an amorphous polymer composed of the phenolic basic units (monolignols) such as p-coumaryl alcohol, coniferyl alcohol and sinapyl alcohol [24]. Several factors like the complex structure, the crystallinity of cellulose and the lignin content are responsible for the recalcitrance of ligocellulose [25]. Most industrial relevant microorganisms cannot directly utilize lignocellulose due to its recalcitrance, but require free sugars obtained after pre-treatment [25]. The use of industrial lignocellulosic waste stream that already contain utilizable sugars as a consequence of the processing of the lignocellulose circumvents the need for separate pre-treatment and is in accordance with the concept of a circular bio-economy.

1.1.3 Spent sulfite liquor (SSL)

Paper production generally involves three steps: the pulping, washing and bleaching, paper making and finishing [26]. In the pulping process the components of the lignocellulose are seperated, mechanically or chemically, to allow the extraction of the cellulose fibers [26]. In chemical pulping processes, this is achieved by dissolving lignin and hemicellulose, usually with sulfides (kraft pulping) or sulfites (sulfite pulping) at elevated temperatures [26]. In addition to the pulp, those processes produce a waster water stream, the liquor, containing remaining pulping chemicals and dissolved by-products. Due to the high organic content (carbon, sulfur) this waste water can not be discarded in the sewage and poses a significant enviremental polution load to the pulp industry [27]. While the alkaline kraft process degrades the polysaccharides to C2–C6 hydroxy- and dicarboxylicacids, the (acidic) sulfite process achieves partial hydrolysis of the hemicellulose into fermentable oligo- and monosaccharides [28].

Consequently, the spent sulfite liquor (SSL) produced in the sulfite process offers the potential as sustainable feedstock for biotechnological processes. The composition of SSL is highly dependent on the raw material used for the pulp, in general soft woods yield higher hexose (mostly glucose and mannose) concentrations while hard wood SSL contains more pentoses (mostly xylose) [28]. However, SSL also contains several inhibitory substances produced during the degradation of lignocellulose, which

may present a considerable obstacle in designing a bioprocess employing SSL as a feedstock [29, 28]. Sugar derived inhibitors like furfural and 5-hydroxymethylfurfural are obtained in the dehydrasation of hexoses and pentoses, respectively [29, 28]. The degradation of lignin can result in a wide range of phenolic compounds, such as lignosulfunates and phenolic acids that are cytotoxic [29, 28]. Further, acetic acid, formed from acetylated hemicelluloses, is inhibitory to many microorganisms due to the uncoupling and intracellular anion accumulation [29]. Currently, the biotechnological utilization of SSL is hindered by presence of those inhibitors and is therefor mostly limited to the recovery of pulping chemicals and combustion for heat. In some cases SSL is used for the production of lignocellulosic ethanol [28]. Economic rather than technological constraints are limiting the industrial use of SSL [30], driving the need to establish manufacturing of high-value products as opposed to low-value bulk commodities such as ethanol. Various detoxification techniques [31] have been suggested for addressing this issue; however, they have the potential to increase expenses and complexity, thus rendering the procedure unfeasible from an economic standpoint [31, 32]. Rather than expensive pre-processing, a bioprocess on SSL should rely on a microorganism capable of dealing with the challenges of SSL.

1.1.4 *Corynebacterium glutamicum*

Corynebacterium glutamicum is a promising candidate for the biotechnological conversion of lignocellulose-containing waste streams into high value products. It is a frequently used platform in the field of biotechnology, with an extensive track record in producing glutamate and other amino acids on an industrial scale [33, 34]. Advancements in modern molecular biology techniques have widened the scope of potential products beyond amino acid production, with over 70 products published so far [35]. The success of *C. glutamicum* is based on a number of factors, including its generally recognized as safe (GRAS) status, ability to secrete correctly folded proteins combined with minimal extracellular protease activity, and its history as a well-characterised and extensively researched production system [36, 37, 38].

Moreover, *C. glutamicum* is particularly suitable for bioprocesses that use renewable substrates due to its natural capacity to utilize a wide range of sugars and organic acids present in lignocellulosic biomass [39]. Moreover, genetic modifications have been made to improve its ability to take up substrates [40] and to utilise additional substrates such as xylose [41]. Furthermore, *C. glutamicum* exhibits high tolerance against organic acids and aromatic compounds and has dedicated genes for the detoxification of typical inhibitors associated with lignocellulose, such as HMF and furfural [42].

1.1.5 Bacteriocins/Pediocin

Bacteriocins are antimicrobial peptides that are ribosomally synthesized by bacteria. The production of bacteriocins in gram-positive bacteria and lactic acid bacteria in particular has been extensively studied as they show some promising candidates for the use of food preservatives. Those bacteriocins can be categorised into lantibiotics, that

contain the non-proteinogenic aminoacid lanthionine (class I), heat-stable unmodified bacteriocins (class II) and large (>30 kDa) heat-labile bacteriocins (class III) [43]. So far only Nisin (class I) is the only for food application approved bacteriocin and is used as bio-preservative with the number E234 mostly in dairy products [44]. In the search for further novel bio-preservatives, class IIa, the pediocin-like bacteriocins, has proved to be particularly promising. Pediocins are the bacteriocins produced by bacteria of the genus *Pediococcus* and are often referred to as antilisterial bacteriocins due to their selectivity against *Listeria* spp. [45].

Listeria monocytogenes is a food-borne human-pathogen that causes listeriosis [46]. Listerioses is a severe sickness with a mortality of around 20 % and a threat especially for at-risk groups like neonates, pregant women, elderly people as well as immunodeficient people in general [47]. *L. monocytogenes* are found in many foods, including dairy products, meat and fish, due to their ability to survive in low pH and high osmolarity enviroments and endure low temperatures they are a significant risk for food safety [48]. With their antilisterial activity pediocins are promising biological food preservation agents that could help to contain this risk.

The primary sequence of pediocins contains two regions; a highly conserved, hydrophilic and cationic N-terminal region that contains a Y-G-N-G-V/L motif known as pediocin box, and an amphiphilic or hyrophobic C-terminal region. Pediocins interact with the extracellular surface of target cells by attaching to a membrane-associated receptor of the mannose phosphotransferase system (manPTS) specifically with the N-terminal region. Subsequently, the C-terminal region penetrates the membrane and forms a pore, permealizing the cytoplasmic membrane [49]. In addition to their antimicrobial activity pediocins show important properties for the use as food preservatives; they are stable to high temperature treatments, as encountered in sterilization procedures as well as in low temperatures down to -80°C. They are further active in a wide pH range from pH 2 - 10, allowing for their potential use in different products including fermented foods and acidic dairy products [45]. However, despite their desirable characteristics, the commercial use of pediocins is limited by the uneconomic production in natural producers that require costly media and yield low titers [50]. One of the most well-researched members of class IIa bacteriocins is pediocin PA-1, derived from *Pediococcus acidilactici*.

The identification and sequencing of the pediocin PA-1 coding sequence, the operon pedABCD, has allowed for the recombinant expression in industrially relevant hosts [51, 52]. In 2021, the heterologous production of pediocin PA-1 in *C. glutamicum* was successfully established by Goldbeck et al [53]. Combined with the ability of *C. glutamicum* to utilise lignocellulosic side streams, such as SSL, this provides a foundation for a sustainable bioprocess to produce high-value antimicrobial peptides. The integration of this bioprocess into lignocellulosic biorefineries has the potential to boost economic feasibility and promote the transition towards a bio-based circular economy.

1.1.6 Bioprocess intensification

Shifting towards higher value products and reducing material costs is certainly one way to increase profitability of a process. However, processes should further be design and developed with efficiency in terms of material and energy use as well as cost in mind. Process intensification is often cited as a promising pathway for the improvement and development of sustainable and cost efficient processes in the chemical industry [54, 55, 56]. Process Intensification refers to a set of innovative principles applied to process and equipment design which deliver significant benefits in terms of process and supply chain efficiency, reduced capital and operating expenditure, improved product quality, reduced waste and improved process safety [57]. Similarly, process intensification principles can be applied in biotechnology, referred to as bioprocess intensification (BPI). The goal of bioprocess intensification is the increase in bioproduct output relative to cell concentration, time, reactor volume or cost [58]. Intensification is to be distinguished from optimization as a step change in technology that achieves not only said goals but also improving other metrics like waste production, energy consumption or CAPEX/OPEX rather than an incremental improvement in regards to some parameters within the same process technology [58, 59]. BPI does not only involve changes in the process design but does also include improvements in the utilised materials and instrumentation. [58]

Currently, most industrial bioprocesses involve batch or fed-batch cultures, that involve cleaning and sterilization, inoculation of the reactor, the bioconversation process and the harvest [60]. Before each production process, the reactors (cleaning, sterilization) as well as the inoculum have to be prepared again. One approach to intensify those processes is the transition towards a repetitive fed-batch (sometimes referred to as semi-continuous or repeated fed-batch). In a repetitive process, the culture broth is only harvested partially at the end of one repetition and the reactor is filled up with fresh medium to initiate the next repetition, reducing down-times and resource consumption while increasing the space time yield of a process. By intensifying a process towards a repetitive cultivation, the advantages of fed-batch processes such as diminishing of substrate/product inhibition or overflow metabolism through a controlled inflow of medium are retained [61]. Further, the cultivation mode has significant influence on the following separation and downstream process. Since repetitive do not produce a continuous stream of harvest but are harvested once per cycle, they do not conflict with existing downstream procedures and are viable when continuous separation and downstream is not feasible [62].

Given the potential of such processes, numerous studies have explored the application of repetitive fed-batch strategies for various organisms and products. For instance, Kopp et al. found that a repetitive fed-batch with two cycles resulted in a higher STY in recombinant protein production in Escherichia coli, in contrast to continuous and batch cultures [60]. Other researchers have documented approaches for a wide variety of microorganisms such as the methylotrophic yeast *Pichia pastoris* [62, 63] and the

marine algae *Crypthecodinium cohnii* [61] or the bacterium *Gluconobacter oxydans* [64]. Thorough understanding of the parameters that affect process stability and efficiency is crucial for successful implementation of intensification strategies. Important factors in repetitive fed-batches are often reported to include the number of repetitions, timing of the transition, and medium exchange ratio [60, 62, 61]. It is crucial to identify the respective parameters for the desired process and establish appropriate control measures to guarantee an effective outcome.

1.1.7 Bioprocess modeling

With the advancement of data acquisition and processing, the digitalisation of bioprocesses is receiving growing attention and is frequently emphasised as a key enabler for digital biomanufacturing and Industry 4.0 initiatives. Additionally, digital biomanufacturing is often considered a tool encompassed within the scope of bioprocess intensification. As a result, these trends are believed to enable each other in a mutually beneficial way. Within the digitalization of bioprocesses, bioprocess modeling is an important field that aims to establish mathematical relationships accurately describing the process that can be further used to estimate, predict or control parameters of interest. Consequently, modeling and simulation are often used as tool during development, intensification and implementation of bioprocesses [56].

There are various approaches and methods for modeling bioprocesses, but in general 2 strategies can be distinguished: mechanistic, data-driven models [65]. Furthermore, mechanistic and data-driven aspects can be combined in hybrid models [66]. All of them however have in common that they try to establish a mathematical relationship between the time progression of the measured process data (e.g. feed rates, substrates concentrations etc.) and the model state variables (e.g. biomass or product concentration). In data-driven modelling this is achieved purely based on the experimental data by utilizing different techniques including, but not limited to, partial least squares (PLS) regression or artificial neural networks (ANNs). Data-driven models and their parameters can be used to predict desired states within the design space. However, they typically lack physiological meaning and do not allow for extrapolation [65]. In contrast, mechanistic models utilise a priori knowledge or assumptions about the underlying mechanisms of a system to mathematically describe it. These models use a fixed set of equations and parameters, which can be related to physiological variables and used to extract more knowledge or optimize the process [65]. Bioprocesses can generally be described by ordinary differential equations (ODE) that are derived from the mass balance of the system, combined with equations for the reaction kinetics that serve as mechanistic links containing the model parameters [67]. Numerous kinetic equations have been established over the years [68], most prominently the monod kinetics that simplifies the complex biological process to one enzymatic reaction that is limited in rate by one substrate [69]. The development of mechanistic models is a complex undertaking that necessitates prior knowledge of the system and to date there exists no algorithm for a fully automatic set up. However, there are workflows and good practices that can aid in the process [70, 67, 71].

1.2 Aims of this Study

Motivation

The utilization of industrial lignocellulosic side streams to produce high-value products, as opposed to incineration or ethanol fermentation, is an important step towards a bio-based circular economy. Antimicrobial peptides such as bacteriocins have gained more attraction in the last years as potential biopreservatives for the food and health care market and thus are an interesting product for a renewable bioprocess. However, the production in lactic acid bacteria is not economically viable due to low achievable titres and expensive cultivation media. The heterologous expression of bacteriocins in a host utilizing lignocellulosic side streams has the potential to resolve those problems and enable an economically viable and sustainable production as part of a bio-based circular economy.

State of the Art

As part of a larger interinstitutional initiative, our laboratory investigated the use of SSL as a substrate for the biotechnological production of the antimicrobial peptide pediocin PA-1 using *Corynebacterium glutamicum*. In the framework of this initiative Goldbeck et al. established the heterologous expression of pediocin PA-1 in *C. glutamicum* and achieved with up to 20.000 BU/ml, titres comparable or higher than those reported for natural producer strains [53]. In a recent study, Christmann et al. further optimized the production and investigated the influence of several cultivation conditions, among them the pH value of the medium, on the pediocin formation. The pH value is known to affect the production and maturation of pediocin and other bacteriocins in their natural producers. Christmann et al. showed that the cultivation pH value also impacts pediocin PA-1 production in *C. glutamicum* and subsequently achieved 7-fold increased pediocin titres (135.000 BU/mL) in batch cultivations under acidic conditions [72].

In a first step toward a sustainable bioprocess, Sinner et al. investigated the cultivation of *C. glutamicum* on the defined media CGXII supplemented with UF-SSL as carbon source. Building on this research, Kitzmüller et al. developed a fed-batch process utilizing UF-SSL as sole medium with only the addition of antibiotics and anti-foam for pediocin production in *C. glutamicum* [73]. In this process, the nitrogen and phosphorous requirements of *C. glutamicum* were satisfied using an additional nutrition feed to avoid precipitation issues. The phosphorus ratio was subsequently identified as an important factor in influencing the pediocin titres. Reducing the carbon to phosphorous ratio in the feed and thereby limiting the phosphorus supply resulted in increased titres. However, the optimal value was estimated at the edge of the design area and may therefore be outside of the range tested. Additionally, the experimental design employed (2^3 factorial with triplicate center point) did not allow for the estimation of potential quadratic effects of the C/P-ratio that were detected. Nevertheless, The work of Kitzmüeller et al. demonstrated the feasibility of the envisioned sustainable bioprocess and achieved pediocin titres of up 5.000 BU/mL.

Problem statement

To ensure optimal efficiency and sustainability, potential process intensification possibilities should already be considered and investigated during development. Transitioning the process mode towards a repetitive fed-batch retains the advantages of a fed-batch cultivation while reducing down-times, energy and material usage for reactor preparation, thus resulting in an overall increased efficiency. As a starting point for this work, the process outlined by Kitzmüller was evaluated regarding this option and preliminary repetitive fed-batch experiments were conducted. In the course of this, several issues have been identified that negatively impact the efficiency of the process and further the implementation of a repetitive fed-batch and therefor have to be addressed:

i) Long and unpredictable lag phase

ii) Low biomass at the end of the batch phase

iii) High proportion of unused substrates in the batch phase

iv) Overfeeding and accumulation of substrates in the fed-batch phase

iiv) Low achieved titres compared to the production in *C. glutamicum* with complex media

Resolving those problems is the first step towards a reliable process and the basis for any further intensification.

Hypothesis

Based on the prior knowledge obtained from the literature and evaluating the process described by Kitzmüller et al. several hypothesises were established that should be investigated in this work.

Lignocellulosic derived inhibitors cause an inconsistent lag phase.
Elongated Lag phases and decreased biomass yields in the use of lignocellulosic side streams are often reported due to the presence of inhibitors, such as furfural and HMF, and the associated necessary detoxification by the microorganisms. Reducing the detoxification load per cell by modifying the inoculum size, the lag phase can be reduced both in duration and variability, ensuring consistent batch cultivation.

The problems in the fed-batch originate from the unoptimized batch phase.
The high variability, as well as the low final biomass concentrations and the incomplete consumption of the substrate provide poor starting conditions for the fed-batch phase and thus lead to further problems in the fed-batch such as overfeeding. By minimizing the end of batch variability, consistent starting conditions for the fed-batch can be be achieved.

Unoptimized fed-batch conditions limit realisation of Pediocin production potential.
A gap between pediocin PA1 production on complex medium and SSL-based minimal medium has been identified. Closer investigation of the promising factors pH value and C:P-ratio in the fed-batch should subsequently be employed to increase the production on SSL and close the previously observed gap.

Goals

This work aims to contribute to the on going development of an intensified bioprocess for the production of pediocin PA-1 using *C. glutamicum* and SSL as renewable substrate. For this reason, problems identified in a previously established fed-batch process should be addressed to allow further intensification to a repetitive fed-batch later on. Specifically, the presented study tries to achieve the following goals:

i) Resolving the identified problems in the batch phase to improve the reliability of the process and provide stable starting conditions for any further testing in the fed-batch phase. In detail, the lag-phase should be at least halved, to 5 hours, while maximising the substrate utilization and biomass concentration in the batch phase. According to the previously established hypothesis, this will be achieved by investigating and subsequently adjusting the inoculating conditions.

ii) Investigation the influence of the fed-batch parameter, pH value and carbon to phosphorous ratio on the pediocin PA-1 production in *C. glutamicum* on SSL. To estimate potential quadratic effects as well as interaction of the investigated factors, a three level full-factorial design of experiment will be employed.

iii) Extend the obtained knowledge and support the on going process development by establishment of a mechanistic model for growth, substrate utilization and pediocin formation. The model should be able to predict the respective states with a NRMSE of $\leq 10\%$.

2 Materials and Methods

2.1 Strains

C. glutamicum CR099::U *pXMJ19-pedACD* was used for all processes conducted in this work. The strain used was provided and developed by the Institute of Microbiology and Biotechnology of the University of Ulm and the Institute of Systems Biotechnology, Saarland University. *C. glutamicum* CR099 is a reduced genome strain with increased genome and plasmid stability, based on the prophage free strain MB001, with further removed insertion sequence elements ISCg1 and ISCg2 [74]. Additionally, the strain has been engineered for the xylose utilization and enhanced mannose uptake (denoted by '::U') by genomic introduction of the respective genes, described in [75] as plasmids. Production of pediocin PA-1 was facilitated by the pedACD cluster on the shuttle vector pXMJ19, containing the genes encoding for the pre-pediocin, as well as for processing and export of pediocin, controlled by the Isopropyl-β-thiogalactosid (IPTG) inducible promoter P_{tac} [53].

Listeria innocua pNZ44 was used as indicator strain for the antimicrobial activity assays.

2.2 Media and solutions

Inoculum preparation was carried out using 2x tryptone-yeast extract (2TY) medium (16 g/L tryptone, 10 g/L yeast-extract, 5 g/L NaCl) with 12 mg/L chloramphenicol (CM) as antibiotic. Culture plates were prepared by the addition of 18 g/L agar-agar.

Bioreactor cultivations were performed with UF-SSL (Borregaard, Sarpsborg, Norway) as batch-medium and feed. UF-SSL from the same production batch was used for the experiments to minimize raw material variability. For the batch medium the SSL was diluted 1:4, filtered sterile (0.2 µm) and supplemented with Biotin (0.2 mg/L) and polypropylene glycol 2000 as antifoam (5 ml/L). The SSL feed was prepared by further addition of IPTG (0.2 M) to the supplemented sterile SSL. Samples were drawn from the fully supplemented SSL to quantify the substrate concentration. The composition of the SSL used in this work is shown in table 2.1. Lactate and glutamate were measured but below the detection limit in all SSL samples.

Table 2.1: Composition of the diluted SSL (25 %) used in this work

	Glucose [g/L]	**Mannose [g/L]**	**Xylose [g/L]**	**Galactose [g/L]**	**Arabinose [g/L]**	**Acetate [g/L]**
mean	10,44	32,45	14,10	6,69	3,18	1,73
st. dev.	0,44	1,53	0,61	0,35	0,25	0,12

In addition to the SSL, a nitrogen and phosphorous (NP) solution was used to statisfy the nutrient requirements during the cultivation. Different concentrations were employed depending on the experimental plan and phase of the process (table 2.2).

Table 2.2: Used nitrogen & phosphorous (NP) solutions

	$r_{C:P}$	**Urea [g/L]**	**KH_2PO_4 [g/L]**
Batch		66.4	73.8
Fed-Batch	45	33.2	33.5
	60	33.2	25.1
	75	33.2	20.1

The indicator strain for the antimicrobial activity assay was cultivated in brain heart infusion (BHI) medium. 37.5 g/L BHI were dissolved in water and sterilized by autoclaving.

For saline solution 9 g/L NaCl were dissolved in distilled water and autoclaved.

2.3 Inoculum preparation

C. glutamicum CR099::U *pXMJ19-pedACD* was streaked out from glycerol cryostocks on 2TY agar plates and grown for 48 hours at 30 °C. Cells for the bioreactor cultivation were prepared by two consecutive liquid precultures grown in an orbital shaker-incubator at 30 °C and 230 rpm. Single colonies were used to inoculate the first precultures in 50 ml tubes containing 12.5 ml 2TY medium. The second stage of the precultures were grown in 1000 ml unbaffled shake flasks with 225 ml 2TY medium and 25 ml 100 % SSL buffered with 100 g/L MOPS for approximately 18 hours. The cells were harvested by centrifugation (10 min, 3420 g, 4 °C) and resuspended in saline to inoculate the reactor.

2.4 Bioreactor cultivations

Bioreactor cultivations were carried out using a bench-top bioreactor system (Labfors 5, Infors HT, Switzerland) with a jacketed glass vessel of 3.0 L working volume. The temperature during the fermentation was held at 30 °C using a thermostat connected

to the cooling jacket. The reactor was equipped with 3 baffles and two six-blade Rushton turbine impellers for stirring. An optical oxygen probe (VisiFerm DO Arc 325, Hamilton, Switzerland) and a potentiometric pH probe (EasyFerm Plus PHI K8 325, Hamilton, Switzerland) were installed to monitor the dissolved oxygen (DO) and the pH value in the reactor. The DO was controlled by adapting the stirrer speed (400-1200 rpm) while sparging air at a constant aeration rate (0.3 vvm) into the reactor. The pH was controlled by a PID controller by adding 2.5 M H_2SO_4 and 2.5 M KOH. The Off-gas stream was analyzed for the oxygen and carbon dioxide concentration with a ZrO_2 and IR sensor respectively (BlueInOne Ferm, BlueSens). Sampling was performed automatically every three hours with a custom made autosampler device. Approximately 30 ml of sample volume was drawn from the bottom of the reactor and stored at 4 °C until further analysis. Process data was collected using the process information management software (PIMS)(Lucullus, SecureCell, Switzerland). For process control MatLab was used over an open platform connection (OPC) and the PIMS. For process control, real-time data was imported into Matlab via an open platform connection (OPC), the setpoints calculated and returned to the PIMS.

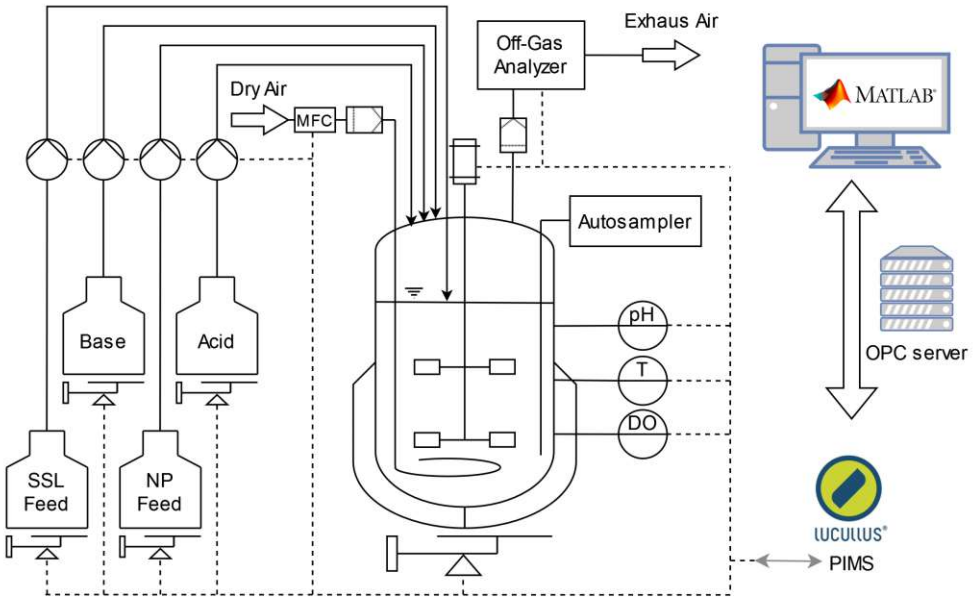

Figure 2.1: Reactor setup for the conducted cultivations.

For batch cultivations 1 L batch medium was transferred sterile into the reactor. During the batch phase, the pH was held at 7 while the DO was maintained at 30 %. The process was started by inoculating the reactors with the resuspended cells. The volume of the inoculum was chosen to reach a starting biomass of approximately 1 g/L in the reactor. Nitrogen and Phosphorous source in the form of urea and KH_2PO_4 (table 2.2) was fed into the reactor over the duration of the batch (100 ml, 4.5 ml/h).

To investigate the influence of the fed-batch parameter, pH value and C/P ratio of the feed, a 3 level full factorial experimental plan was employed (figure 2.2). The fed-batch phase of the process was initialized by adjusting the pH value according to the experimental plan (6.0 - 7.0) and lowering the DO setpoint to 15 %. To start the production, the cells were induced by the addition of 0.2 M IPTG into the reactor. The SSL feed was controlled with an open loop predefined exponential feed profile (1 l, $\dot{V}_0 = 30$ [ml·h^{-1}], $\mu = 0.03$ [h^{-1}]) During the production phase, the feed profile of the NP-stock (table 2.2) was changed from linear to exponential feeding (200 ml, $\dot{V}_0 = 6$ [ml·h^{-1}], $\mu = 0.03$ [h^{-1}]) to obtain a constant C/P ratio.

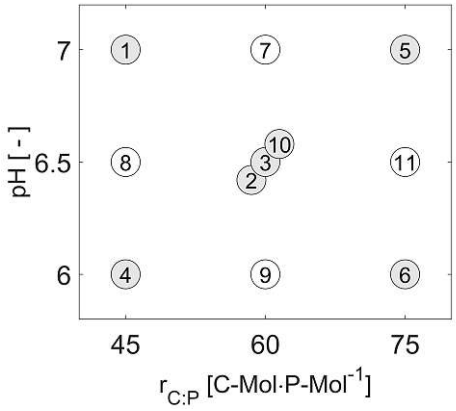

Figure 2.2: Full factorial experimental design for the fed-batch conditions with the respective run numbers. The C/P-ratio was

Repetitive Fed-batch processes were conducted by draining the reactor to a desired remaining volume of culture broth and re-filling it with fresh batch medium. One repetitions consisted of a batch and fed-batch phase with a duration of 24 h each. Draining an re-filling were performed with peristaltic pumps.

2.5 Sample Analysis

To evaluate the process, the samples were analyzed for their biomass concentration, dry weight, antimicrobial activity, sugar and organic acid concentrations as well as phosphate and ammonia concentration. For the dry mass estimation 3 x 1.8 ml sample volume were centrifuged (14000 g, 4 °C, 10 min) and the pellet was dried at 115 °C for 72 h. The dry weight of the samples was determined gravimetrically by weighting of the dried pellets. The supernatants were collected and used for the quantification of sugars, organic acids, phosphate and ammonium.

For determination of the sugar concentration, the supernatants were diluted 1:20 with ultra-pure water, filtrated (0.2 µm) and analysed using high-performance liquid chromatography (UltiMate U3000, Thermo Scientific, USA) with a refractive index detector (RI100, Shodex, USA). For separation, a lead column (Nucleogel Sugar Pb, Macherey-Nagel GmbH, Germany) at 79 °C and an isocratic flow (0.4 ml/min, 65 min runtime) of ultrapure water were employed.

The supernatants were further analysed photometrically for organic acids (glutamate, lactate, acetate), phosphate and ammonium ions using enzymatic assays (CEDEX Bio HT, Roche, Switzerland).

The Pediocin activity was determined with a photometric assay similar to that described by Kyrill et al. [76]. The indicator strain was grown overnight in 15 ml falcon tubes containing 5 ml BHI medium with 5 µg/ml CM on a rotary shaker incubator (37 °C, 230 rpm). Two-fold dilution series of the culture supernatants with BHI medium were prepared in 96-well plates. No sample was added to the last row, that served as blank. The indicator culture was diluted 1:25 with BHI medium and added to all wells (ratio 1:1). The plates were incubated for 5-6 hours at 37 °C and the OD600 was measured to estimate the biomass in each well (Infinite M200 PRO, TECAN, Switzerland). The obtained growth inhibition data were normalized with the absorption of the blank and used to fit dosage-response curves. The equation for the dosage-response curve (equation 2.1) was adapted from Veroli et al. [77] and fitted using an implementation of a nonlinear iterative least square algorithm in MatLab 2022b. The inflection points (ID_{50}) of the fitted curve where then used to calculate the activity of the sample. The pediocin activity, given in BU·ml^{-1}, was defined as the amount of active pediocin per volume that results in growth inhibition of 50 %.

$$OD_{600} = LB_{OD_{600}} + \frac{UB_{OD_{600}} - LB_{OD_{600}}}{1 + (ID_{50}/D)^k} \tag{2.1}$$

Previous experiments have shown that traditional methods for determination of the biomass like cell dry weight and OD600 are not applicable to our process due to precipitation. An assay based on the fluorescence of amino acid side chains in the cell mass was used thereby used. For this reason, 3 x 900 µl of the sample were centrifuged (3420 g, 4 °C, 10 min) and the pellets were washed in 900 µl saline and centrifuged again. The washed pellets were resuspended in 900 µl saline and serially diluted two-fold with saline in a 96-well plate. Relative fluorescence units (RFU) were measured on a plate reader with 280/15 nm excitation wavelength and 340/20 nm emission wavelength. RFU were converted to the biomass concentration with a pre-determined standard calibration (linear range: 8500 - 16000, slope: 0.980, intercept: 4.680) and the corresponding dilution factor.

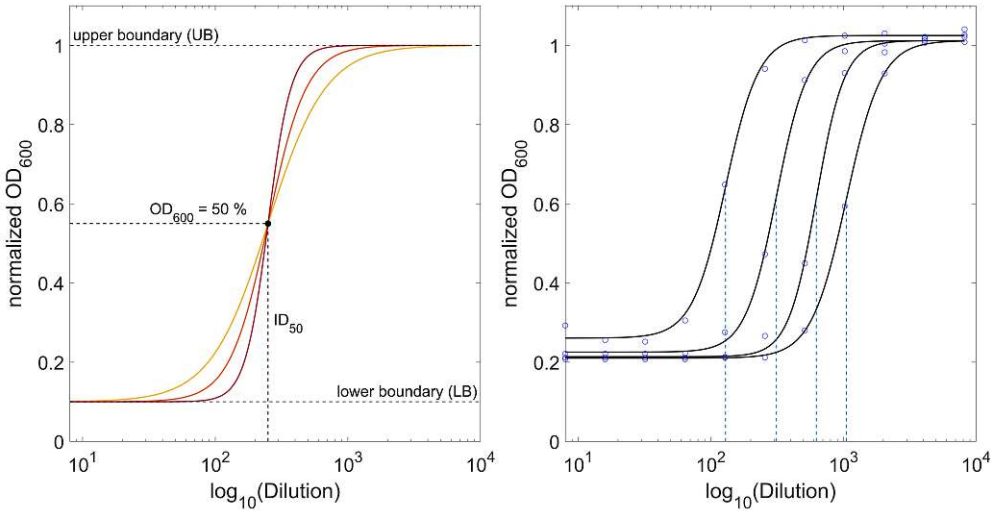

Figure 2.3: Dosage-response curve and the corresponding parameters according to equation 2.1; Different values of k (2, 3, 5) are illustrated in color (left). Example of samples with increasing activity (right).

2.6 Data evaluation

The obtained data was processed and evaluated using MatLab 2022b (Mathworks, USA). For continuous signals (weight signals, gas flow) outliers were removed using a hampel filter before smoothing the data with matlabs smooth function with the 'rloess' mode (robust quadratic regression smoothing).

Respiratory rates were calculated according to eqation 2.3- 2.4. The respiratory rates were compensated for errors arising from humidity in the off-gas stream using the correction factor r_{inert}. r_{inert} was calculated using the water fraction in the exhaust gas measured with the humidity sensor of the off-gas analyzer (equation 2.2). The respiratory rates were further used to calculate the respiratory quotient (RQ, equation 2.5):

$$r_{inert} = \frac{1 - x_{CO_2,Air} - x_{O_2,Air}}{1 - x_{CO_2,Offgas} - x_{O_2,Offgas} - x_{H_2O}} \left[- \right] \tag{2.2}$$

$$r_{O_2} = OUR = -\frac{\dot{V}_{in} \cdot (x_{O_2,Air} - r_{inert} \cdot x_{O_2,Offgas})}{M_V} \left[\frac{mol}{h} \right] \tag{2.3}$$

$$r_{CO_2} = CER = \frac{\dot{V}_{in} \cdot (r_{inert} \cdot x_{CO_2,Offgas} - x_{CO_2,Air})}{M_V} \left[\frac{mol}{h}\right] \tag{2.4}$$

$$RQ = \frac{CER}{OUR} [\,\text{-}\,] \tag{2.5}$$

Volumetric rates were calculated according to equation 2.6 using the respective concentrations. The specific rates were calculated from the volumetric rates (equation 2.7).

$$r_i = \frac{\Delta m_i}{V_R \cdot \Delta t} \left[\frac{g_i}{Lh}\right] \tag{2.6}$$

$$q_i = \frac{r_i}{c_X} \left[\frac{g_i}{g_X h}\right] \tag{2.7}$$

Balances were established based on the following reaction equation:

$$\begin{gathered} O_2 + \text{SSL} + \text{urea} + PO_4 \longrightarrow \\ CO_2 + \text{by-products} + \text{urea} + NH_3 + PO_4 + \text{X} + \text{sample} \end{gathered} \tag{2.8}$$

The term SSL summarizes the substrates according to table 2.1. For the balances only the utilizable substrates were considered (Glucose, Mannose, Xylose, Acetate). The overflow metabolites glutamate and lactate were measured and included as by-products in the equation. The composition of the biomass (X) of *C. glutamicum* was taken from the literature [75]:

$$C_1H_{1.832}N_{0.176}O_{0.615}P_{0.0157}S_{0.0033}K_{0.0005}Mg_{0.0005}Ca_{0.0058}Na_{0.0267}Cl_{0.0034}$$

For the electron balance the degree of reduction (DoR, γ) of a substances ($CH_aO_bN_c$) was calculated according to equation 2.9:

$$\gamma = 4 + 1 \cdot a - 2 \cdot b - 3 \cdot c \tag{2.9}$$

The balance ratio was determined by considering the relevant terms on both sides of the reaction equation for the respective elemental balance (equation 2.10).

$$r_{balance} = \frac{\sum_{i=1}^{n} n_{product,i}}{\sum_{j=1}^{m} n_{educt,j}} \tag{2.10}$$

Design of experiments was performed in MODDE pro 13 (sartorius, Göttingen, Germany). The influence of the factors incorporated in the DoE on the respective response was evaluated in MODDE using multiple linear regression (MLR) at a significance level of 0.05.

2.7 Modeling workflow

The different models and all scripts for the analysis and evaluation of the models and model outputs were coded in MatLab 2022b. The workflow for setting up and analysing the mechanistic models was similar to the approach described in [67] and broadly involved the following steps:

i Assessment of prior knowledge and experimental data

ii Model definition

iii Model analysis

iv Parameter estimation

v Evaluation of the fit

Model definition

All models were derived from the mass balance for an ideally stirred tank reactor (equations 2.11 - 2.13). The total volume flow rate into the reactor ($\dot{V}_{in}$) is influenced by the the SSL and NP feed as well as the addition of acid and base for the pH control. During batch operation no SSL was fed into the reactor ($\dot{V}_{SSL,in} = 0$). The biomass formation is influenced by the specific growth rate and changing reaction volume. The change of substrate concentration was described by the flow of substrate into the reactor and the decrease due to uptake by the cells.

$$\frac{dV_R}{dt} = \dot{V}_{in} \tag{2.11}$$

$$\frac{dX}{dt} = X \cdot \left(\mu - \frac{\dot{V}_{in}}{V_R}\right) \tag{2.12}$$

$$\frac{dc_{S_i}}{dt} = \frac{\dot{V}_{SSL,in}}{V_R} \cdot c_{S_i,in} - \frac{\dot{V}_{in}}{V_R} \cdot c_{S_i} - q_S \cdot X \tag{2.13}$$

The model for the pediocin formation (equation 2.14) was based on the equation proposed by Luedeking and piret [78] and further modified to include degradation/oxidation of the product as well as dilution due to the inflow of volume during the fed-batch.

$$\frac{dP}{dt} = q_P \cdot X - P \cdot \frac{\dot{V}_{in}}{V_R} - q_{dO} \cdot P \tag{2.14}$$

Model analysis

The model analysis was performed in a methodology similar to that described by Brun et al [79]. The model was analysed in regards to parameter sensitivity, overall parameter importance on the model and identifiability of the parameter. The sensitivity of the model parameters was estimated as the influence of a perturbation by 1 % of the individual parameters (θ_p) on the model outputs ($\hat{y}_i$) (equation 2.15). The parameter importance (δ_i^{msqr}), a measure of the mean sensitivity of the model output to a model parameter, was calculated as the mean square root of the sensitivity (equation 2.16). For the parameter estimation, identifiable parameter sets (K) were determined based on the collinearity index for the respective set (γ_K)(equation 2.17). The collinearity index is calculated from the eigenvalues (λ_K) of a submatrix for the respective parameter set ($\tilde{S_K^T}\tilde{S_K}$). According to Brun et. al. [79], a parameter subset can be considered identifiable if its collinearity index is below the threshold of 20.

$$S_{i,p} = \frac{\partial \hat{y}_i}{\partial \theta_p}\theta_p \tag{2.15}$$

$$\delta_p^{msqr} = \sqrt{\frac{1}{n}\sum_{i=1}^{n} S_{i,p}} \tag{2.16}$$

$$\gamma_K = \frac{1}{\sqrt{\lambda_K}} \tag{2.17}$$

Parameter estimation

The parameter were estimated using the fminseach algorithm, a Matlab implementation of the Nelder-Mead simplex algorithm [80], and a log likelihood (l) objective

function (equation 2.18). The estimation was carried out with the optimization criterion ($\hat{\Theta}$) of minimizing the mean negative log likelihood of the observed (y_i) and predicted model states ($\hat{y_i}$) (equation 2.19).

$$l = -\frac{n}{2} \cdot ln\left(2\pi\right) - \frac{n}{2} \cdot ln\left(\sigma^2\right) - \frac{1}{2\sigma^2}\left(\hat{y_i} - \overline{y_i}\right) \tag{2.18}$$

$$\hat{\Theta} = arg\ min\left(mean\left(-l\right)\right) \tag{2.19}$$

Evaluation of the fit

The fit of a model in respect to one model state was evaluated by calculating the root-mean-square-error (RMSE) for that state (equation 2.20). The RMSE was further normalised using the range of the state to obtain the normalised root-mean-square-error (NRMSE)(equation 2.21).

$$RMSE = \sqrt{\frac{1}{n}\sum_{l=1}^{n}\left(\hat{y_{i,l}} - y_{i,l}\right)^2} \tag{2.20}$$

$$NRMSE = \frac{RMSE}{max(y_i) - min(y_i)} \tag{2.21}$$

3 Results and Discussion

3.1 Process evaluation

The batch and fed-batch phases were assessed individually due to distinct objectives being targeted. A reliable batch phase is crucial for subsequent exploration in the fed-batch phase. Firstly, the problems encountered in the initial batch phase were addressed. Secondly, the effect of pH and C:P ratios in the fed-batch phase was investigated in the cultures using the improved batch phase. The batch phase remained constant throughout those experiments to establish consistent initial conditions, while the examined fed-batch parameters were altered following a three-level full-factorial experimental design.

3.1.1 Batch phase

This subsection takes a detailed look on the improvements for the batch phase and evaluates the batch phases of the conducted processes. The purpose of the batch phase in this work is to generate biomass that is then further induced in the fed-batch phase to produce pediocin PA-1. Since differences in the batch phase will carry over throughout the process, a stable batch phase is a requirement for any further investigations in the fed-batch. To provide comparable starting conditions the batch phase should thereby have a low variability in both duration and achieved end biomass. The batch phase of the previous process struggled with problems such as low biomass yields, slow and incomplete substrate utilization as well as a high batch-to-batch variability. As a consequence it was decided to address those issues before proceeding to the fed-batch.

Optimization of the batch phase

Slight modifications were made to the composition of the medium. The original process established a very minimalistic medium only based on SSL supplemented with antibiotics, antifoam and IPTG for the feed. During development of the initial process, the provided SSL was analysed for nutrients and trace elements by a reference laboratory and the data were compared to the common GCXII medium. Based on this comparison it was decided that no trace elements needed to be added. Nitrogen and Phosphorous requirements were provided as external feed to circumvent solubil-

ity problem and no vitamins were supplemented. Although this minimalistic medium allowed growth, the achieved biomass concentrations achieved at the end of the batch were very low ($\leq$ 3 g/L) despite the excess of available carbon sources. Additionally, unwanted glutamate production (up to 600 mg/L) was observed in the original process. While the glutamate concentrations seem low, the production of side- and overflow metabolites can reveal unfavorable cultivation conditions and thereby aid in improving said conditions. Glutamate production and secretion in *C. glutamicum* have been extensively studied [33, 81] and have been linked to cell stress like biotin limitation [82, 83], temperature shift [84] or addition of chemicals (most notably tween and penicilin) [85, 86]. Since the temperature was controlled within a narrow margin and no known glutamate-inducing agents were added, it was concluded that the lack of biotin in the medium is the most probable reason for the glutamate production. Unfortunately, no biotin quantification of the SSL provided was available during the course of this study. Biotin is reported to be present in lignocellulosic biomass, with considerable variation depending on the raw material of origin [87, 88, 89]. However, the only reported value for SSL (0.5 - 0.9 µg/L [87]) is well below typical supplementation levels for *C. glutamicum* cultivation. To avoid limitations, it was decided to add biotin equal to the concentration (0.2 mg/L) that is supplemented into GCXII cultivation medium [90]. A possible biotin limitation and the resulting glutamate side production are very likely to reduce the biomass yield [91] and thereby the efficiency of the batch. Nevertheless, additional factors have to play a role in the observed problems of the original batch-phase.

One of the main problems identified was an unpredictable long lag phase with a duration of up to 42 hours. The lag phase is the first phase in bioreactor cultivation and is characterised as the period the cells take to start replicating after being introduced to the reactor [92]. The exact mechanisms of the lag phase are still poorly understood, however it is usually assumed that the cell adapt to the changed environment and repair macro-molecular damage accumulated from the stationary phase of the inoculum [93]. Common ways to reduce the lag phase therefore include cultivation of the inoculum in the same or similar conditions as the reactor culture. Measures to reduce the lag phase were already present in the original process. A two-staged liquid pre-culture with increasing fraction of SSL was used to inoculate the reactor. The second stage was prepared with 10 % SSL , which should lead to the cells expressing genes required for the uptake and metabolization of the sugars present in SSL. Another stage of pre-culture with a SSL fraction of 25 % was not considered to be practicable. Similarly, it was considered that elevating the proportion of the second stage to 25 % SSL might lengthen the pre-cultivation period and increase the risk of unsuccessful pre-cultivation. A simple method to reduce the lag phase duration could be the increase of inoculum size. Several studies have been focused on the effect of the inoculum size on the lag phase for different microorganisms, media and applications. However the results of those studies are not consistent. While some did not not find a reduction in lag phase with increasing starting cell density, which is inline with the the theory that the lag phase is caused by intracellular adaptions of the cells [94, 95, 96].

Other studies found that increasing inoculum sizes in fact decrease the lag phase, indicating the influence cooperative effects on the lag phase [97, 98]. It has to be noted that inoculum-size independent lag phases were mostly reported for optimal cultivation conditions, while decreasing lag phases were mainly observed under restricting conditions (poor nutrients, high osmolarity, altered pH etc.) [99, 100]. SSL contains several lignocellulose-derived toxic compounds, most notably furfural and HMF, that lead to non replicating and dying cells [29]. *C. glutamicum* has dedicated genes to detoxify those inhibitors, however growth is greatly reduced during this initial detoxification [42, 101], further increasing the lag phase. Based on this, the hypothesis was established that the prolonged lag-phase is heavily influenced by the growth inhibition of the cells during detoxification. In theory, an increase of the inoculum size should reduce the time for the detoxification and thereby reduce the observed lag-phase. To test this hypothesis the duration of the lag phases from a series of cultivations differing in the amount of inoculum were compared.

Samples were drawn every three hours, which equals the sampling interval in the original process and the later performed bioreactor cultivations for the evaluation of the pediocin production. The determination of the lag phase duration based on the biomass would however require a higher sampling frequency. To minimize the influence of the sampling on the experiment it was decided to determine the length of the lag phase based on the respiratory rates. The oxygen uptake rate and the carbon evolution rate were calculated from the exhaust gas signals of the respective gas. During aerobic microbial cultivation, oxygen is required as terminal electron receptor in the respiratory chain and gets oxidized to water. Additionally, carbon dioxide is released as a result of the step-wise degradation of the carbon source in metabolism. The metabolic activity of the cells can thereby be observed in the change of the off-gas signals. Additionally, the substrate and biomass concentrations were measured and compared. In accordance with the original process the batch end was chosen to be the point of complete glucose utilization.

Figure 3.1 shows the CER data for the comparison of different inoculum sizes. Further, the time point of depletion for acetate and glucose are represented in the plot by by vertical lines. Shortly after the start of the batch a fast increase of the CER, caused by the introduction of the inoculum can be seen in all processes. This initial increase is followed by a plateau phase that is indicative of the lag-phase. The original process was inoculated with a start OD of 1, which equals 0.23 g/L biomass. A start OD of up to 1 is commonly used for *C. glutamicum* in conventional media. Increasing the start biomass concentration to 1 g/L reduced the duration of the lag phase significantly and resulted in about 4 times higher achieved biomass concentrations. An increase from 1.0 g/L to 1.5 g/L did further shorten the lag phase but did not show a beneficial effect on the biomass yield like the first increase. In a next cultivation the SSL fraction for the batch medium was raised to 30 %, which increases the substrate concentration as well as the inhibitor concentration. The batch with elevated SSL fraction and 1.0 g/L suffered from a prolonged lag phase compared to the cultivation with the same

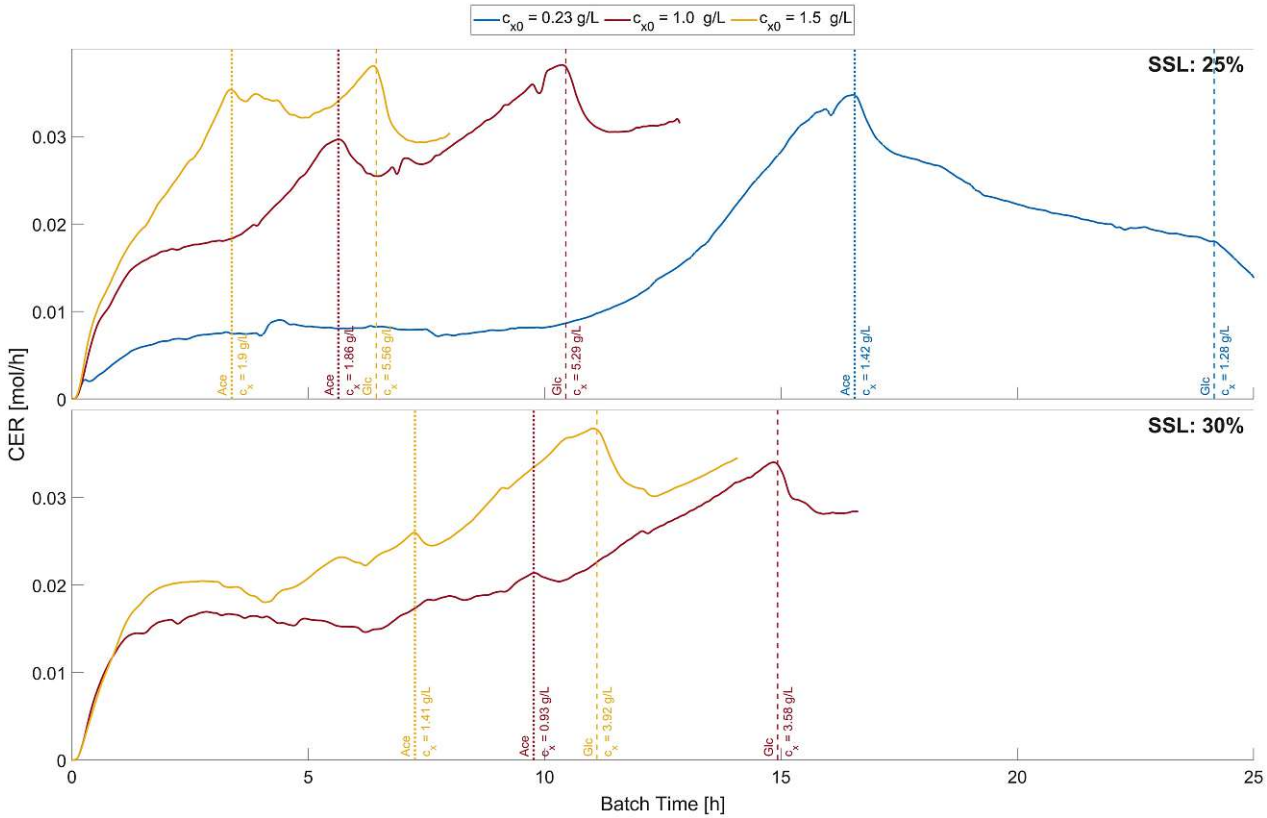

Figure 3.1: Investigation of the starting conditions for the batch cultivation. The original process utilized OD_{600}=1.0 (0.23 g/L) for inoculation, displaying a lag phase of approximately 10 hours. Increasing the inoculum to 1.0 g/L resulted in significant reduction of the observed lag phase (approx. 3 hours) and increase of the biomass concentration. Further increase shortened the lag (below 1 hour) further but did not show any beneficial effects on the biomass concentration. Raising the SSL concentration resulted in again prolonged lag phases, probably due to the higher concentration of inhibitors. The effects of elevated SSL levels can be compensated with an additional increase of inoculum, further reinforcing the established hypothesis.

inoculum size and 25 % SSL. By raising the start biomass concentration to 1.5 g/L the effect of the increased SSL level was compensated and the lag phase and batch duration almost identical to the cultivation with 25 % SSL and 1.0 g/L inoculum. Against expectations the higher substrate concentration of the higher SSL fraction did not yield higher biomass concentrations. In fact the achieved biomass concentrations were about 30 % lower compared to the experiments with 25 % SSL. In both batches with 30 % SSL the biomass concentration did decrease slightly up to the depletion of acetate. It is possible that the increased inhibitor concentrations lead to a die-off of a part of the initial biomass and thereby decreased the number of viable cells in the reactor. Further, the detoxification process could be a possible explanation for the decreased biomass yields. While the detoxification metabolism for lignocellule derived inhibitors like furfural and HMF is not yet fully understood in *C. glutamicum*, it is reported that furfural is either reduced to furfuryl alcohol or oxidized to furoic acid under aerobic conditions [42]. An alcohol dehydrogenase, FudC, was identified as key enzyme for the conversion path to furfuryl alcohol, reducing furfural at the expense of NADPH [102]. No exact mechanism is known to this date for the oxidation to furoic acid. Similarly to furfural, HMF is converted to HMF acid and HMF alcohol [103]. It is safe to assume that the detoxifaction is a burden to the cells energy household and therefor leads to reduced biomass yields.

The obtained results did reinforce the established hypothesis, that the detoxification of the inhibitors inherent to SSL is the main cause of the prolonged lag phase. It was decided to change the starting conditions for future experiments and proceed with 1.0 g/L inoculation biomass. The gathered data was further used to link peaks in the off-gas signals to the substrate utilization in the batch phase. Correct assignment of changes in the off-gas signals to the corresponding event, like the depletion of a particular sugar, can help with process monitoring and control. Since off-gas analysis is an online measurement, the signals can be used to evaluate a prolonged lag phase or the end of the batch in real-time without time consuming measurements if the process understanding allows it. The previous process defined the end of the batch as the complete utilization of glucose, which was identified as peak in the respiratory after approximately 16-20 hours process time. However, it was later discovered that the observed peak was misidentified and instead coincided with the depletion of acetate. Therefore glucose was not completely utilized at the start of the feed, probably contributing to the overfeeding in fed-batch. For the chosen stating conditions two peaks in the respiratory rates are visible during the batch phase. These two peaks were found to coincide with the depletion of acetate (approx. 5 h) and glucose (approx. 11 h), respectively. For practicality reasons it was decided to change the end of batch criterion and set the batch duration to 24 h for the upcoming fed-batch experiments. It was observed that the respiratory rates increased further after the depletion of glucose, due to the utilization of xylose and mannose. By increasing the batch duration beyond the complete uptake of glucose, the cells will utilize those remaining sugars, which should result in higher achieved biomass concentrations.

Demonstration and evaluation of the optimized batch phase

For the fed-batch processes the batch-phase was conducted with the mentioned optimizations. In total 11 processes were performed with the optimized batch conditions. In the following the results of the batch phases are presented. Samples were drawn in intervals of 3 hours, totalling to 9 samples for the duration of the batch. For practicality reasons, no separate fed-batch start sample was drawn, but the fed-batch was started shortly before the last batch sampling time point. Thereby this sample was used as both batch-end and fed-batch start sample. It should therefore be noted that the conditions (pH, DO, etc.) during the sampling interval do not correspond continuously to those of the batch, but for a short time ($\leq$ 10 min at the end) to those of the fed-batch. Although it is highly unlikely that these few minutes of changed conditions will affect the results to such an extent that they are no longer representative of the batch, this must be taken into account when considering the results.

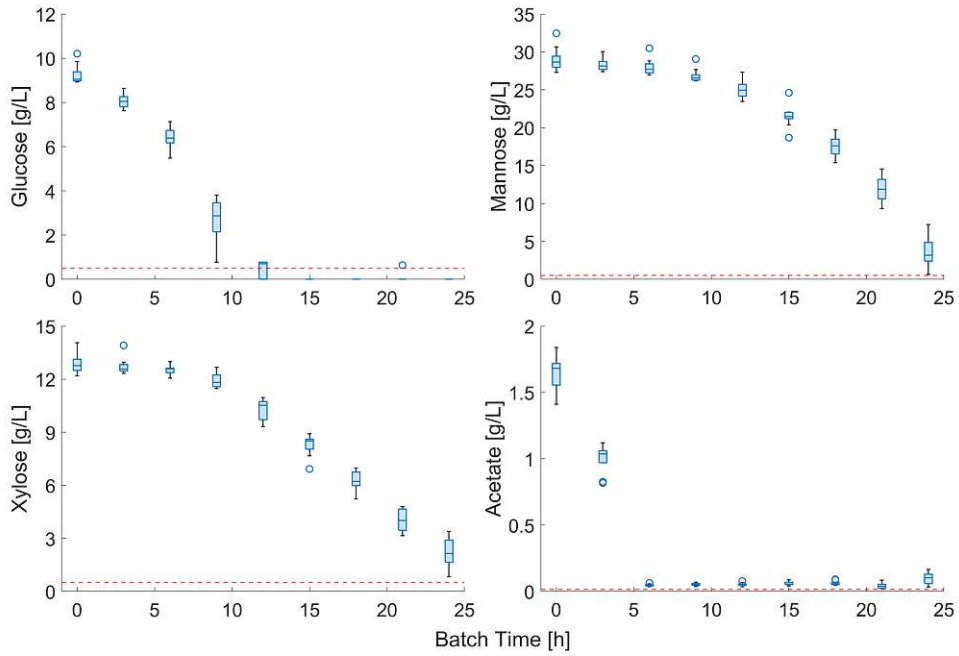

Figure 3.2: Box chart for the substrate concentrations (fermentable sugars + acetate) of the batch phases. The red dashed line represents the LOQ of the measurement for the respective substrate.

In figure 3.2 boxplots of the substrate concentrations (sugars and acetate) of the batch phases are shown. To minimize the influence of the inherent variance of SSL on the starting conditions for the process the same production batch was used for all experiments. Additionally, process-to-process variability minimized by diluting up

to 10 L medium (5 fed-batches) together. It can be seen that the spread for the starting concentration is very narrow, with the exception of two outliers for glucose and mannose. Regarding the utilization of the substrates it can be observed that the uptake of acetate and glucose starts immediately with no sign of a lag phase. Acetate is the first substrate to be depleted after around 6 hours, followed by glucose after approximately 12 hours. In contrast the concentrations of xylose and mannose stay almost constant for the first hours of the process. In contrast, the xylose and mannose concentration remain constant for the first hours of the process and start to decrease once glucose concentrations approach zero. This observation is in line with the literature, that suggests that the uptake of xylose [41] and mannose [40] is down-regulated in the presence of glucose. Both xylose and mannose decrease till the end of the batch but are not consumed completely during the batch phase. For the complete uptake of the remaining sugars the batch phase would have to be prolonged for about 2-3 hours. However, an increase of the batch duration should only be conducted if a significant gain for the process yield is to be expected and the decision thereby not based solely on the substrate utilization.

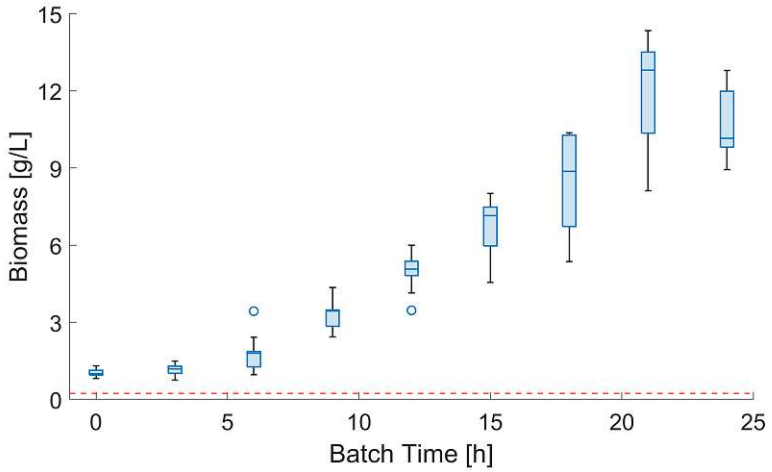

Figure 3.3: Box chart for the biomass concentration of the batch phases. The red dashed line represents the LOQ the measurement.

The achieved biomass concentration is one of the most important attributes to judge the success of the batch phase. Figure 3.3 illustrates the biomass concentration for the batch phases of the conducted experiments. The processes were inoculated with a start biomass concentration of 1.0 g/L. The required volume of the preculture to reach this start concentration in the reactor was determined using the OD_{600} of the preculture broth. Directly after inoculation of the process a start sample was drawn from the reactor. It can be seen that the biomass concentration for the start sample (1.04 ± 0.14 g/L) has a narrow spread around the expected concentration of 1.0 g/L. The biomass concentration increases exponentially almost from the beginning for ap-

proximately 21 hours. A short delay in growth can only be observed for the first three hours of the process where the concentration increases slightly to 1.14 ± 0.24 g/L. During batch cultivations, substrate is provided in excess to the cells, as a consequence the cells grow exponentially with a specific growth rate of $\mu = \mu_{max}$ for the provided condition. For the exponential growth in performed batch phases a mean $\mu = 0.118 \pm 0.009\ h^{-1}$ was observed. However, the biomass concentration did not increase exponentially throughout the entire batch phase in the conducted processes; instead, it decreased or stalled towards the end of the batch. This event event occurred between 21-24 h process time, with most processes peaking in biomass concentration around 21 h. The biomass concentration at the start of the fed-batch (10.8 ± 1.35 g/L) decreases compared to the maximum reached mean concentration (12.0 ± 2.14 g/L) about 10 % due to this drop. The drop did not coincide with the depletion of any carbon source or other measured nutrients. When the biomass concentration decreases, acetate and glucose are long depleted, however mannose ($\simeq$ 5 g/L) and xylose ($\simeq$ 3 g/L) are still available and taken up by the cells. Regarding reproducibility, a minimal variation can be observed in the biomass concentration during the initial 12 hours of the process when glucose is primarily consumed. The spread of biomass is significantly increased in the samples from 15 hours on wards. After the depletion of glucose and thereby the lack of repression, xylose and mannose are utilized by the cells. The employed strain was engineered for the utilization of xylose and enhanced uptake of mannose compared to wildtype *C. glutamicum*. Variations between the runs in this phase could potentially be related to differences in the stability and expression levels of those genetically engineered pathways compared to the naturally inherent pathways of *C. glutamicum*. The increased variability in the biomass formation is most likely a consequence of the co-utilization of xylose and mannose. Significant variations can be observed especially between 18 and 21 hours process time. However, the spread decreases slightly before the end of the batch due to the biomass drop.

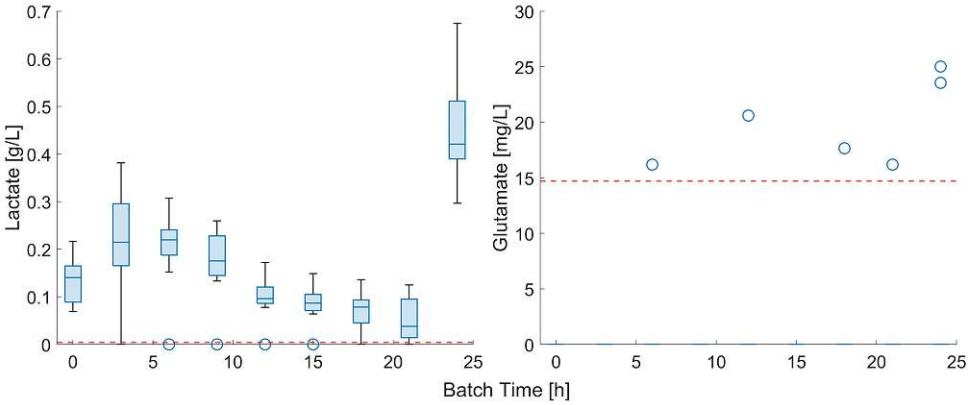

Figure 3.4: Concentrations of the organic acid metabolites during the batch phase. The red dashed line represents the LOQ the measurement.

Further, typical overflow metabolites such as the organic acids lactate and glutamate were monitored for the duration of the process (figure 3.4). The production of these metabolites can be indicative for unfavorable conditions such as limited oxygen supply or presence/lack of certain chemicals. The data may thus help to detect explain the observed sudden decline in biomass at the end of the batch. Considerable variability in lactate production was observed between the different batch phases. This applies especially for the second sample were the concentration ranges from no lactate detected to above 4 mmol/L. Despite this, a trend can be observed: in general a small increase in the first hours of the batch seems to be followed by a decrease due to the (re)utilization of lactate. However, it has to be mentioned that the concentrations are generally very low in the performed cultivations. For the transition from batch to fed-batch a steep increase of the lactate concentration was detected in all processes. Events in this time interval are of particular interest as they may aid in comprehending the die-off at the end of the batch. If the lactate production is linked to the drop in biomass, the extend of the lactate rise should correlate with the decrease of biomass. The search of a potential mathematical relationship is particularly interesting for future mechanistic modelling of the biomass drop. However, no numerical correlation was found between biomass and lactate concentrations, volumetric or specific rates. Although this does not necessarily mean that there is no correlation between the increase in lactate and declining biomass, the available data cannot be employed to predict cell death or deduce its cause. Another possible reason for the rise in lactate levels could be the start of the fed-batch phase and the associated changes. *C. glutamicum* is known to secrete organic acids, mainly lactic acid, into the medium when being cultivated under oxygen deprived conditions [104, 105]. In the transition to the induced fed-batch, the DO setpoint was reduced from 30 to 15 % in order to minimize the oxidation of pediocin. The DO control was accomplished using a PID controller for the stirrer. Reducing the setpoint led to the controller undershooting, resulting in a brief period of reduced oxygen supply (<5% DO), which may have contributed to the lactate production. If this proves to be the cause of the lactate rise, improving the transition could reduce the unwanted lactate production. Tuning the PID parameters could reduce the undershoot, however, stability and responsiveness during the remaining process should not be compromised, which could prove difficult. Instead, a gradual reduction in the DO setpoint could be a possible and simple way around this problem without the need for timely PID tuning.

In preliminary experiments, unwanted glutamate production was identified in the original process design. Lack of biotin in the SSL-based cultivation medium was found to be the most probable cause for the occurrence of this side product. To provide suitable cultivation conditions for the biotin-auxotrophic *C. glutamicum*, biotin was added to the medium for all further experiments. No significant amounts of glutamate were produced in any of the batch-phases. In the vast majority of the samples the concentration was below the detection limit. Very low concentrations of glutamate were measured in a small number of samples. In those samples, the concentration did range from 0.12 to 0.15 mmol/L (about 17-25 mg/L), slightly above the lower boundary

of the measuring range (0.1 -10 mmol/L) according to the manufacturer. It has to be mentioned that the samples with glutamate were not within one process but distributed among several cultivations, with no pattern or identifiable trigger for the production. It cannot be ruled out that these low results may have been caused by measurement errors due to the difficult nature of the SSL matrix and the problems it poses for photometric assays. Either ways, it can be concluded that the secretion of glutamate as a by-product was effectively reduced to zero. While no biotin quantification of the provided SSL was feasable, it can be assumed that biotin limitation caused the glutamate production, which was revoked by the supplementation.

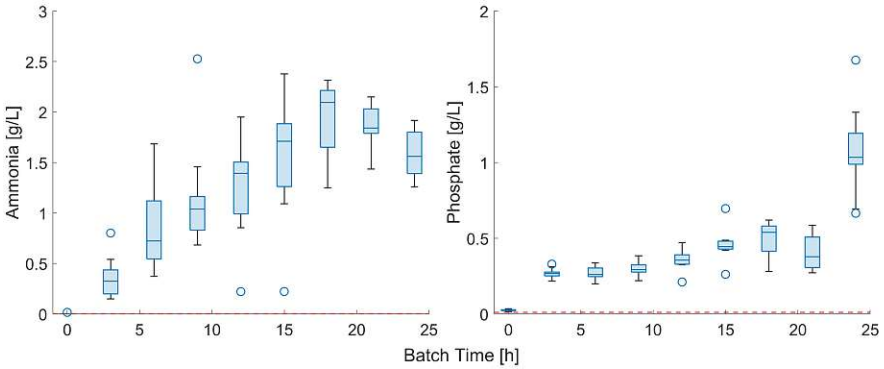

Figure 3.5: Ammonium and phosphate concentrations over the course of the batch phase. The red dashed line represents the LOQ the measurement.

For a successful cultivation nitrogen limitations or even starvation has to be avoided. Since SSL lacks available nitrogen, the required nitrogen was supplied in the form of urea. Despite this, urea was not detected at any sampling time point of any of the processes (data not shown), raising thoughts about possible nitrogen limitations. Additionally to urea, the ammonium concentration was tracked throughout the processes (figure 3.5). In microorganisms capable of utilization of urea as nitrogen source urea is hydrolyzed by urease to ammonia and carbon dioxide [106]. Ammonia is in equilibrium with ammonium, which is then accumulated into the metabolism via the glutamate dehydrogenase pathway [107]. Since urease is a cytosolic enyzme in *C. glutamicum*, the lack of detectable urea suggests the immediate uptake of the provided urea [106, 108]. Under sufficient nitrogen supply the transport of urea into the cell occurs rapidly through passive diffusion in *C. glutamicum* [108, 109]. Similarly, the in the cell released ammonia is able to pass the cell membrane by diffusion [110], which is most likely the cause for the presence of ammonium in the broth. The ammonium concentrations did rise linearly for the first 18 hours and decreased slightly in the remaining batch phase. This is to be expected because the linear feed profile used in the batch causes an oversupply of nitrogen until the exponentially growing biomass has reached an equal or greater nitrogen demand. However, ammonium levels were still above 100 mmol/l at batch end, suggesting that nitrogen limitation was not causing

the biomass drop. Based on this data it can further be concluded that the linear addition of nitrogen is sufficient even with the increased biomass growth compared to the original process.

Figure 3.5 further shows the concentration of soluble phosphate in the cultivation broth during the batch. Providing phosphate to satisfy the phosphorous requirement of the cells is impaired by precipitation issues most likely caused by the high concentration of bivalent ions, mostly calcium, in the SSL. To circumvent this solubility problem, phosphate was fed into the reactor. After an initial increase due to start of the NP feed the phosphate concentration remained relatively stable in all cultivations, with values ranging between 3 - 5 mmol/L. Increased phosphate concentrations with a considerable spread can be observed at 24 hours, at the transition to the fed-batch. This increase can most likely be attributed to the changes associated with the start of the feed. While for most parameters, a short period (below 10 minutes) of changed conditions will not have an immediate impact of the measurement, for phosphate this holds not true. In the course of starting the fed-batch, the pH of the broth is adapted according to the experimental design to values between 6 and 7. The solubility of calcium phosphate salts depends heavily on the pH value, with generally higher solubility at lower pH values [111]. The rise and the high variability of the phosphate concentration in this sample is thereby most likely caused by the adaption and the range of different pH values in the fed-batch.

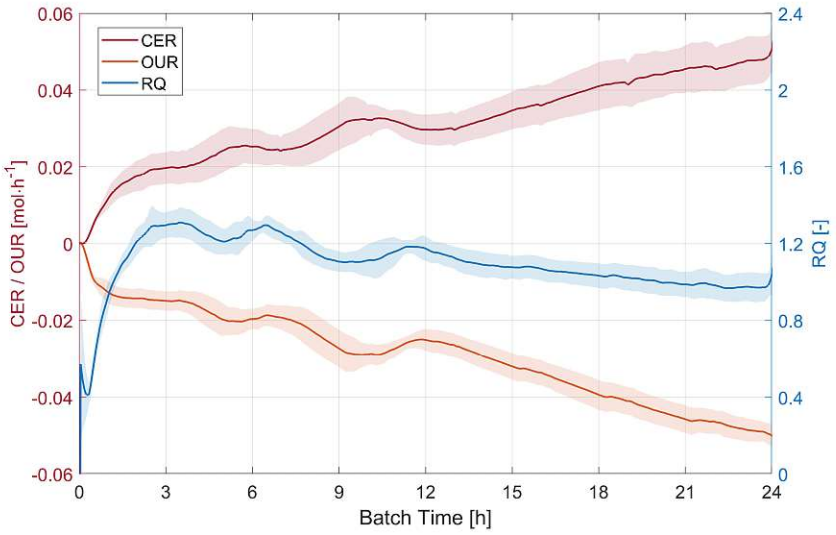

Figure 3.6: Mean respiratory rates and RQ for the batch phase. The areas around the lines represent the standard deviation for the respective signal

In addition to the results obtained through the sample analysis, the concentration of oxygen and carbon dioxide in the off-gas stream was monitored during the process. The

on basis on those online measurements calculated respiratory rates for the batch phase are illustrated in figure 3.6. Process knowledge about the off-gas signals is especially valuable not only for process evaluation or monitoring but also in the view of potential process control strategies. A potential link between the observed biomass drop and the exhaust gas measurements could be employed to reassess the end of batch criterion used as an indicator for the feed start. The off-gas signals had previously been attributed to the utilization of specific substrates during batch optimisation and were later used to identify their depletion in cultivations. The peaks that were attributed to the complete uptake of acetate and glucose in the consequence remained reproducible at 5-6 h and 10-11 h throughout the performed batch phases. This is inline with the substrate concentrations in the broth during the process (figure 3.2). After the drop caused by glucose depletion, the respiratory rates continued to increase until the start of the feed. During this steady rise, small perturbations probably caused by the sampling are visible. In some processes, a decrease in the slope of the exhaust gas signals was recorded at the end of the batch phase, between 20 h and 23 h. However this event did not occur consistent in the performed processes and could not be numerically correlated to the observed loss of biomass. The RQ is calculated from the respiratory rates and gives the ratio of the consumed oxygen and the generated carbon dioxide during the cultivation [112]. Hence the RQ is inherently independent of the biomass concentration but linked to the metabolic state of the cells and it stoichiometrie. Changes in the metabolism of the cells like utilization of different substrates or the formation of side products will lead to an altered reaction stoichiometrie and are therefor reflected in the RQ [113]. In theory, the RQ can be calculated for a given metabolism, however with the complexity due to multiple substrates and inhibitors in SSL this is not feasible for this process. In the performed batch phases, the RQ rises to approximately 1.4 in the first hours of the process and approaches 1.0 from 3 hours onwards. The increased RQ in the beginning is most likely related to the formation of lactic acid and the uptake of acetic acid.

Batch kinetic parameter

The specific uptake rates and the specific growth rate (μ_{max}) were calculated for the batch phases of the performed cultivations (table 3.1). The specific uptake rates were determined for the duration until the respective substrate was completely consumed, while μ_{max} was calculated for the exponential part of the growth.

Table 3.1: Batch kinetic parameters

Parameter	Value	Std dev	unit
$q_{Glc,max}$	0.310	0.046	$g{\cdot}g^{-1}{\cdot}h^{-1}$
$q_{Man,max}$	0.160	0.037	$g{\cdot}g^{-1}{\cdot}h^{-1}$
$q_{Xyl,max}$	0.079	0.018	$g{\cdot}g^{-1}{\cdot}h^{-1}$
$q_{Ace,max}$	0.204	0.063	$g{\cdot}g^{-1}{\cdot}h^{-1}$
μ_{max}	0.118	0.009	$g{\cdot}g^{-1}{\cdot}h^{-1}$

3.1.2 Fed-Batch phase

After the batch phase the feeding was started and the biomass was induced to produce the peptide pediocin PA-1. In the feeding phase the influence of two process parameters, namely the pH and the Carbon-Phosphorous ratio of the feed on the productivity was investigated. The parameters were varied according to a full factorial design to evaluate potential interactions and quadratic effects.

Feed profile evaluation

Overfeeding was a problem in the previous process that led to accumulation of unutilized substrates in the medium and therefore to an inefficient process. In a carbon-limited fed-batch process the growth of the microorganisms is controlled by limiting the supply of substrate entering the reactor. During the fed-batch the substrate concentration is assumed to be zero within the reactor and the with the feed provided substrate is utilized immediately.

In this work the feed rate was controlled by a predetermined exponential feed ramp, resulting in a constant specific growth rate throughout the fed-batch phase. Depending on the biomass concentration at the start of the fed-batch, an initial feed rate is calculated for the desired feed-ramp using physiological parameters (q_x, $Y_{x/s}$). However, with the different substrates and inhibitors present in SSL, as well as competitive substrate inhibition, setting an appropriate feed rate is not a trivial task. Further, the difficult matrix and dark color of SSL require a time and labor intensive biomass quantification, preventing the calculation based on real-time measurements. Therefore, the initial feed rate was to a fixed value for all fed-batches, based on the expected end biomass according to previously performed processes. In the original process, the initial feed rate was set to high, exceeding the substrate uptake capabilities of the cells and resulting in the observed accumulation. In the optimized batch phase, among other things, the biomass concentration achieved was significantly increased, implying changed conditions for the feed start. In the following the substrate and biomass data for the feeding phase of the conducted processes are presented to evaluate the success of the feed profile.

The feed ramp was calculated for a feed duration of 24 hours. However, inaccuracies in the feed preparation (sterile filtering, aliquoting) and dead volumes in the feed line lead to a difference between the expected feed volume the actual available feed volume in some processes. This insufficient feed volume lead to a premature feed stop and a shortened fed-batch phase in those processes. It was therefor decided to cut the last sampling interval from the data as the conditions can not be considered representative for the fed-batch phase.

In Figure 3.7 the substrate concentrations for the fed-batch are illustrated. During the fed-batch the glucose concentration remains constant below the detection limit for all processes. The acetate concentrations decrease slightly in the first hours of the fed-batch and remain at a low level for the rest of the process. However, the

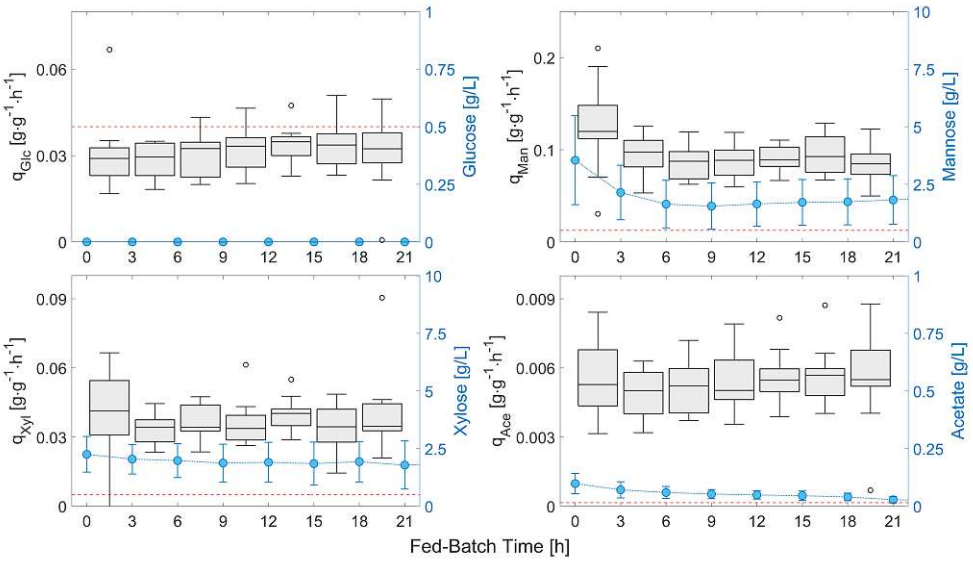

Figure 3.7: Mean substrate concentration with standard deviation over the duration of the feed phase. The red dashed line represents the LOQ the measurement. The box plots represent the specific rates for the respective substrate in the sampling interval.

concentrations are close to the lower border of the the measuring range (0.015-2.3 g/L) with values ranging from 0.02 g/L to 0.07 g/L throughout the fed-batch. It has to be mentioned that the dark color and complex matrix of SSL might lead to a greater variance and inflated results for the photometric acetate measurements. In contrast to glucose, xylose and mannose were not depleted in the batch phase. The concentration of xylose in the feed phase is consistent with the residual concentration at the end of the batch (2.5 g/L). As for mannose, the concentration reduces during the initial two sampling intervals and remains stable at a residual concentration of around 2.4 g/L from then on.

Figure 3.7 further shows the specific substrate uptake rates for the sampling intervals. It can be observed that the specific substrate uptake rates are constant for the majority of the fed-batch (27 h - 45 h). The specific uptake rates for xylose and mannose are elevated for the first sampling interval, which is attributed to the utilization of the remaining xylose and mannose from the batch above the residual concentration.

The specific growth rate (q_X / µ) was calculated for each sampling interval in the fed-batch phase and compared to set point of 0.03 g/g/h (figure 3.8). The data suggests that the specific growth rate remains constant throughout the fed-batch phase but below set point. It has to be noted that the values show a significant spread both

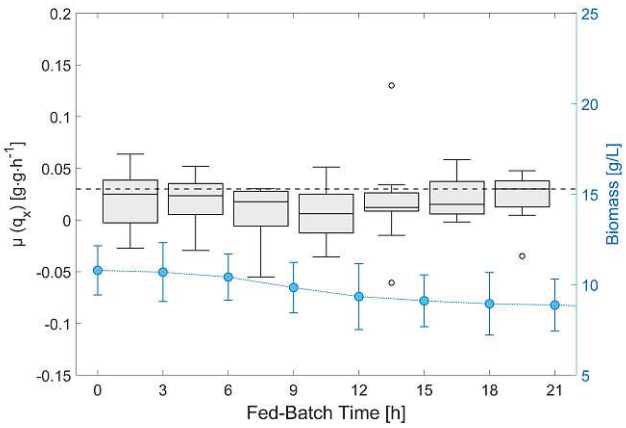

Figure 3.8: Set point (black dashed line) in comparison with the calculated specific growth rate (box plot) throughout the fed-batch. Mean Biomass concentration concentration with standard deviation (blue line)

above and below the set point for most of the time. The low set point and dilution during the fed-batch process result in only minimal changes in biomass concentrations among the individual measurement points. Further, it has to be mentioned that the biomass concentration stays almost constant and decreases slightly due to the dilution, however the total biomass increased over the fed-batch phase. Additionally, the low absolute value of the set point amplifies the impact of measurement inaccuracy on the final result.

While the target growth rate was not reached in most process, it can be considered that the specific growth rate was controlled stable within the fed-batch phase. However, a spread between the mean specific growth rates of the fed-batch phase was observed between the processes. Several parameters influence the process to process variability of the specific growth rate in the fed-batch. One cause of the variability is the variation of the biomass concentration at the start of feeding. As previously noted, the timely measurement of the biomass concentration on SSL is currently not feasible. Therefore, the same initial feeding rate was used in all experiments, regardless of the biomass concentration present at the start of feeding. By improving the reproducibility of the batch phase this source of variability was minimized to ensure comparable conditions in the fed-batch.

During the fed-batch, the pH was varied between 6.0 and 7.0. The pH value of the cultivation medium is known to greatly influence the growth of bacteria. To reject the possibility that the observed variation is caused by the varied fed-batch parameters, the influence of the pH and C:P ratio on μ_{FB} (table 3.2) was analyzed by Multiple linear regression (MLR) and Analysis of Variance (ANOVA). There was no significant influence detected (coefficients: $p = 0.19$ & $p = 0.76$, F-test: $p = 0.38$, LoF: $p = 0.47$), which suggests that growth rate control was effective, despite the different conditions.

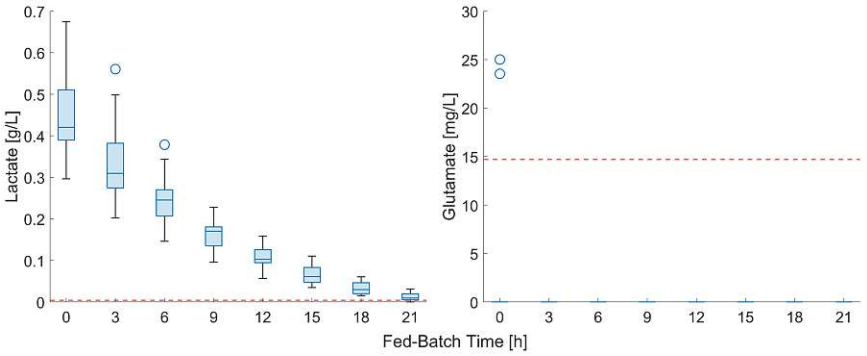

Figure 3.9: Concentration of lactate and glutamate throughout the fed-batch

Lactate and glutamate levels were monitored throughout the fed-batch as they are indicative of unfavourable culture conditions. Figure 3.9 illustrates the lactate and glutamate concentrations throughout the fed-batch. In the fed-batch the DO level was reduced to 15 % in order to reduce peptide oxidation. The transition from batch to fed-batch was accompanied by an increase in lactate concentration. This lactate was utilized throughout the fed-batch and no further lactate build up was observed despite the lowered DO levels. Similar to the batch medium, biotin was added to the feed to prevent potential limitations and the consequent metabolic changes. No glutamate was detected in any of the samples during the fed-batch.

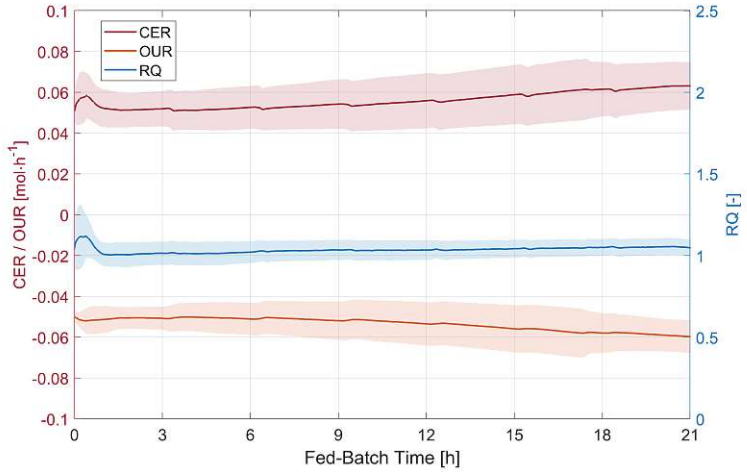

Figure 3.10: Mean respiratory rates and RQ for the fed-batch phases. The areas around the lines represent the standard deviation for the respective signal

The respiratory rates and the RQ for the fed-batch phase are displayed in figure 3.10. Apart from small disturbances caused by the start of the feed, the respiratory rates are increasing steady throughout the fed-batch. The observed slope of the respiratory rates however is very small as expected due to the low feed ramp and the subsequent small growth. The RQ remained constant at approximately 1 in the fed-batch phase indicating a stable metabolism. The shown data further shows the success of the feed control.

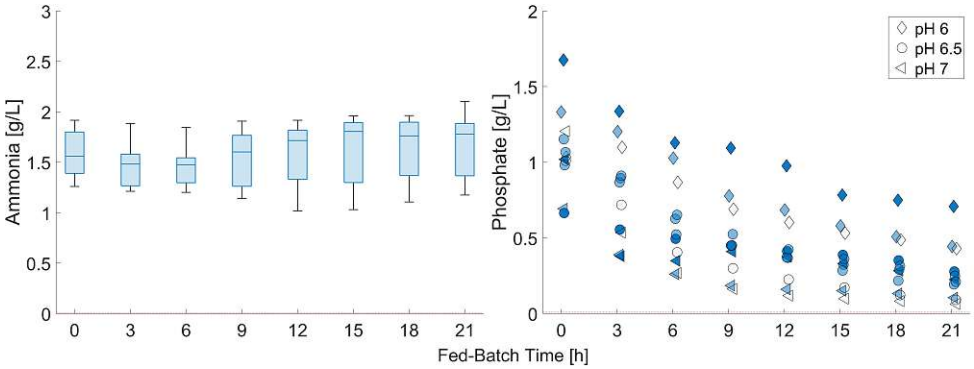

Figure 3.11: Concentration of Ammonium and Phosphate for the fed-batch phases. The red dashed line represents the LOQ of the respective measurement. Phosphate feed ratios (45, 60, 75) are displayd by descending blue-tones.

In contrast to the batch, the NP solution was feed into the reactor according to an exponential feed ramp. The exponent has been set to the same value for both the SSL and NP feed ramps. The ratio of the carbon to phosphorous moles entering the reactor was controlled by adjusting the concentration of phosphate in the NP solution. It was previously found that the nitrogen supply in the fed-batch did not have any effect on the pediocin titers achieved. Consequently, the same urea concentration was used in all experiments. Figure 3.11 shows the ammonium and phosphate concentrations in the fed-batch. Similarly to the batch, no urea was detected in any sample of the fed-batch, suggesting rapid uptake into cells. Ammonia concentrations remained stable at the same level as at the end of the batch throughout the fed-batch phase, indicating that no nitrogen limitation occurred. The phosphate concentration did increase in the transition to the fed-batch and decreased from there on over the course of the feeding phase. As the solubility of phosphate is highly dependent on the pH of the medium [111], distinct levels of phosphate concentration can be observed for the different pH set points in the fed-batch. Additionally, gradations are observable within these levels based on the carbon-to-phosphorous ratio of the feed. However, the decrease in phosphate is similar for all experiments.

Based on the concentration profiles and the stable specific rates (q_{s_i}, q_x) presented it can be stated that no overfeeding of either feeds occurred during the fed-batch. While the specific growth rate was below the set point for a majority of the experiments, the feed control was deemed appropriate. No significant variations between the growth rates in the fed-batch of the different experimental conditions were found, providing comparable conditions for the evaluation of the fed-batch.

Evaluation of the pediocin PA-1 production

The influence of the pH value and C:P ratio on the pediocin production in the fed-batch was evaluated. Pediocin production is generally described to follow primary product kinetics[114, 115, 116, 117], where the production rate is depending on the growth rate. Most of those studies, performed with natural pediocin producers, therefor investigated the production in batch experiments. The only studies focusing on the recombinant production of pediocin in *C. glutamicum* to this day, also utilized batch cultivations for pediocin production[53, 72].

In the original process described by Kitzmüller, the basis for this work, pediocin production in the fed-batch was investigated and product formation was observed to be mostly growth independent. As described earlier, the specific growth rate in the fed-batch was controlled constant with an exponential feed ramp and a set point of 0.03 h^{-1}. It was shown that the specific growth rate was stable throughout the fed-batch. The actual specific growth rate was calculated to be even below the set point in the most processes. The extremely low value and the absence of significant differences in μ_{FB} between the experimental groups indicate that the differences in pediocin production observed subsequently are likely to be caused by growth-independent production differences.

The original process relied on a semi-quantitative critical dilution assay for the determination of the antimicrobial activity. This simple method defines the activity of a sample through the dilution factor in a two-fold dilution series that is needed to reduce the OD_{600} below 50 % of that of an untreated culture. Consequently, the resolution of the activity measurements is limited to steps resulting from the two-fold dilutions. In order to improve the resolution, a dosage-response curve fit was implemented for the evaluation of the assay. The dosage-response curve was fitted to the growth inhibition data obtained in a similarly way as in the critical dilution assay. However, the activity is calculated from the infection point of the resulting curve. This allows activity to be measured on a continuous scale with no intervals, ultimately increasing the resolution of the assay. In the original process the antimicrobial activity of the samples was converted to a concentration by comparing the activity with that of a commercial pediocin PA-1 standard. The evaluation of the experimental design was then carried out using this pediocin concentration. In contrast to the previous process, a drop in the antimicrobial activity of more than 80 % was observed in some experiments of this work. It is highly improbable that the pediocin was degraded extracellular at the rate

and extent observed, given the low extracellular protease activity known to exist in *C. glutamicum*[118]. Furthermore, pediocin exhibits remarkable stability across a wide pH range of 2 to 10[119]. The most likely reason for the observed decrease in activity is oxidation, since pediocin is known to be to sensitive to oxidation[120]. Efforts to establish a HPLC method for quantification of the pediocin concentration in addition to the activity assay were not successful to this day due to the difficulties associated with SSL matrix. Since it is not possible to distinguish between active or oxidised peptide, converting the activity into a concentration based on fixed specific activity appears inadequate. Consequently, the evaluation was carried out based on the antimicrobial activity.

Table 3.2: Summary of the factors and responses for performed fed-batch experiments

Exp. No	pH	C:P ratio	max. Activity [BU/ml]	μ_{FB} [g/g/h]
1	7	45	9639	0.0112
2	6.5	60	18955	0.0144
3	6.5	60	28815	0.0247
4	6	45	53933	0.0126
5	7	75	7329	0.0340
6	6	75	17751	0.0052
7	7	60	17277	0.0204
8	6.5	45	10258	0.0283
9	6	60	52757	0.0180
10	6.5	60	31470	0.0105
11	6.5	75	3547	0.0194

The antimicrobial activity in the supernatant of the samples was measured throughout the fed-batch. Major differences in the maximum as well as the course of the activity were observed in the performed experiments. In the first hours of the process the activity increases with the slope of the rise greatly varying. A number of processes showed a significant increase in activity in the initial hours, followed by a subsequent steep decrease. In contrast, for some processes the activity increased slowly or remained consistent after an initial rise throughout the fed-batch phase. In order to address the sharp peaks in the activity, it was determined that the assessment would be based on the highest activity during the fed-batch phase rather than the average activity. Therefore, the maximum antimicrobial activity achieved was selected as the response for the evaluation of the experimental design (table 3.2).

A linear regression model was fitted to the data using MLR to estimate the effects of the pH and the C:P-ratio on the maximal achieved activity. For the evaluation, both main effects and quadratic effects as well as interactions of the factors were considered (equation 3.1).

$$Y = \beta_0 + \beta_{C/P} \cdot X_{C/P} + \beta_{pH} \cdot X_{pH} + \beta_{C/P^2} \cdot X_{C/P^2} + \beta_{pH^2} \cdot X_{pH^2} + \beta_{C/P \cdot pH} \cdot X_{C/P \cdot pH} + \epsilon \tag{3.1}$$

All analysis were conducted at a significance level of 0.05. To eliminate the influence of the varying magnitudes of the factors on the coefficients, the factors were orthogonally scaled. No transformation was performed on the independent variables.

For the chosen significance level all coefficients were found significant, consequently no terms were omitted from the model (Figure 3.12, bottom left). Several metrics were calculated to assess the validity and quality of the obtained model (Table 3.3). ANOVA was used to analyze the goodness-of-fit of the regression as well as detect a possible lack of fit. No lack of fit was detected in the presented model (p = 0.62). Further, the p Value of the regression model (0.005) is below the significance level, meaning that the coefficients deviate significant from 0. The coefficient of determination (R2) for an acceptable model should be at least 0.5. For the fitted model shows a R2 of 0.94 which indicates that the model is able to explain the majority of the observed variance of the response. The predictive power of the MLR is characterized by Q2. Generally, a higher Q2 should result in less prediction error. For a valid model Q2 should be above 0.1. The Q2 of 0.64 suggests that the obtained model will generalize well and should have a relative small prediction error on new unseen samples. The validity of the model is calculated from the lack-of-fit metric and should exceed 0.25. The high validity metric (0.8790) of the MLR model indicates that the chosen terms are adequate to fit the data. The reproducibility of the experiments is estimated from the variation of the replicates (center point) compared to the overall variation.

Table 3.3: Summary of the MLR model and anlysis

Model summary			
	Number of observations	11	
	Coefficients	6	
	Degrees of freedom	5	
Model analysis			Threshold
ANOVA	p Model	0.0047	<0.05
	p Lack of Fit	0.6168	>0.05
Summary of fit	R2	0.9387	>0.5
	Q2	0.6385	>0.1
	Validity	0.8790	>0.25
	Reproducibility	0.8553	>0.5

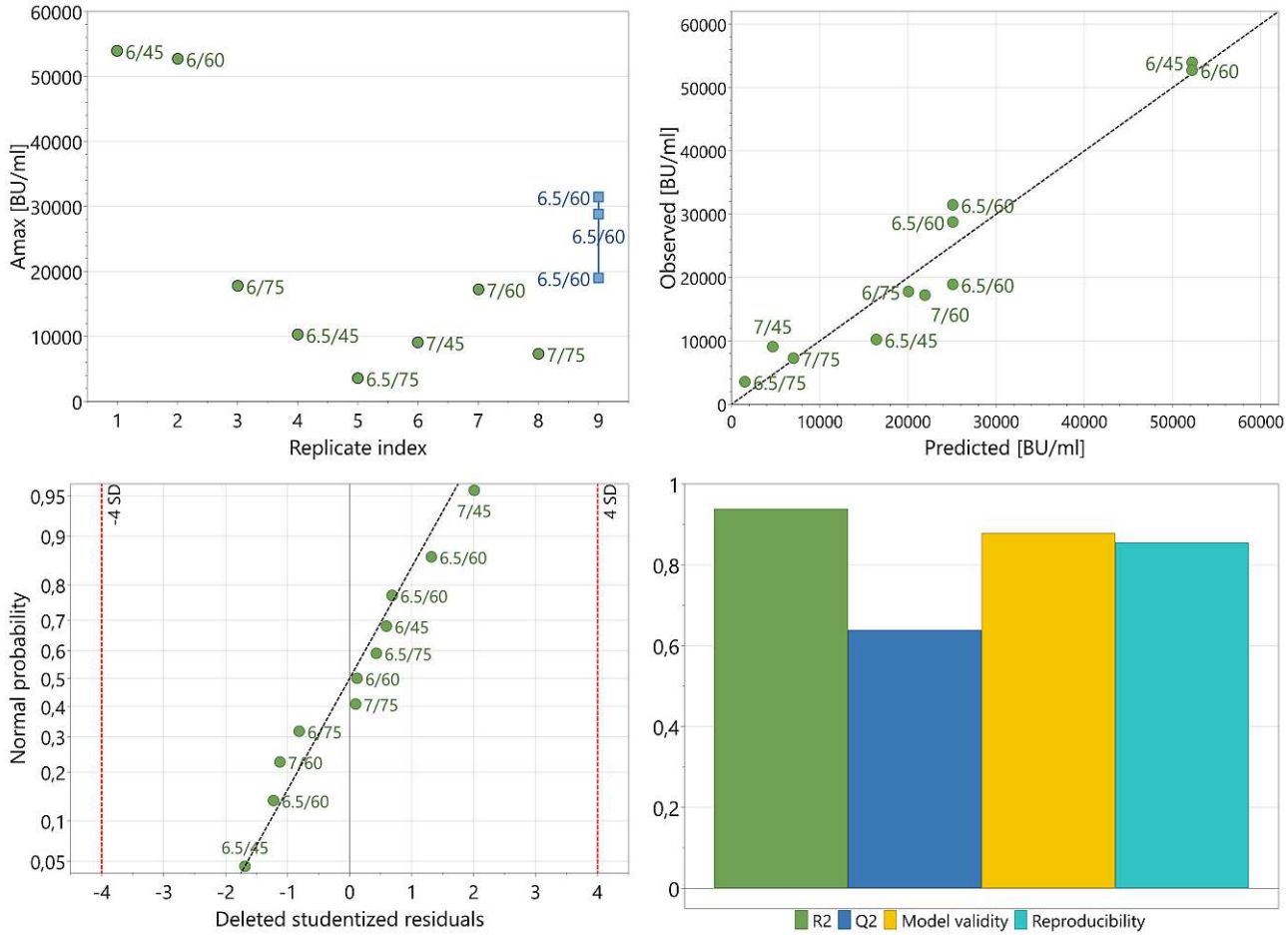

Figure 3.12: Response values for each experiment, replicates are marked as rectangle (Top, Right). Normal probability plot for the deleted studenized residuals (Bottom, Right). Coefficients of the MLR and their corresponding uncertainty range (Bottom, Left). Summary of the fitted linear regression model (Top, Left).

Further, the residuals of the regression were examined as part of the analysis. For this reason the deleted studenized residuals were calculated. One of the assumptions that must to be met for a multiple linear regression is the normal distribution of the error terms. To check for this assumption, the residuals were plotted against their normal probability (figure 3.12, top right). The dashed line in the plot represents the theoretical location of perfectly normally distributed residuals. The residuals show no signs of skewness or tailed course, indicating that they follow a normal distribution. The residuals can further be used to detect potential outliers. Outliers are characterised by a considerable deviation from the standard distribution line and a larger absolute deleted studenized residual value. Since all residuals fall within the outlier threshold (red dashed lines) and can be considered normally distributed it is likely that no outliers are present.

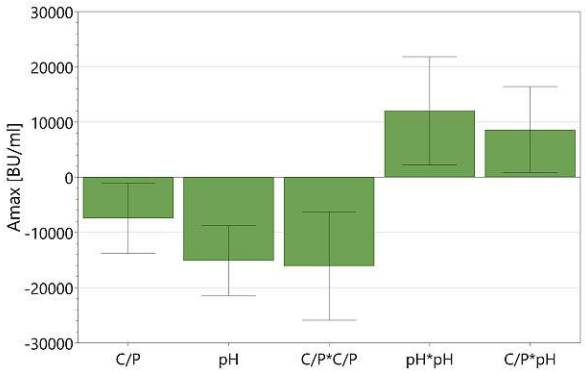

Figure 3.13: Observed vs. Predicted max. antimicrobial activity for the experiments

Based on the analysis of the MLR, it can be summarised that a valid and significant fit was obtained involving first order and second order terms for the pH value and C/P-ratio and their interaction (first order). The coefficients of the regression (figure 3.12, lower left) make it possible to draw conclusions about the influence of these parameters on the maximum antimicrobial activity that can be achieved in the fed-batch. For the main effects of the pH value and C/P-ratio, negative coefficients were obtained, indicating that a lower pH value and less phosphate is generally favorable for a high activity. While both parameters show a significant effect, the absolute value of coefficient shows that the activity is primary influenced by the pH value of the fed-batch. Already in the previous investigation carried out by Kitzmüller, a quadratic effect of the C/P-ratio was detected but was confounded due to the lack of face centered points in the DoE. This observation was confirmed and quantified by the experiments of this work with the quadratic coefficient exceeding that of the primary effect of the C/P-ratio. Similarly, the pH value showed quadratic effects on the activity. Since both the C/P-ratio and the pH-value influence the phosphate concentration, it comes to no surprise that an interaction of those factors was detected.

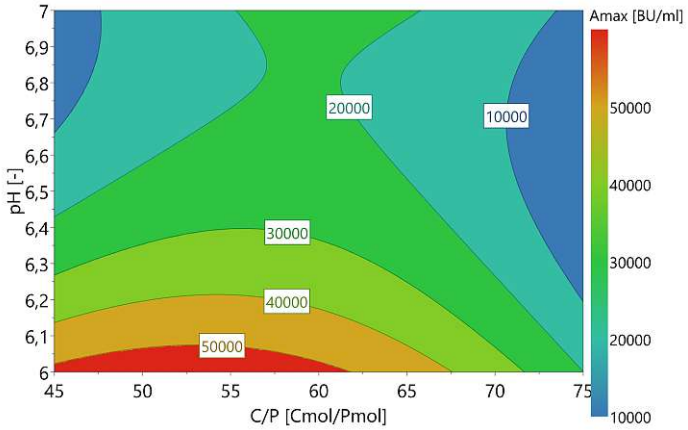

Figure 3.14: Surface plot of the MLR model within the design space

Figure 3.14 illustrates a surface plot of the expected maximum antimicrobial of a fed-batch based on the MLR. The highest activity was observed at the edge of the design space at a fed-batch pH of 6. Thereby it is possible that the optimum for the pH value lies outside of the tested range and lowering the pH below 6 will yield higher activities. However, the reported minimal pH value for *C. glutamicum* is 5.5, below that point the cell is no longer able to maintain the pH homeostasis [121, 122]. Consequently extending the design space to this or even beyond this limit is unlikely to benefit the productivity. Further, a decrease beyond pH 6, the limit for exponential growth, may pose a risk for the envisioned repetitive fed-batch. Cell stress and subsequent adaptions to the lowered pH can cause a lag phase when the cells are confronted with the changed conditions in the batch phase of the next repetition. While this may be the case for processes with pH 6, the probability for an extended lag phase increases significant by lowering the pH below the physiological limits of *C. glutamicum* [123].

The carbon-phosphorous-ratio in the fed-batch shows a significant quadratic effect on the maximum pediocin activity. As the C/P ratio increases and the available phosphate reduces, the resulting activity demonstrates an increase up to a certain threshold, beyond which the activity subsequently decreases. Interactions between the pH value of the medium and the phosphate concentration have already been stated earlier when discussing the phosphate concentration in the fed-batch. It comes thereby to no surprise that the optimal C/P-ratio was found to be dependent on the pH value of the fed-batch phase For pH 6 the optimal ratio was determined to be between 50 and 55. It should be noted that, while the activity assay's resolution has been significantly improved, the results are still subject to considerable biological variability due to the nature of the assay. However, as there are no analytical methods available to quantify the pediocin concentration and determine the ratio of active and oxidised peptide, the activity assay remains the only feasible means of assessing the fed-batch.

3.2 Mechanistic Model Formulation

The collected data was further utilized to set up a mechanistic model of the presented fed-batch process. The data were produced by a range of offline and online measurements, wherein each is influenced by measurement errors. The use of SSL, with its multiple substrates and inhibitors, adds further complexity and uncertainty compared to processes using defined media based on a single carbon source. Therefore, it is crucial to assess the quality and consistency of the data before using it to develop and parameterise a model. Accordingly, the first step was to check the consistency of the data by establishing elemental balances.

3.2.1 Elemental Balances

Elemental Balances for the bioreactor were established based on the reaction equation (equation 2.8). Balances were set up for the elements carbon, nitrogen and phosphorous as well as for electrons based on the degree of reduction (DoR). According to the law of conservation of mass, mass can not be destroyed or created. This rule also applies to the bioreactor and the cells with their complex metabolic reactions. For the balancing, the metabolism of the cells is simplified to the net exchange of the cells and the medium. On the assumption that the reaction equation is an adequate description of the system, then the balance ratio for the corresponding balance should equal to 1. Measurement errors of the different measurements included in the balance and compounds that are not accounted for will lead to deviances from this value. The balances can thereby be used to check the consistency of the data. Table 3.4 shows the individual measurements and the total number of measurement that are considered for each balance and are consequently checked by the respective balances.

Table 3.4: Considered measurements for each balance

Balance	**Nr. of Measurements**	**Measuruments**
C	8	X, Glc, Man, Xyl, Ace, CO_2, Lac, Glu
N	4	X, Urea, NH_3, Glu
P	3	X, PO_4, (Cell weight)
DoR	8	X, Glc, Man, Xyl, Ace, O_2, Lac, Glu

Figure 3.15 shows box plots of the balance ratios for each balance of the eleven fed-batches. In consideration of the complexity of the SSL matrix and the amount of different substances and consequently measurements, an acceptance criterion of 10 % was set.

It can be observed that the carbon balance is within the set borders for the majority of the batch phase. For the first samples, the ratios are distributed approximately around 1 with minimum variance. After 12 hours, the ratio drifted slightly towards the lower limit of the acceptance criteria. Nevertheless, the carbon balance remains within the limits until the start of feeding at 24 hours. For the fed-batch, the balance

ratio suggests a constant underestimation of the measured carbon. Similar to the carbon ratio, the DoR balance can be deemed acceptable in the batch but remains below the threshold for the entirety of the fed-batch phase. For both carbon and DoR the balance shows a constant gap after 24 hours and no further drift from the theoretical value, indicating that a singular event caused this.

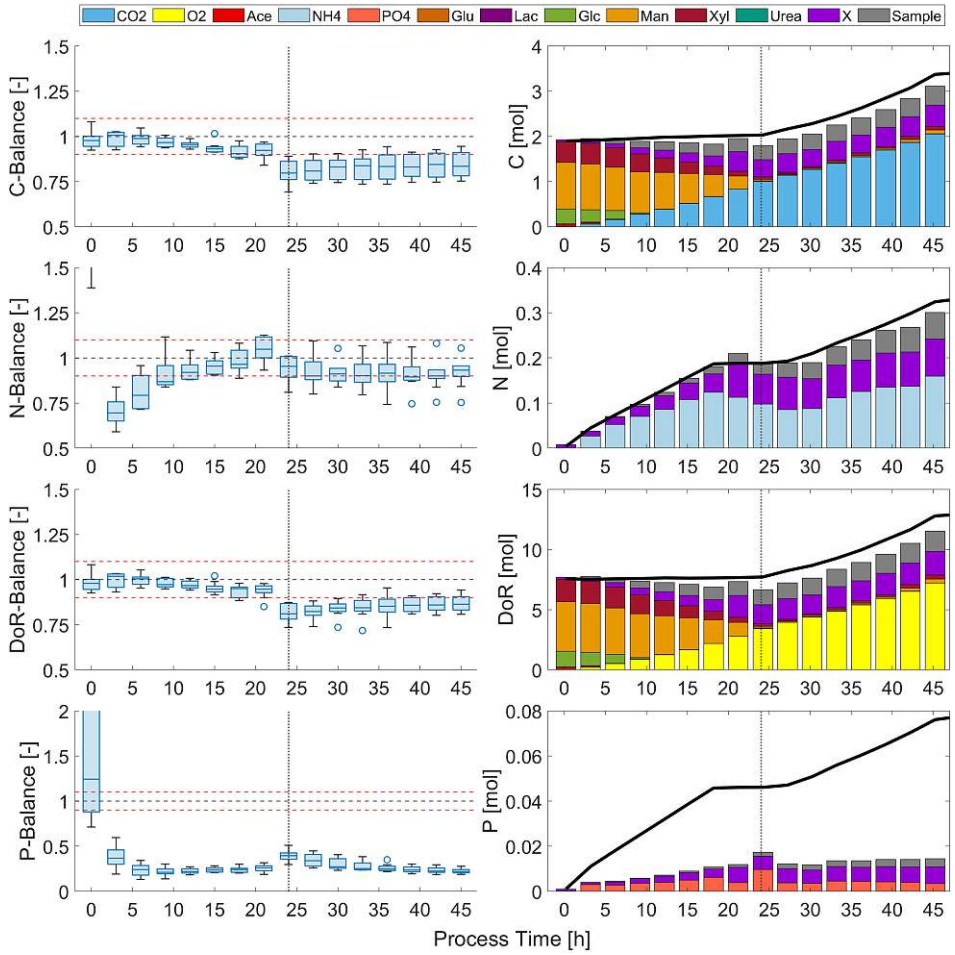

Figure 3.15: Graphical summary of the elemantal and DoR balances. Left: Boxplots of the balance ratio. The dashed grey line represents a perfectly closed balance ($r_{balance} = 1$). The dashed red lines show the 10% acceptance interval. Right: Example of the balances for a single process.

It has to be noted that due to the lack of quantification methods, the produced and secreted pediocin PA-1 is not included in the balance. Even though the antimicrobial activity of the samples can be used to evaluate the success of a process and compare

processes among each other, it can not reliably quantify the peptide concentration. Depending on the achieved product concentration in a fed-batch, a small disparity in the balance ratio caused by this simplification is thereby expected. It is further very likely that the previously mentioned decrease of biomass concentration at the end of the batch, is the most contributing factor to the gap in the C- and DoR-balance.

Significant differences in the nitrogen balance can be observed in the first hours of the process. The first sample exhibits a spread in the nitrogen balance ratio between 1.4 and 17 (not shown). This is cause by inaccuracies in the control of the NP feed rate at the start of the process combined with the very low total amount of total nitrogen present at that point. In the following samples the balance indicates a slight underestimation of nitrogen. However the nitrogen balance approaches the acceptance limit and stays within the acceptance criterion after 9 hours. In the fed-batch the nitrogen balance ratio decreases slightly and is distributed narrowly around the 90% line. The previously discussed decline in biomass concentration towards the end of the batch is most likely contributing to the decreased balance ratios in the fed-batch.

The ratio of the P-balance is constantly too high throughout the process. In the previous process a high underestimation of the phosphate was observed and attributed to precipitation of calcium phosphate. Therefor a precipitation term, defined as the difference between the total dry weight and the biomass of a sample, was included in the P-balance. In similar fashion the weight of the precipitate was determined in this work and included in the balance under the assumption that the precipitate is composed only of tricalcium phosphate ($Ca_3(PO_4)_2$, TCP). However with the precipitate included under that assumption, the P-balance is significantly overestimating the amount of phosphorous in the reactor for the whole process. Calculating the balance without a precipitate term resulted in median balance ratios between 0.17 and 0.36. In a next step, the assumption that the precipitate is composed solely of TCP was questioned. Calcium phosphate precipitation is a complex process, the precipitated species and amount depends heavily on the pH value[124], the Ca-P ratio[125], the temperature[126] and factors such as the occurrence of other ions[127] and organic ligands[128]. Several different calcium phosphate forms are obtainable at neutral to slightly acidic pH values and low temperatures (approx. 30 °C), including but not limited to octacalcium phosphate (OCP, $Ca_8H_2(PO_4)_6{\cdot}5H_2O$), Hydroxyapatite (HA, $Ca_{10}(PO_4)_6(OH)_2$) or dicalcium phosphate dihydrate (DCPD, $CaHPO_4{\cdot}H_2O$)[129, 124]. The literature reports that the direct precipitation of TCP from aquaeous solution is not possible and TCP is only achieved after treatment of the precipitate with high temperature[130, 131, 132]. To further complicate the matter, it is possible that mixtures of different calcium phosphates precipitate or the phases change[129] during the process or the drying of the samples. With different pH values in the fed-batch, various levels of phosphate concentration, and the presence of additional cations and organic compounds in SSL, it is challenging to predict the type of precipitate without conducting a thorough analysis. Several efforts were taken to improve the analytic for the precipitate and thereby the P-balance. Efforts to separate the precipitate and the cells quantitatively re-

mained unsuccessful for the duration of this thesis. Phosphate quantification using ion chromatography after dissolving the precipitate (including cells) in concentrated hydrochloric acid did not yield any improvements. Additional sample preparation steps, e.g. washing the pellet with ultra pure water or diluted acids or dissolving the cells with organic solvents, did also not result in a plausible balance. It was not possible to determine the phosphate content of the precipitate with the analytical instrumentation available during this thesis. Consequently, the precipitate term was removed from the balance.

Based on the balances, possible inconsistencies in the data were detected, especially in the fed-batch. The carbon and DoR balance are particularly important for a potential model as they include the substrates along with the biomass and overflow metabolites. The gap in the C- and DoR-balance are most likely caused by the fact that cell death and the produced pediocin were not considered. Additionally, the DoR- and C-balance are subject to highest number of individual measurements and consequently measurement errors. In contrast, only the ammonium concentration and the biomass have a significant contribution to the nitrogen balance. The nitrogen balance is within the acceptance limits for the majority of the process. However, it is greatly affected by the low amount of nitrogen in the first hours of the process. For the P-balance a significant disparity was observed. As it was not feasible to determine the majority of phosphorus within the system, it was concluded that the phosphate values would not be incorporated into the model. For a potential model of the pediocin production, the total carbon to phosphorous ratio of the fed-batch was used as a workaround instead.

3.2.2 Modeling of *C. glutamicum* growth on SSL

The modeling conducted for this thesis was split into two major parts: modeling of the substrate uptake and growth on SSL and the modeling of pediocin production. Formulation of the models was based on the previously presented experimental data as well as extensive literature research. For readability and convenience, the substrates were abbreviated as S_1 - S_4 (glucose, mannose, xylose, acetate) and biomass as X.

Batch growth

The model building was started by modeling the substrate uptake and biomass formation in the batch phase. This batch model was subsequently extended to the fed-batch and the product formation. For modeling of the growth on SSL, especially the work of P. Sinner et. al. [75, 133] was used as basis for establishing the equation system. The substrate utilization was described using monod kinetic equation, with the half affinity constant (K_{Si}) and the maximum specific uptake rate for each substrate ($q_{Si,max}$) as parameters. In the process evaluation it was shown that the utilization of acetate and glucose started immediately. The uptake of xylose and mannose was inhibited by the presence of glucose in the initial hours of the cultivation. Consequently, a competitive inhibition term was included for the uptake equation of xylose and mannose. It is

Table 3.5: Equations for the substrate utilization of the batch models

state	model 1		model 2	
S_1	$q_{S_1} = q_{S_1,max} \cdot \frac{S_1}{S_1 + K_{S_1}}$	(3.2)	$q_{S_1} = q_{S_1,max} \cdot \frac{S_1}{S_1 + K_{S_1}} \cdot \left(1 - \frac{S_4}{S_{4,max}}\right)$	(3.3)
S_2	$q_{S_2} = q_{S_2,max} \cdot \frac{S_2}{S_2 + \frac{K_{S_2}}{K_{S_1}} S_1 + K_{S_2}}$	(3.4)		
S_3	$q_{S_3} = q_{S_3,max} \cdot \frac{S_3}{S_3 + \frac{K_{S_3}}{K_{S_1}} S_1 + K_{S_3}}$	(3.5)		
S_4	$q_{S_4} = q_{S_4,max} \cdot \frac{S_4}{S_4 + K_{S_4}}$	(3.6)	$q_{S_4} = q_{S_4,max} \cdot \frac{S_4}{S_4 + K_{S_4}} \cdot \left(1 - \frac{S_1}{S_{1,max}}\right)$	(3.7)

reported that glucose/acetate mixtures result in decreased utilization rates in *C. glutamicum* for both substrates compared to growth on the each alone. Therefor, a second model was proposed that considers the mutual inhibition of glucose and acetate. Accordingly, inhibition terms were introduced to the equation for glucose and acetate. The inhibition was adapted from luong's equation, a generalization of the monod kinetic with substrate inhibition [134]. In variation of luong, the inhibition from acetate was applied to the substrate uptake of glucose and vice a versa. The addition of the inhibition terms increased the number of parameters by two: the maximum concentrations of acetate and glucose that allow growth ($S_{1,max}$, $S_{4,max}$). These parameters proofed to be unidentifiable with the data obtained from the experiments. Instead they were approximated from the literature: Khan et. al. [135] determined that the maximum glucose concentration for growth of *C. glutamicum* is between 300 - 350 g/L while Kiefer et. al. [136] reported that *C. glutamicum* tolerates acetate concentration beyond 60 g/L in batch cultivations. Therefore, $S_{1,max}$ and $S_{4,max}$ were set as constants to 320 g/L and 70 g/L, respectively.

The growth was modelled as the sum of the four specific substrate uptake rates and their corresponding biomass yield coefficients.

$$\mu = \sum_{i=1}^{4} q_{Si} \cdot Y_{X/Si} \tag{3.8}$$

As described in section 3.1.1, a drop in the biomass concentration at the end of the batch was observed in most of the performed processes. However, it was not possible to establish a mechanistic link between this decrease and any of the measured

substrates or metabolites. For the possibility to include a cell death term into the model, the efforts to find a potential connection were intensified and the biomass data and specific growth rate were correlated with all available process data and variations thereof (quadratic, logarithmic, inverse). Despite this, no mathematical relationship was found to describe the decline in biomass concentration. There is the possibility that metabolites or inhibitors that were not measured in the processes were responsible for this event. Further, it is possible that the sampling rate (3 hours) was not high enough to detect a potential cause for the biomass decrease. Either way, without a mathematical link, it was not possible to include a plausible cell death term to the batch model. Therefore, the period between 21 and 24 hours was not used for the parameter estimation and subsequent evaluation of the batch models.

Table 3.6: Model parameters for both batch models

Parameter	**Value**		**Unit**
	model 1	model 2	
$q_{S_1,max}$	0.290	0.288	$g{\cdot}g^{-1}{\cdot}h^{-1}$
$q_{S_2,max}$	0.138	0.130	$g{\cdot}g^{-1}{\cdot}h^{-1}$
$q_{S_3,max}$	0.097	0.089	$g{\cdot}g^{-1}{\cdot}h^{-1}$
$q_{S_4,max}$	0.200	0.200	$g{\cdot}g^{-1}{\cdot}h^{-1}$
K_{S_1}	0.060	0.060	$g{\cdot}L^{-1}$
K_{S_2}	0.228	0.207	$g{\cdot}L^{-1}$
K_{S_3}	0.452	0.714	$g{\cdot}L^{-1}$
K_{S_4}	0.010	0.010	$g{\cdot}L^{-1}$
Y_{X/S_1}	0.327	0.413	$g{\cdot}g^{-1}$
Y_{X/S_2}	0.410	0.443	$g{\cdot}g^{-1}$
Y_{X/S_3}	0.351	0.268	$g{\cdot}g^{-1}$
Y_{X/S_4}	0.038	0.038	$g{\cdot}g^{-1}$
$K_{S_1,max}$	-	320	$g{\cdot}L^{-1}$
$K_{S_4,max}$	-	70	$g{\cdot}L^{-1}$

The parameters obtained are shown in table 3.6. Both models yielded, except for a few cases, very similar parameters . This is especially true for the maximum substrate uptake rates. Furthermore, the obtained values agree well with the experimentally determined substrate uptake rates, which further indicates that the model accurately described the underlying kinetics. Contrary to expectations, the yield coefficient for glucose is lower than that for xylose and mannose. This may be attributed to the detoxification of the inhibitors present in SSL in the beginning of the batch phase reducing the biomass yield, which coincides with the time period of glucose and acetate uptake. Consequently, the biomass yield for glucose and acetate is reduced in contrast to the yield on the sugars that are utilized later on in the batch (xylose, mannose), when no more detoxification burden is present.

A comparison of the RMSE and NRMSE for the prediction of all states and both batch models is shown in table 3.7. In figure 3.16 and 3.17 the predicted values for each sample time point of all process are ploted against the observed experimental data. Based on the NRMSE below 10 % for all substrates, it can be stated that both models are able to accurately predict the substrate concentration in the batch phase. The sugar concentrations showed a narrow spread around the diagonal line that represents a theoretical perfect prediction, indicating that no outliers are present and both models describes the substrate uptake adequately. Towards lower concentration the spread increases slightly due to increased variation in the experimental data between the processes. For acetate a slight underprediction can be observed at concentrations around 1 g/L. The estimation of the parameters for acetate struggled from the small sample size relevant for acetate (sample 1 - 3). Further, the acetate concentration (2 g/L) is low in comparison to the other substrates (10 - 30 g/L). Due to those reasons, the sensitivity of the acetate related parameters as well as the parameter importance in the model is reduced. Thereby, the estimation of the acetate parameters probably yielded less accurate parameters compared to the parameters relevant to the sugar utilization. Nevertheless, the model delivered acceptable predictions for the acetate concentrations in the cultivation. The biomass shows the highest error of the model states with a NRMSE of 15.8 and 13.3 %, respectively for model 1 and 2. In the observed vs. predicted plots the biomass further exhibits a higher spread at higher biomass concentrations. This is partly attributed to the batch-to-batch variation observed in the biomass concentration especially in the end of the batch phase. The biomass state (X) in the model is composed of the individual predicted sugar uptake rates and the corresponding yields. Consequently, the predicted biomass is subject to the errors of the prediction in the substrates and thereby expected to show higher errors. A slight overprediction of the biomass is apparent in both models in concentrations below 10 g/L, although to a lesser extend in model 2.

Table 3.7: RMSE/NMRSE with standard deviation for all states of the batch models

	RMSE [g/L]		**NMRSE [%]**	
	model 1	model 2	model 1	model 2
X	1.56 ± 0.64	1.41 ± 0.58	15.78 ± 9.24	13.34 ± 5.58
S_1	0.44 ± 0.07	0.46 ± 0.16	4.8 ± 0.72	5.06 ± 1.78
S_2	1.23 ± 0.56	1.25 ± 0.46	7.39 ± 4.19	7.35 ± 3.12
S_3	0.52 ± 0.22	0.63 ± 0.22	5.91 ± 2.64	7.09 ± 2.44
S_4	0.09 ± 0.05	0.07 ± 0.05	5.49 ± 3.78	4.72 ± 3.32

It can be summarised that both models accurately predicted the substrate concentrations in the batch phase with NRMSE below 10 %. With NMRSE of around 15 % the predictions for the biomass concentration are above the desired accuracy limit of 10 %. Additionally it has to be considered that the last 3 hours of the batch were not included in the evaluation due to the lack of a cell death term. Thereby the biomass

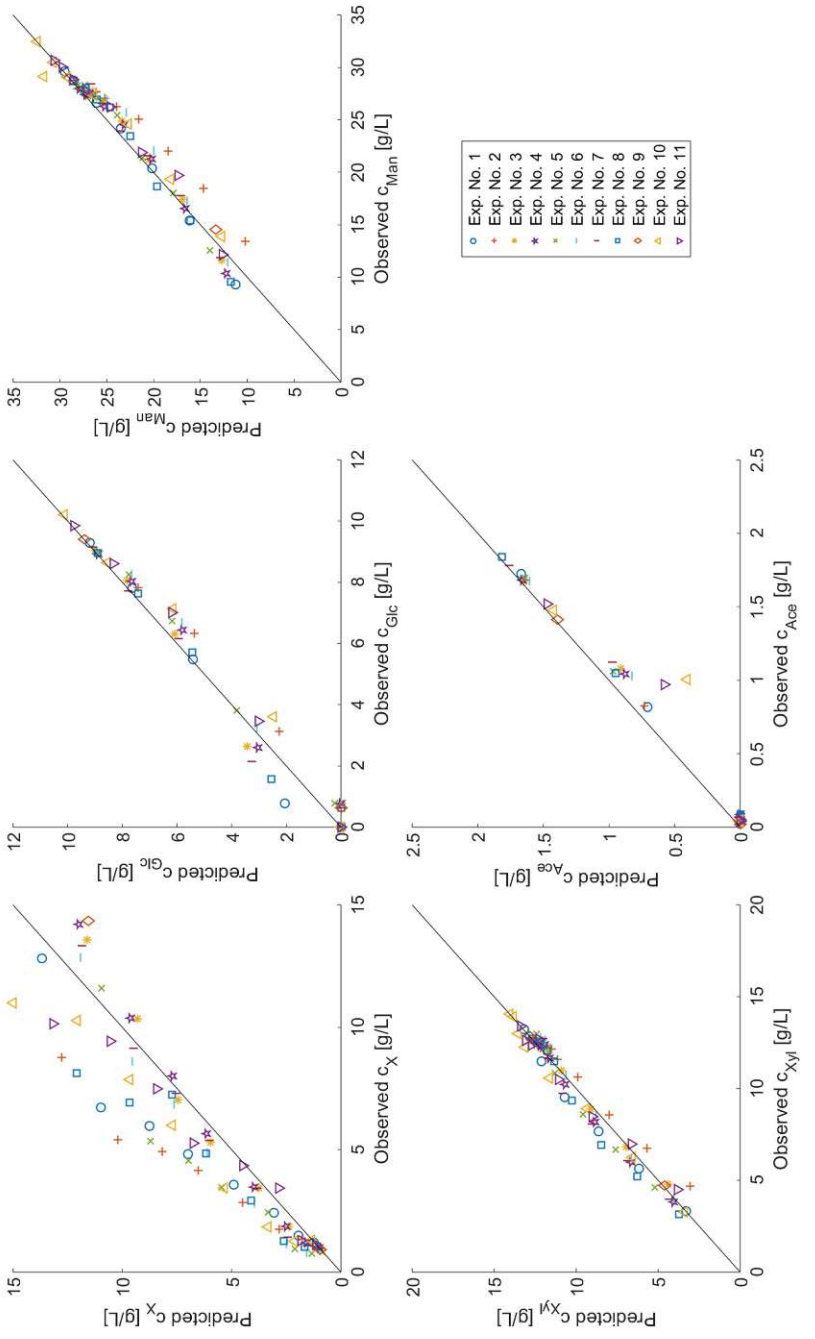

Figure 3.16: Observed vs. predicted plot for each state of the batch model 1. The diagonal line represent observed = predicted.

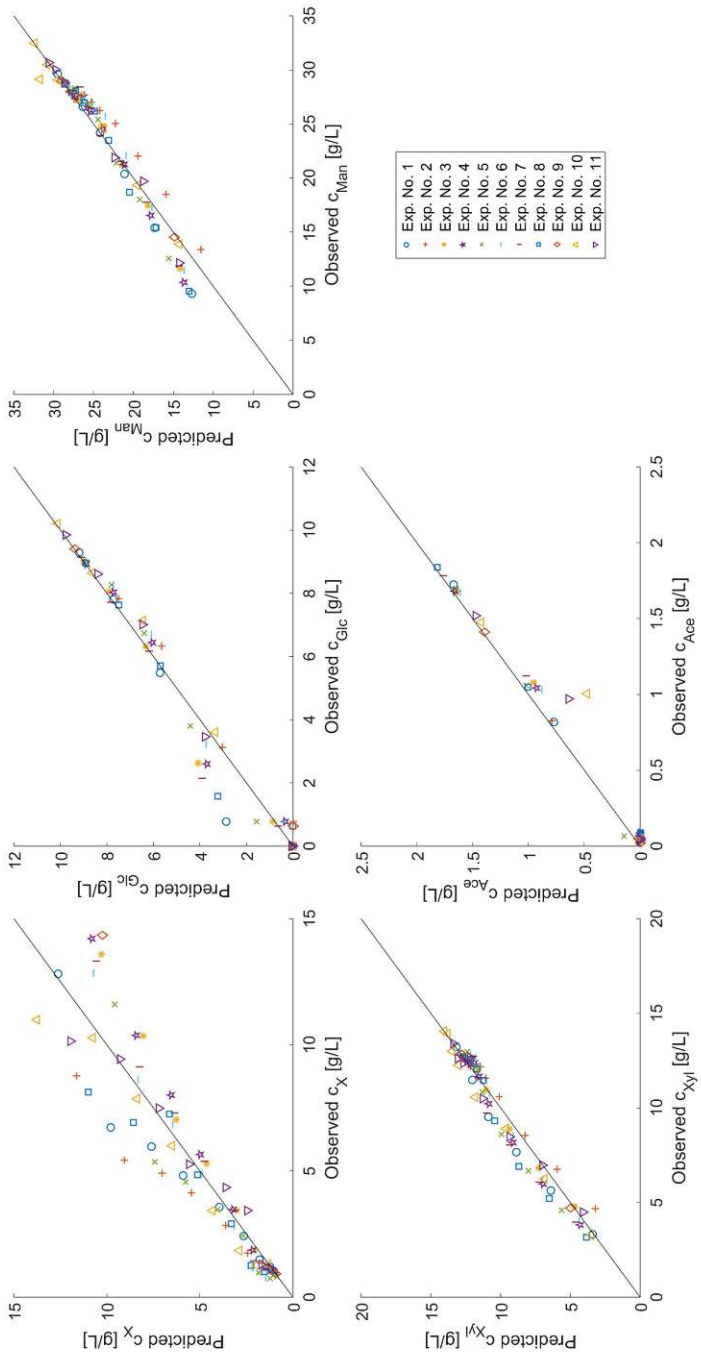

Figure 3.17: Observed vs. predicted plot for each state of the batch model 2. The diagonal line represent observed = predicted.

concentration at the end of the batch can not be predicted accurately independent from the RMSE obtained by the models. However to include a cell death term and possibly improve the biomass state in the batch model, further investigations of the cause of the decline in biomass are needed. With regard to the two models no significant difference was found. Model 2 exhibited slightly better predictions of the states biomass and acetates, while displaying larger errors for the xylose concentration. However, the differences are generally negligible, especially considering the process variability and analysis accuracy. This is most likely attributed to the fact that the mutual inhibition term of glucose and acetate only affects a very short time span due to the small number of samples with acetate. Furthermore, the concentration of substrate and thus the influence on the biomass is much lower than that of the sugars. However, it should be noted that the reduced variability due to the precise control of substrate concentrations means that any inhibitions are included in the value of the other parameters. Therefore, if acetate concentrations fluctuate between processes, as they may due to the variability of SSL, the predictions of model 1 may be worse. Model 2 could therefore be used as a framework for future applications and studies in which the ratios of acetate and sugars change between processes. For the given use-case and process, the simplification (no inhibition of glucose and acetate) can be justified and do not reduce the quality of the predictions. Therefore, it was decided to proceed only with model 1 for further modeling of the fed-batch process.

Extension of the model to the fed-batch

Despite the mentioned difficulties, it was attempted to extend the batch model over the whole process. During the fed-batch phase, growth is significantly reduced due to the carbon limited feeding strategy, with average specific growth rates below 0.03 h^{-1}. Further, the induction of the production of recombinant pediocin PA-1 puts additional metabolic load onto the cells. It is therefore expected that an increasing proportion of the energy from the substrate is used for cell maintenance. Similar conditions are often present in continuous cultures with low dilutions rates. Accordingly, some process models for continuous cultures acknowledge this fact by the addition of maintenance terms. For instance, P. Sinner et. al. introduced maintenance parameters for all substrates in the corresponding uptake equations [133]. For the mentioned reasons a maintenance term was added to the equation system (equation 3.9). This was implemented by introducing a general maintenance term (ms) that is subtracted from the growth rate after the fed-batch is started. The induction parameter is a boolean variable (on/off) that describes the current phase of the process (fed-batch/batch). In contrast to the approach of Sinner et. al., less parameters are required this way, however no distinguishing between the different contribution of the substrates is considered.

$$\mu = -induction \cdot ms + \sum_{i=1}^{4}(q_{Si} \cdot Y_{X/Si}) \tag{3.9}$$

The parameter estimation for the fed-batch model was particularly difficult due to the inconsistent data at the end of the batch and the lack of a cell death term. Attempts to parametrize the model with data of the whole process duration resulted in fits that did not describe the course of the experimental data and were consequently not used for any further analysis or interpretation. Due to the lack of a mathematical link for cell death, the optimization algorithm tries to match the reduction in biomass by changing the other parameters. Thus, the predicted biomass is artificially adjusted to the data and the obtained parameters lose any physiological meaning.

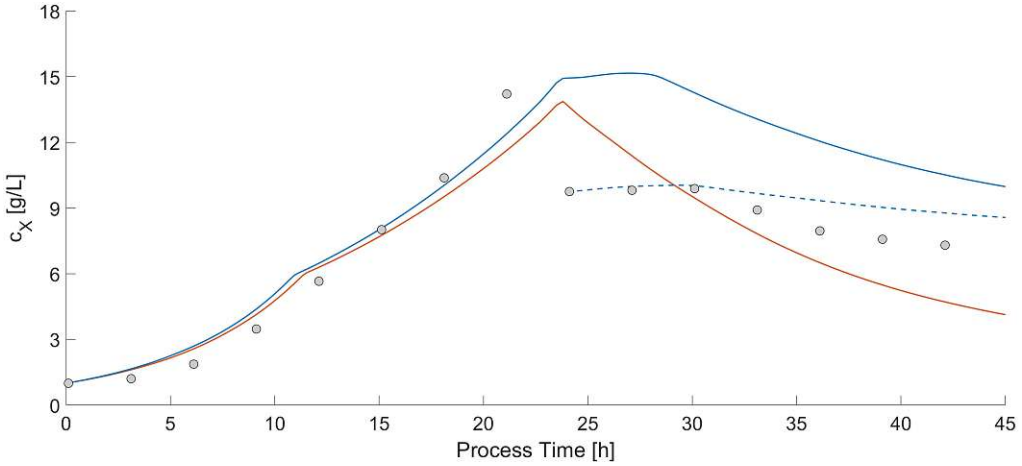

Figure 3.18: Demonstration of the optimization issue due to the biomass drop. The blue fit describes the course of both the batch and fed-batch phase accurately. However, a constant error is obtained due to the lacking cell death term (blue). Parametrizing the equation on the whole data set yields a fit (orange) that is artificially better in terms of RMSE but does not describe the data realistically. This was circumvented by splitting the data set (dashed blue).

Figure 3.18 illustrates this problem bases on two example fits to one of the processes. The model parameterized this way shows a lower RMSE but cannot realistically describe the data and therefore cannot be considered a valid model. Due to the almost constant substrate and biomass concentration in the fed-batch, parametrizing exclusively on the fed-batch did not yield satisfying results. Instead it was decided to split the data by removing the interval between 21 - 24 hours. The same set of parameters was applied to both phases of the process. However, for the fed-batch the experimental data from the 24 h sample was used as start values of the simulation. This way, the constant off-set of the biomass concentration in the fed-batch was avoided. For the parameter estimation, the parameter set obtained for model 1 in the batch phase were used as initial values.

Table 3.8: Model parameters for the fed-batch process model.

Parameter	Value	Unit
$q_{S_1,max}$	0.295	$g{\cdot}g^{-1}{\cdot}h^{-1}$
$q_{S_2,max}$	0.138	$g{\cdot}g^{-1}{\cdot}h^{-1}$
$q_{S_3,max}$	0.070	$g{\cdot}g^{-1}{\cdot}h^{-1}$
$q_{S_4,max}$	0.200	$g{\cdot}g^{-1}{\cdot}h^{-1}$
K_{S_1}	0.070	$g{\cdot}L^{-1}$
K_{S_2}	0.074	$g{\cdot}L^{-1}$
K_{S_3}	0.783	$g{\cdot}L^{-1}$
K_{S_4}	0.001	$g{\cdot}L^{-1}$
Y_{X/S_1}	0.393	$g{\cdot}g^{-1}$
Y_{X/S_2}	0.410	$g{\cdot}g^{-1}$
Y_{X/S_3}	0.323	$g{\cdot}g^{-1}$
Y_{X/S_4}	0.038	$g{\cdot}g^{-1}$
ms	0.04	$g{\cdot}g^{-1}{\cdot}h^{-1}$

The with this split approach obtained parameter set is shown in table 3.8. Since the fed-batch model is an extension of the batch model 1, similar parameters were obtained. According to this model, the cell maintenance parameter was estimated to be 0.04 [$g{\cdot}g^{-1}{\cdot}h^{-1}$]. Given the observed growth rate in the fed-batch of less than 0.03, this suggests that over half of the substrate used by the cells is allocated to cell maintenance. However, it has to be mentioned that product formation is not considered in this model and the energy/carbon required for product formation is thereby probably a part of the maintenance parameter.

Table 3.9: RMSE and NMRSE values including their standard deviation for the states of the fed-batch model.

	RMSE [g/L]	NRMSE [%]
X	1.45 ± 0.31	12.99 ± 3.78
S1	0.31 ± 0.16	3.38 ± 1.83
S2	1.46 ± 0.72	5.3 ± 2.82
S3	1.09 ± 0.29	9.45 ± 2.98
S4	0.07 ± 0.02	4.16 ± 1.25

Table 3.9 shows the errors of the states for the fed-batch model. Similar to the batch model it was based upon, it accurately predicted the concentration of all substrate (NMRSE below 10 %). The error for the biomass did decrease slightly compared to the batch, but still fails to meet the 10 % criteron. Further, the biomass prediction can not be considered accurate for the whole process without a suitable cell-death term. Figure 3.19 illustrates the observed vs. predicted plot for the fed-batch model

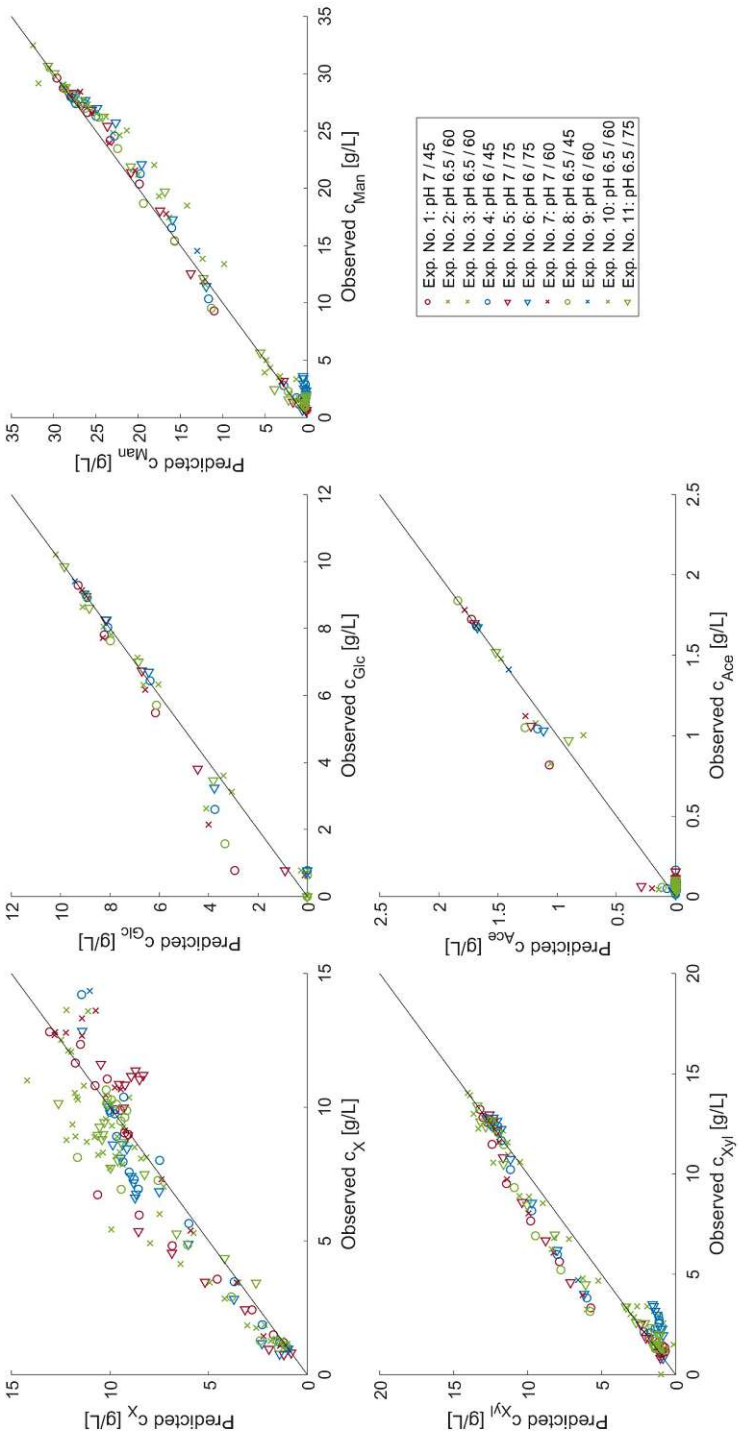

Figure 3.19: Observed vs. predicted plot for each state of the batch model 1. The diagonal line represent observed = predicted.

(using the split approach). The observed vs. predicted plot for the biomass shows overprediction at concentrations from 1 to 9 g/L followed by wide spread at higher values (above 10 g/L), reinforcing the previous mentioned statement. It can be seen that the data for glucose, mannose and acetate are narrowly distributed around the diagonal line, suggesting that the these states are accurately predicted. The model exhibited an overestimation of the xylose concentration during the batch phase, ranging from approximately 4-11 g/L. In contrast, the model is slightly underpredicting the concentration of xylose during the fed-batch phase at lower levels but is generally more accurate in the fed-batch. Those deviations from the measured concentration are also reflected in the state error for xylose which is with approximately 10 % about twice as high as for mannose and acetate (5 % and 4 %).

3.2.3 Modeling of the pediocin PA-1 formation

In the fed-batch phase the influence of the pH value and the carbon/phosphorous ratio of the feed on the production of pediocin PA-1 was investigated. Based on the obtained data it was attempted to establish a kinetic model of the production of pediocin in *C. glutamicum*. A potential model should be able to accurately describe the course of the activity in the fed-batch and consider the effect of the relevant parameters.

The formulation of a model for the pediocin formation (equation 2.14) was based on a modified Ludeking-Piret equation. The equation proposed by Ludeking and Piret (equation 3.10) [78] is commonly used to describe product formation in bioprocess in general and has been sucesfully adapted for modeling bacteriocin production in natural producer strain in several cases [137, 117, 138]. The Luedeking-Piret equation can be used to describe both growth dependent and independent product formation as well as mixed types. For primary product kinetics (growth associated), β equals 0 and α can be interpreted as the product yield ($Y_{P/X}$). Strictly growth independent production is described only by the second part of the equation ($\alpha = 0$, $q_P = \beta$).

$$\frac{dc_P}{dt} = \alpha \cdot \frac{dc_X}{dt} + \beta \cdot c_X \tag{3.10}$$

Pediocins and bacteriocins in general are often reported to follow primary product kinetics in their natural producer strains [45]. However, as previously outlined, the results from the DoE suggest that growth independent product formation characteristics predominate in the performed fed-batch experiments. It was thereby assumed that the heterologous pediocin PA-1 production in *C. glutamicum* follows mainly secondary metabolite kinetics. Further, the very low and stable specific growth rate in the fed-batch phase (≤ 0.03 h^{-1}) would result in poor identifiability and importance of the parameter α in a model that considers mixed metabolite kinetics. Consequently, the model building for the pediocin formation was based on the Luedeking-Piret equation for secondary metabolites.

The differential equation was further expanded to consider the decrease of the activity due to dilution and degradation. It was previously outlined that the observed decrease in activity is most likely caused by oxidation pediocin. Further, the extend of degradation did vary greatly between the different fed-batches. In general, experiments with higher activity would decline faster and to a greater extend (up to 80 %), while the ones with lower activity did decrease less or stayed stable. It was thereby assumed that the degradation/oxidation is dependent on the total produced amount of pediocin (equation 3.11).

$$q_{dO} = \sum_{t=0}^{t} (P \cdot V_R) \cdot b \tag{3.11}$$

pH dependence

To describe the impact of the fed-batch pH value on the pediocin production, a corresponding mechanistic link has to be incorporated into the model. To this day, no studies that attempted the mechanistic modeling of heterologous pediocin production have been published. Several studies however investigated the production of various pediocins in their natural producers, lactic acid bacteria, and subsequently proposed models describing the data [137, 117, 138]. In lactic acid bacteria, a decreasing pH value during the fermentation is necessary for the secretion of active pediocin [45]. Mechanistic models describing the pediocin formation in lactic acid bacteria therefor commonly include pH dependent terms. However, adaption of those models was not successful, as they considered a pH gradient rather than a steady controlled pH value for the cultivation.

Published mechanistic models that consider pH dependent pediocin production were found to be very specific towards natural producer strains and not deemed suitable for the here presented process. Instead, it was decided to take a more general approach for the model building. The pH-dependence of many physiological processes such as enzymatic reactions can be described by bell-shaped curves, where the activity rises towards an optimal pH and decreases once the optimum is surpassed [139]. Lin et. al. proposed a basic bell curve equation [140], which was then effectively employed by Li et. al. to model the pH-dependent activity of immobilized enzymes [141]. According to the results of the DoE, the pH range of the performed fed-batches did most likely not exceed the optimal pH value. Therefor, the bell curve equation can be shortened to to a one sided curve and adapted to the specific production rate (q_P):

$$q_P = q_{P,max} \cdot \frac{1}{(1 + e^{k \cdot (pH - pH_{de})})} \tag{3.12}$$

Influence of the C/P ratio

In addition to the pH-value, the model needs to incorporate the influence of phosphorous on the production. However, it was not possible to allocate (cell, SSL, precipitate) or accurately quantify the phosphate in the reactor. Therefore it was attempted to build a hypothesis based on solely on the carbon to phosphorous ratio entering the reactor through the feeds instead of the experimental measured phosphate concentrations. Investigation of nutritional requirements and limitations are very specific to the utilized microorganism and product and can thereby not be generalized from other producer strains or products. The formulation of a mechanistic link was further complicated by the limited metabolic knowledge of heterologous pediocin production in *C. glutmacium* on SSL and the impact of phosphorous. Instead the influence of phosphorous on the production was described using a quadratic relationship as indicated by the results of the DoE.

$$q_P = q_{P,max} \cdot \frac{r_{C/P}}{r_{C/P,max} + r_{C/P} + \frac{r_{C/P}^2}{r_{C/P,max}}} \tag{3.13}$$

Equation 3.13 was subsequently used to model the influence of the C/P-ratio. The inverse of the ratios was used for modelling to obtain an equation where the production falls steeply to zero when the ratios approach very high values and consequently very little to no phosphate is provided. $r_{C/P,max}$ denotes the maximum of the quadratic function and can thereby be seen as the optimal C/P-ratio of the feed.

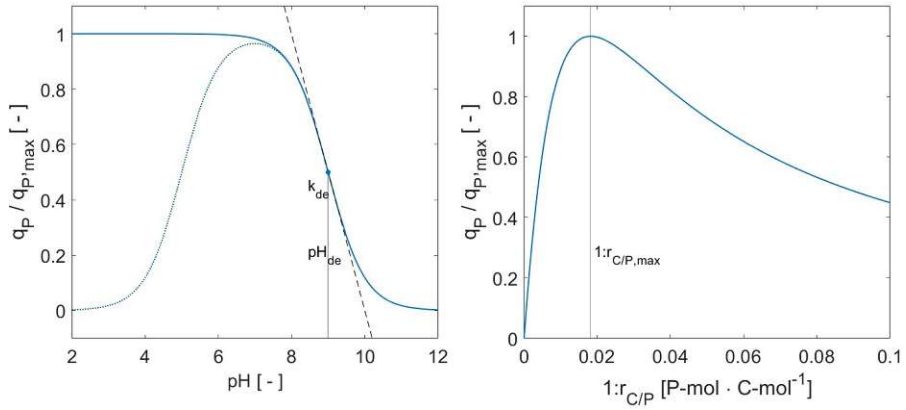

Figure 3.20: Illustration of the equations used to describe the influence of pH and carbon to phosphorous ratio. Left: original bell shaped curve (dotted blue line) and the single sided curve (eqation 3.12) used for the pH contribution. Right: Quadratic equation for the impact of the carbon phosphorous ratio on the production (equation 3.13).

The evaluation of the experimental design further suggested an interaction between the factors pH and C/P-ratio. To consider interactions, the equations for the pH and phosphorous ratio were combined in a multiplicative way. Ultimately, the used model equation for the specific pediocin formation rate is the product of the equations 3.12 and 3.13:

$$q_P = induction \cdot \left(q_{P,max} \cdot \frac{1}{(1 + e^{k \cdot (pH - pH_{de})})} \cdot \frac{r_{C/P}}{r_{C/P,max} + r_{C/P} + \frac{r_{C/P}^2}{r_{C/P,max}}} \right) \tag{3.14}$$

To avoid additional uncertainties in the parameter estimation, the model relied on the measured biomass concentrations rather than the biomass predictions of the fed-batch model. The obtained parameters for the pediocin model are displayed in table 3.10. The parametrized model displayed a RMSE of 5550 ± 2768 BU/ml which equals to a NMRSE of 46.26 ± 52.13 % for the pediocin state.

Table 3.10: Parameter of the pediocin model

Parameter	**Value**	**Unit**
$q_{P,max}$	3590	$BU \cdot g^{-1} \cdot h^{-1}$
pH_{de}	6.20	-
k	5.10	-
$r_{C/P,max}$	58.14	$C\text{-}mol \cdot P\text{-}mol^{-1}$
b	$2.70 \cdot 10^{-9}$	$BU^{-1} \cdot h^{-1}$

Figure 3.21 further shows the observed versus predicted plot for the pediocin model. The model can roughly estimate the overall trend of activity in a process on basis of the given parameters. However, it can be observed that the model is unable to accurately estimate the pediocin activity throughout the process. Based on the data presented, it can be stated that the proposed model equations do not accurately describe the production of Pediocin. Consequently, a more detailed interpretation of the parameters was dispensed with. There are several reasons for the large errors in the estimation of the pediocin production by the model.

There are numerous factors contributing to the significant discrepancy in the model's prediction of pediocin production. First and foremost, the challenges regarding analytical methods and their development, associated with the use of SSL as medium, must be addressed. This issue is particularly highlighted by the restricted capacity to assess crucial key parameters for the production, such as the phosphate concentration within the system. As previously demonstrated, it is highly likely that the

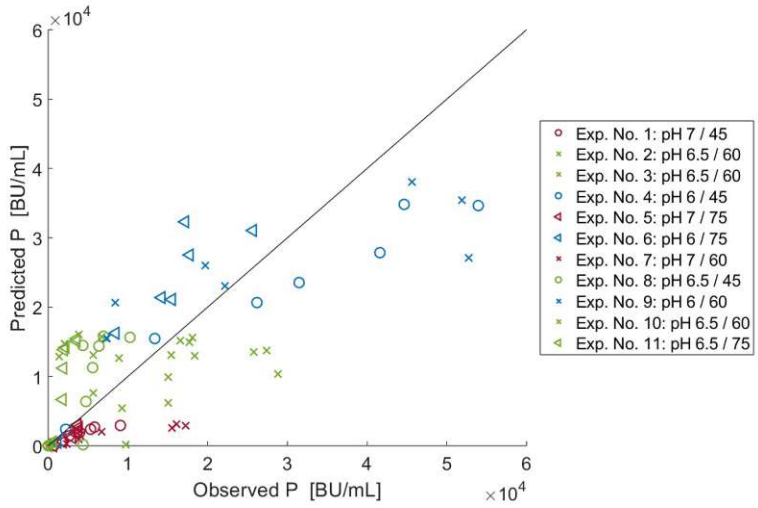

Figure 3.21: Observed vs. Predicted plot for the pediocin model. The diagonal line represent observed = predicted.

majority of supplied phosphate did precipitate during the process, most likely due to the high calcium concentrations present in the SSL used. It was however not possible to establish the elemental composition of the precipitate due to insufficient analytical instrumentation. Accurate determination necessitates specialized and expensive techniques like inductively coupled plasma mass spectrometry (ICP-MS), usually not present in biotechnology laboratories. Furthermore, no suitable reversed-phase HPLC method was available during the study to quantify the concentration of pediocin and determine the ratio of degraded to active peptide. Instead, the production was determined based on the antimicrobial activities of the sample supernatants. While there were significant improvements in the resolution of the acitivity determination by employing evaluation based on dosage response curves rather than semi-quantitave critical dilution assay. It should be noted that solely relying on the activity of antimicrobial peptides on an indicator strain for assessment and modelling has limitations. Additionally, the results may vary depending on the method and indicator strain used, making them only partially comparable. Moreover, the outcomes, usually expressed in arbitrary or biological units (AU, BU), cannot be utilised for mass or elemental balances of the reactor, which are used to check the consistency of the data and derive the differential equations.

In addition to the aforementioned analytical challenges, the formulation of the model is impeded by the limited knowledge about the underlying mechanisms of the production. The heterologous expression of pediocin PA-1 in *C. glutamicum* is a relatively recent accomplishment and therefore has not yet been thoroughly investigated. However, especially investigating the impact of nutrient changes, such as varying the phosphorous

supply, on peptide production and establishing mechanistic links requires thorough research and proper analytics. While some studies have identified a connection between central carbon and energy metabolism and phosphate limitation [142, 143], it remains in question how this relates to heterologous pediocin expression and secretion. It is worth mentioning that altering the carbon to phosphorus ratio may have an effect that is not necessarily directly linked to metabolic changes caused by phosphorus deficiencies.

The precipitation of phosphate also affects the composition and availability of cationic species (e.g. calcium) precipitated as counter ions. Pediocins as cationic peptides were shown to bind to both sensitive and resistant cells due to electrostatic interactions in the first step [144, 145]. Changes in the ionic composition of the medium might thereby influence the interaction of the pediocin molecules with the cells or the export out of the cells. Influence of ions, in particular bivalent ions, on the formation of pediocin are reported for the natural producer *Pediococcus acidilactici* as well as for the heterologous production in *C. glutamicum* [72, 146]. None of those studies however investigated the mechanism of the influence of those ions. Anastasiadou et al. [146] found a supression of pediocin production when incorporating $CaCl_2$ into the growth medium for *Pediococcus acidilactici*, while addition of $MnSO_4$ resulted in a significant increase. On the contrary, Christmann et al. observed a positive influence of $CaCl_2$ on the pediocin production, with a two-fold increase in production with an increase from 0.05 g/L to 2 g/L in *C. glutamicum* [72].

The SSL used in this study was analyzed for trace element composition by an external laboratory in the development of the original process. According to this analysis, the utilized SSL contains 3.5 g/L Ca^{2+} ions and should consequently not be limiting. However, there is the possibility that the concentrations of bivalent ions were well below the reported 2 g/L due to the before mentioned precipitation. The observed influence of the phosphorous ratio could consequently be related to the changed availability of bivalent ions that co-precipitate. Further, it is possible that both, the phosphorous and bivalent ion concentrations influence the production. Without adequate analytical methods to quantify the phosphorous and bivalent ion concentration throughout the fed-batch, it was not feasible to test this hypothesis.

The model evaluation results indicate that the hypothesis proposed for the production of pediocin was inadequate. For the aforementioned reasons, no further modelling was conducted in this work. Nonetheless, possible reasons for the limited estimation capabilities of the present model were included. Upon improvement of the analytical methods, it is necessary to revisit the proposed alternative hypothesis for production of pediocin and subsequently re-examine the formulation of the model equation.

4 Conclusion and Outlook

4.1 Conclusion

The previously in our research group developed SSL-based fed-batch process for the production of pediocin PA-1 was investigated for the possibility of transitioning towards a repetitive fed-batch. Several problems in this bioprocess were identified that reduced the efficiency, hindered the envisioned intensification and consequently had to be resolved beforehand.

Improvement of the batch phase

The batch phase of the original process was analyzed and key problems for a future repetitive fed-batch were identified. The long and unpredictable lag phase of the process (10 hours average, up to 42 hours) was attributed to inhibitors present in SSL and the neccesary detoxification by cells. By increasing the inoculum size from 0.23 g/L to 1.0 g/L at the utilized SSL concentration, the lag phase was reduced significantly (approx. 3 hours), while the substrate utilization and the biomass yield were improved. Inoculum sizes above 1.0 g/L were shown to further decrease the observed lag but were not beneficial for the achieved end biomass. It was additionally shown that higher SSL concentrations can be off-set by adapting the inoculum amount. As a result of the adapted starting conditions, the substrate utilization was enhanced, leading to a reduction in unused substrate and a substantial increase in the achieved biomass concentration from 2.0 g/L to 11 g/L. The reproducibility of the batch phase was demonstrated with eleven successfully performed processes. However, a die-off after 21 hours was observed in most of the cultivations, that could not be correlated to any measured substrate or metabolite. The optimized batch phase was employed in the following investigation of the pediocin production in the fed-batch.

Influence of fed-batch pH and C:P-ration on the pediocin production

The optimized batch phase provided comparable starting conditions requiered for further testing the influence of promising fed-batch parameters. To investigate the influence of the pH value and the C:P-ratio in the envisioned SSL-based process and estimate potential quadratic effects and interactions, a three level full-factorial ex-

perimental plan for the fed-batch phase was employed. Both the pH value and the C:P-ratio as well as their interaction and quadratic terms were shown to have a significant influence on the maximum achieved pediocin titre. For the tested conditions, a maximum antimicrobial activity of 54.000 BU/ml with a pH value of 6.0 and a C:P-ratio of 45 was achieved, equaling to a 10 times increase compared to the original process design. Additionally, the optimal conditions (pH 6, C:P 55) were determined to lie at the edge of the selected design space (pH 6-7, C:P 45-75), suggesting the potential for further production gains by lowering the pH value. However, as the minimal pH value for growth of Corynebacterium has been reported to be 5.7, reducing the pH to below 6.0 was considered unfeasible.

Mechanistic modeling

The obtained data was further exploited for the establishment of a mechanistic model. Elemental balances were established to check the consistency of the data used for the modeling. In the course of this, significant problems were found in the phosphate analytics. This task was seperated into modeling the growth of *C. glutamicum* and the production of pediocin on SSL. For the growth modeling, a batch model considering the duration till the observed die-off (21 hours) was established and further extended to the fed-batch. The batch model was able to accurately estimate the uptake of all substrate (glucose, mannose, xylose, acetate) with an NMRSE of below 10%, did however fail to meet the set acceptance critereon for the biomass concentration. Modeling the complete fed-batch was complicated by the observed cell die-off, that was found to not correlate with any measured variable. Since no plausible cell-death term could be established, the time span in question was not considered in the parameter estimation. The fed-batch model delivered accurate predictions of the substrate concentration throughout the process (NRMSE $< 10\%$). With a NRMSE of 13% and the lack of a cell-death term, the biomass concentration did fail the acceptance critereon for the fed-batch as well. Limited capabilities to quantify the product and phosphate concentrations, caused by the analytical challenges associated with the use of SSL, complicated the modeling of the pediocin production. Nevertheless, it was attempted to establish a model structure for the pediocin formation in the fed-batch. Due to the inability to determine the pediocin concentration, the antimicrobial activity was used to model the pediocin production instead. The model failed to estimate the pediocin titre throughout the process and showed a NRMSE of 45%. Several reasons have been identified for the suboptimal performance of the pediocin model. These issues comprise imprecise measurements of key parameters and the subsequent challenge of identifying mechanistic terms for peptide oxidation and the impact of phosphate. Additionally, there are further unaccounted-for variables to consider, including the impact of bivalent ion concentration, which can be influenced by both pH and the C:P ratio.

It can be summed up that this work was able to tackle the identified problems and achieve substantial improvements in the biomass concentration, substrate utilization, productivity and reliability of the process.

4.2 Outlook

Sustainable biotechnological production represents a crucial step towards addressing the urgent climate change concerns in the industry. The goal of intensifying bioprocesses is to optimize the efficient use of essential resources and enhance productivity through technological advancements. The next step should be to focus on the aforementioned transition towards a repetitive fed-batch to further enhance the overall productivity and efficiency of the process.

In a repetitive fed-batch culture broth is harvested from the reactor and fresh medium is filled back into the reactor to initialize the next repetition. No separate inoculum is required but the remaining cells from the previous cultivation cycle act as inoculum for the next reposition. The inoculum amount is influenced by the volume and the biomass concentration of broth left in reactor and is controlled by the ratio of old broth and new medium. Consequently the established connection between the inoculum amount and the lag-time and reliability of the SSL-based process is from detrimental importance for the upcoming intensification. Further, the reduced lag-phase and variability of the process achieved in this work is the basis for intensification as those factors will add up in the following repetitions and might lead to a uncontrollable and inefficient process. However, several question have to be investigated in the process of transitioning to a repetitive fed-batch in order to guarantee a successful intensification. One of those is the influence of the lowered pH value in the fed-batch phase on the batch phase of the next repetition. Further a drop in the biomass concentration in the end of the batch phase was observed, but was not explainable by any measured substrate or metabolite. Cultivations with higher samplings interval in the time period of interest are necessary to detect possible correlations. Additionally, analytical techniques to determine the viability of the cells such as staining techniques, culture plating or biocapacity probes could provide new insights into the observed die-off. Subsequently, the end of batch and the feed start has to be re-evaluated to circumvent viability issues and potentially improve the productivity. Process models are often considered an important tool in bioprocess intensification. Improvements in the analytical methods could subsequently reduce the modeling error and enhance the ability to predict important parameters such as the biomass and product concentration. A mechanistic process model able to accurately predict the biomass and product concentration could be utilized to control the time points of the feed start or harvesting to achieve optimal productivity in a repetitive fed-batch. Further, additional important parameters such as the media exchange ratio and the number of cycles could be controlled based on the model prediction instead of fixed empiric values that don't consider the actual conditions present in the reactor and consequently might not achieve optimal results.

The practical application of the aforementioned intensification strategy should be explored and implemented in a subsequent stage. The integration of this process into a pulp and paper biorefinery has the potential to enhance the economic viability of sustainable production alternatives through the production of high-quality products.

References

[1] Eunice Foote. Circumstances affecting the heat of the sun's rays. *American Journal of Science and Arts*, 22(66):382–383, 1856.

[2] John Tyndall. I. The Bakerian Lecture.—On the absorption and radiation of heat by gases and vapours, and on the physical connexion of radiation, absorption, and conduction. *Philosophical Transactions of the Royal Society of London*, 151:1–36, 12 1861.

[3] Svante Arrhenius. XXXI. On the influence of carbonic acid in the air upon the temperature of the ground. *The London, Edinburgh, and Dublin Philosophical Magazine and Journal of Science*, 41(251):237–276, 4 1896.

[4] United Nations. United Nations Framework Convention on Climate Change United Nations, 1992.

[5] United Nations. Paris Agreement to the United Nations Framework Convention on Climate Change, 2015.

[6] United Nations Environment Programme. Emissions Gap Report 2022: The Closing Window — Climate crisis calls for rapid transformation of societies. Technical report, United Nations Environment Programme, Nairobi, 2022.

[7] IPCC. *Climate Change 2022: Mitigation of Climate Change. Contribution of Working Group III to the Sixth Assessment Report of the Intergovernmental Panel on Climate Change*. Number 1. Cambridge University Press, Cambridge, UK and New York, NY, USA, 8 2022.

[8] United Nations. Transforming our world: the 2030 Agenda for Sustainable Development, 2015.

[9] Valeria Ferreira Gregorio, Laia Pié, and Antonio Terceño. A Systematic Literature Review of Bio, Green and Circular Economy Trends in Publications in the Field of Economics and Business Management. *Sustainability*, 10(11):4232, 11 2018.

[10] Bert Annavelink, Lesly Garcia Chaves, René van Ree, and Iris Vural Gursel. IEA Bioenergy Task 42 Biorefining in a circular economy: Global biorefinery status report 2022. Technical report, IEA Bioenergy Technology Collaboration Programme, 2022.

[11] Francesco Cherubini, Gerfried Jungmeier, Maria Wellisch, Thomas Willke, Ioannis Skiadas, René Van Ree, and Ed de Jong. Toward a common classification approach for biorefinery systems. *Biofuels, Bioproducts and Biorefining*, 3(5):534–546, 9 2009.

[12] B. Kamm and M. Kamm. Principles of biorefineries. *Applied Microbiology and Biotechnology*, 64(2):137–145, 4 2004.

[13] Kurt Wagemann and Nils Tippkötter. Biorefineries: A Short Introduction. In *Advances in biochemical engineering/biotechnology*, volume 123, pages 1–11. 2018.

[14] G.S. Hossain, L. Liu, and G.C. Du. Industrial Bioprocesses and the Biorefinery Concept. In *Current Developments in Biotechnology and Bioengineering*, pages 3–27. Elsevier, 2017.

[15] Julia Tomei and Richard Helliwell. Food versus fuel? Going beyond biofuels. *Land Use Policy*, 56:320–326, 11 2016.

[16] Tatsuji Koizumi. Biofuels and food security. *Renewable and Sustainable Energy Reviews*, 52:829–841, 12 2015.

[17] Alexandros Gasparatos, Per Stromberg, and Kazuhiko Takeuchi. Sustainability impacts of first-generation biofuels. *Animal Frontiers*, 3(2):12–26, 4 2013.

[18] Alison Mohr and Sujatha Raman. Lessons from first generation biofuels and implications for the sustainability appraisal of second generation biofuels. *Energy Policy*, 63:114–122, 12 2013.

[19] Francisco G. Calvo-Flores and Francisco J. Martin-Martinez. Biorefineries: Achievements and challenges for a bio-based economy. *Frontiers in Chemistry*, 10(November):1–23, 11 2022.

[20] Nicolaus Dahmen, Iris Lewandowski, Susanne Zibek, and Annette Weidtmann. Integrated lignocellulosic value chains in a growing bioeconomy: Status quo and perspectives. *GCB Bioenergy*, 11(1):107–117, 2019.

[21] Brian D. Titus, Kevin Brown, Heljä-Sisko Helmisaari, Elena Vanguelova, Inge Stupak, Alexander Evans, Nicholas Clarke, Claudia Guidi, Viktor J. Bruckman, Iveta Varnagiryte-Kabasinskiene, Kęstutis Armolaitis, Wim de Vries, Keizo Hirai, Lilli Kaarakka, Karen Hogg, and Pam Reece. Sustainable forest biomass: a review of current residue harvesting guidelines. *Energy, Sustainability and Society*, 11(1):10, 4 2021.

[22] U.S. White House. U.S. Plan to Conserve Global Forests. Technical report, Washington, 2021.

[23] Biodiversity, land use and forestry | Fact Sheets on the European Union | European Parliament.

[24] R.H. Marchessault. *Wood Chemistry*, volume 252. Elsevier, 1 1993.

[25] Julie Baruah, Bikash Kar Nath, Ritika Sharma, Sachin Kumar, Ramesh Chandra Deka, Deben Chandra Baruah, and Eeshan Kalita. Recent trends in the pretreatment of lignocellulosic biomass for value-added products. *Frontiers in Energy Research*, 6(DEC):1–19, 2018.

[26] Biermann Christopher. *Handbook of Pulping and Papermaking*. Elsevier, 1996.

[27] MARSHALL LANGTON PRICE. The pollution of streams by sulphite-pulp waste, a study of possible remedies. Technical Report 16, 1909.

[28] Susana R. Pereira, Diogo J. Portugal-Nunes, Dmitry V. Evtuguin, Luísa S. Serafim, and Ana M.R.B. Xavier. Advances in ethanol production from hardwood spent sulphite liquors. *Process Biochemistry*, 48(2):272–282, 2 2013.

[29] Eva Palmqvist and Bärbel Hahn-Hägerdal. Fermentation of lignocellulosic hydrolysates. II: Inhibitors and mechanisms of inhibition. *Bioresource Technology*, 74(1):25–33, 2000.

[30] J. M. Holderby and W. A. Moggio. Utilization of Spent Sulfite Liquor. *Journal (Water Pollution Control Federation)*, 32(2):171–181, 1960.

[31] Niel Bezuidenhout, Daneal C. S. Rorke, Eugéne van Rensburg, Danie Diedericks, and Johann F. Görgens. Ethanol production from non-detoxified hardwood spent sulfite liquor in submerged fed-batch culture using advanced yeasts. *Biomass Conversion and Biorefinery*, (0123456789), 3 2023.

[32] Roger G. Harrison, Paul W. Todd, Scott R. Rudge, and Demetri P. Petrides. Bioprocess Design and Economics. In *Bioseparations Science and Engineering*, number August. Oxford University Press, 4 2015.

[33] Qi Sheng, Xiao-Yu Wu, Xinyi Xu, Xiaoming Tan, Zhimin Li, and Bin Zhang. Production of l-glutamate family amino acids in Corynebacterium glutamicum: Physiological mechanism, genetic modulation, and prospects. *Synthetic and Systems Biotechnology*, 6(4):302–325, 12 2021.

[34] Lothar Eggeling and Michael Bott. A giant market and a powerful metabolism: l-lysine provided by Corynebacterium glutamicum. *Applied Microbiology and Biotechnology*, 99(8):3387–3394, 2015.

[35] Judith Becker, Christina Maria Rohles, and Christoph Wittmann. Metabolically engineered Corynebacterium glutamicum for bio-based production of chemicals, fuels, materials, and healthcare products. *Metabolic Engineering*, 50(April):122–141, 2018.

[36] Joo Young Lee, Yoon Ah Na, Eungsoo Kim, Heung Shick Lee, and Pil Kim. The actinobacterium Corynebacterium glutamicum, an industrial workhorse. *Journal of Microbiology and Biotechnology*, 26(5):807–822, 2016.

[37] Xiuxia Liu, Wei Zhang, Zihao Zhao, Xiaofeng Dai, Yankun Yang, and Zhonghu Bai. Protein secretion in Corynebacterium glutamicum. *Critical Reviews in Biotechnology*, 37(4):541–551, 2017.

[38] Min Ju Lee and Pil Kim. Recombinant protein expression system in Corynebacterium glutamicum and its application. *Frontiers in Microbiology*, 9(OCT), 2018.

[39] Apurv Mhatre, Somnath Shinde, Amit Kumar Jha, Alberto Rodriguez, Zohal Wardak, Abigail Jansen, John M. Gladden, Anthe George, Ryan W. Davis, and Arul M. Varman. Corynebacterium glutamicum as an Efficient Omnivorous Microbial Host for the Bioconversion of Lignocellulosic Biomass. *Frontiers in Bioengineering and Biotechnology*, 10(April):1–14, 2022.

[40] Miho Sasaki, Haruhiko Teramoto, Masayuki Inui, and Hideaki Yukawa. Identification of mannose uptake and catabolism genes in Corynebacterium glutamicum and genetic engineering for simultaneous utilization of mannose and glucose. *Applied Microbiology and Biotechnology*, 89(6):1905–1916, 2011.

[41] Hideo Kawaguchi, Alain A. Vertes, Shohei Okino, Masayuki Inui, and Hideaki Yukawa. Engineering of a xylose metabolic pathway in Corynebacterium glutamicum. *Applied and Environmental Microbiology*, 72(5):3418–3428, 2006.

[42] Yota Tsuge, Yoshimi Hori, Motonori Kudou, Jun Ishii, Tomohisa Hasunuma, and Akihiko Kondo. Detoxification of furfural in Corynebacterium glutamicum under aerobic and anaerobic conditions. *Applied Microbiology and Biotechnology*, 98(20):8675–8683, 2014.

[43] Djamel Drider, Gunnar Fimland, Yann Héchard, Lynn M. McMullen, and Hervé Prévost. The Continuing Story of Class IIa Bacteriocins. *Microbiology and Molecular Biology Reviews*, 70(2):564–582, 2006.

[44] Maged Younes, Peter Aggett, Fernando Aguilar, Riccardo Crebelli, Birgit Dusemund, Metka Filipič, Maria Jose Frutos, Pierre Galtier, Ursula Gundert-Remy, Gunter Georg Kuhnle, Claude Lambré , Jean-Charles Leblanc, Inger Therese Lillegaard, Peter Moldeus, Alicja Mortensen, Agneta Oskarsson, Ivan Stankovic, Ine Waalkens-Berendsen, Rudolf Antonius Woutersen, Matthew Wright, Lieve Herman, Paul Tobback, Fabiola Pizzo, Camilla Smeraldi, Alexandra Tard, Adamantia Papaioannou, and David Gott. Safety of nisin (E 234) as a food additive in the light of new toxicological data and the proposed extension of use. *EFSA Journal*, 15(12), 2017.

[45] Maria Papagianni and Sofia Anastasiadou. Pediocins: The bacteriocins of Pediococci. Sources, production, properties and applications. *Microbial Cell Factories*, 8(1):3, 2009.

[46] J. McLauchlin, R. T. Mitchell, W. J. Smerdon, and K. Jewell. Listeria monocytogenes and listeriosis: A review of hazard characterisation for use in microbiological risk assessment of foods. *International Journal of Food Microbiology*, 92(1):15–33, 2004.

[47] Mehmet Doganay. Listeriosis: Clinical presentation. *FEMS Immunology and Medical Microbiology*, 35(3):173–175, 2003.

[48] Carl A. Batt. LISTERIA | Listeria monocytogenes. *Encyclopedia of Food Microbiology: Second Edition*, pages 490–493, 1 2014.

[49] Liyan Zhu, Jianwei Zeng, Chang Wang, and Jiawei Wang. Structural Basis of Pore Formation in the Mannose Phosphotransferase System by Pediocin PA-1. *Applied and Environmental Microbiology*, 88(3), 2022.

[50] Eldin Maliyakkal Johnson, Dr Yong Gyun Jung, Dr Ying Yu Jin, Dr Rasu Jayabalan, Dr Seung Hwan Yang, and Joo Won Suh. Bacteriocins as food preservatives: Challenges and emerging horizons. *Critical Reviews in Food Science and Nutrition*, 58(16):2743–2767, 2018.

[51] Gi Seong Moon, Yu Ryang Pyun, and Wang June Kim. Characterization of the pediocin operon of Pediococcus acidilactici K10 and expression of his-tagged recombinant pediocin PA-1 in Escherichia coli. *Journal of Microbiology and Biotechnology*, 15(2):403–411, 2005.

[52] J. D. Marugg, C. F. Gonzalez, B. S. Kunka, A. M. Ledeboer, M. J. Pucci, M. Y. Toonen, S. A. Walker, L. C.M. Zoetmulder, and P. A. Vandenbergh. Cloning, expression, and nucleotide sequence of genes involved in production of pediocin PA-1, a bacteriocin from Pediococcus acidilactici PAC1.0. *Applied and Environmental Microbiology*, 58(8):2360–2367, 1992.

[53] Oliver Goldbeck, Dominique N. Desef, Kirill V. Ovchinnikov, Fernando Perez-Garcia, Jens Christmann, Peter Sinner, Peter Crauwels, Dominik Weixler, Peng Cao, Judith Becker, Michael Kohlstedt, Julian Kager, Bernhard J. Eikmanns, Gerd M. Seibold, Christoph Herwig, Christoph Wittmann, Nadav S. Bar, Dzung B. Diep, and Christian U. Riedel. Establishing recombinant production of pediocin PA-1 in Corynebacterium glutamicum. *Metabolic Engineering*, 68(April):34–45, 2021.

[54] Philip Lutze, Rafiqul Gani, and John M. Woodley. *Phenomena-based Process Synthesis and Design to achieve Process Intensification*, volume 29. Elsevier B.V., 2011.

[55] P. A. Ramachandran and R. V. Chaudhari. Sustainable Reactor Design. *Encyclopedia of Sustainable Technologies*, pages 525–540, 1 2017.

[56] Ganapathy Subramanian. *Process Control, Intensification, and Digitalisation in Continuous Biomanufacturing*. Wiley, 3 2022.

[57] Alexandre C. Dimian, Costin S. Bildea, and Anton A. Kiss. Process Intensification. In *Computer Aided Chemical Engineering*, volume 35, pages 397–448. 2014.

[58] K.V.K. Boodhoo, M.C. Flickinger, J.M. Woodley, and E.A.C. Emanuelsson. Bioprocess intensification: A route to efficient and sustainable biocatalytic transformations for the future. *Chemical Engineering and Processing - Process Intensification*, 172(January):108793, 2 2022.

[59] John M. Woodley. Bioprocess intensification for the effective production of chemical products. *Computers & Chemical Engineering*, 105:297–307, 10 2017.

[60] Julian Kopp, Stefan Kittler, Christoph Slouka, Christoph Herwig, Oliver Spadiut, and David J. Wurm. Repetitive Fed-Batch: A Promising Process Mode for Biomanufacturing With E. coli. *Frontiers in Bioengineering and Biotechnology*, 8(November), 2020.

[61] Liangsen Liu, Fangzhong Wang, Guangsheng Pei, Jinyu Cui, Jinjin Diao, Mingming Lv, Lei Chen, and Weiwen Zhang. Repeated fed-batch strategy and metabolomic analysis to achieve high docosahexaenoic acid productivity in Crypthecodinium cohnii. *Microbial Cell Factories*, 19(1):1–14, 2020.

[62] Tomoshi Ohya, Masao Ohyama, and Kaoru Kobayashi. Optimization of human serum albumin production in methylotrophic yeast Pichia pastoris by repeated fed-batch fermentation. *Biotechnology and Bioengineering*, 90(7):876–887, 2005.

[63] Sanja Martens, Sven Oliver Borchert, Bart W. Faber, Gesine Cornelissen, and Reiner Luttmann. Fully automated production of potential malaria vaccines with Pichia pastoris in integrated processing. *Engineering in Life Sciences*, 11(4):429–435, 2011.

[64] R. Bauer, N. Katsikis, S. Varga, and D. Hekmat. Study of the inhibitory effect of the product dihydroxyacetone on Gluconobacter oxydans in a semi-continuous two-stage repeated-fed-batch process. *Bioprocess and Biosystems Engineering*, 28(1):37–43, 2005.

[65] Dörte Solle, Bernd Hitzmann, Christoph Herwig, Manuel Pereira Remelhe, Sophia Ulonska, Lynn Wuerth, Adrian Prata, and Thomas Steckenreiter. Between the Poles of Data-Driven and Mechanistic Modeling for Process Operation. *Chemie-Ingenieur-Technik*, 89(5):542–561, 2017.

[66] Apostolos Tsopanoglou and Ioscani Jiménez del Val. Moving towards an era of hybrid modelling: advantages and challenges of coupling mechanistic and data-driven models for upstream pharmaceutical bioprocesses. *Current Opinion in Chemical Engineering*, 32, 2021.

[67] R. E. Spier and J. B. Griffiths. *Animal Cell Biotechnology*, volume 2095 of *Methods in Molecular Biology*. Springer US, New York, NY, 2020.

[68] Dimpal Jyoti Mahanta, Munindra Borah, and Pallabi Saikia. A Study on Kinetic Models for Analysing the Bacterial Growth Rate. pages 68–72, 2014.

[69] Jacques Monod. THE GROWTH OF BACTERIAL CULTURES. *Annual Review of Microbiology*, 3(1):371–394, 10 1949.

[70] Harold Van Waveren. *Good Modelling Practice Handbook*. Dutch Dept. of Public Works, 1999.

[71] Joachim Almquist, Marija Cvijovic, Vassily Hatzimanikatis, Jens Nielsen, and Mats Jirstrand. Kinetic models in industrial biotechnology – Improving cell factory performance. *Metabolic Engineering*, 24:38–60, 7 2014.

[72] Jens Christmann, Peng Cao, Judith Becker, Christian K. Desiderato, Oliver Goldbeck, Christian U. Riedel, Michael Kohlstedt, and Christoph Wittmann. *High-efficiency production of the antimicrobial peptide pediocin PA-1 in metabolically engineered Corynebacterium glutamicum using a microaerobic process at acidic pH and elevated levels of bivalent calcium ions*, volume 22. 2023.

[73] Jakob Kitzmüller. *Optimization of recombinant Corynebacterium glutamicum fed-batch processes*. PhD thesis, Technische Universität Wien, 2022.

[74] Marten Linder, Markus Haak, Angela Botes, Jörn Kalinowski, and Christian Rückert. Construction of an IS-Free Corynebacterium glutamicum ATCC 13 032 Chassis Strain and Random Mutagenesis Using the Endogenous ISCg1 Transposase. *Frontiers in Bioengineering and Biotechnology*, 9(December):1–10, 12 2021.

[75] Peter Sinner, Marlene Stiegler, Christoph Herwig, and Julian Kager. Noninvasive online monitoring of Corynebacterium glutamicum fed-batch bioprocesses subject to spent sulfite liquor raw material uncertainty. *Bioresource Technology*, 321:124395, 2021.

[76] Kirill V. Ovchinnikov, Thomas F. Oftedal, Sebastian J. Reich, Nadav S. Bar, Helge Holo, Morten Skaugen, Christian U. Riedel, and Dzung B. Diep. Genome-assisted Identification, Purification, and Characterization of Bacteriocins. *Bio-protocol*, 12(14):1–15, 2022.

[77] Giovanni Y. Di Veroli, Chiara Fornari, Ian Goldlust, Graham Mills, Siang Boon Koh, Jo L. Bramhall, Frances M. Richards, and Duncan I. Jodrell. An automated fitting procedure and software for dose-response curves with multiphasic features. *Scientific Reports*, 5(1):14701, 10 2015.

[78] Robert Luedeking and Edgar L. Piret. A kinetic study of the lactic acid fermentation. Batch process at controlled pH. *Journal of Biochemical and Microbiological Technology and Engineering*, 1(4):393–412, 12 1959.

[79] Roland Brun, Peter Reichert, and Hans R. Künsch. Practical identifiability analysis of large environmental simulation models. *Water Resources Research*, 37(4):1015–1030, 4 2001.

[80] Jeffrey C. Lagarias, James A. Reeds, Margaret H. Wright, and Paul E. Wright. Convergence Properties of the Nelder–Mead Simplex Method in Low Dimensions. *SIAM Journal on Optimization*, 9(1):112–147, 1 1998.

[81] Theodora Tryfona and Mark T. Bustard. Mechanistic understanding of the fermentative L-glutamic acid overproduction by Corynebacterium glutamicum through combined metabolic flux profiling and transmembrane transport characteristics. *Journal of Chemical Technology and Biotechnology*, 79(12):1321–1330, 2004.

[82] ISAMU SHIIO, SHIN-ICHIRÔ ÔTSUKA, and MANSAHIRO TAKAHASHI. Effect of Biotin on the Bacterial Formation of Glutamic Acid. *Journal of Biochemistry*, 51(1):56–62, 1 1962.

[83] ISAMU SHIIO, S I OTSUKA, and NOBORU KATSUYA. Effect of biotin on the bacterial formation of glutamic acid. II. Metabolism of glucose. *Journal of biochemistry*, 52(2):108–16, 8 1962.

[84] S. Delaunay, P. Gourdon, P. Lapujade, E. Mailly, E. Oriol, J.M. Engasser, N.D. Lindley, and J.-L. Goergen. An improved temperature-triggered process for glutamate production with Corynebacterium glutamicum. *Enzyme and Microbial Technology*, 25(8-9):762–768, 11 1999.

[85] ISAMU SHIIO, SHIN-ICHIRO ÔTSUKA, and NOBORU KATSUYA. Cellular Permeability and Extracellular Formation of Glutamic Acid in Brevibacterium flavum. *The Journal of Biochemistry*, 53(5):333–340, 5 1963.

[86] Koichi Takinami, Hiroe Yoshii, Haruo Tsuri, and Hiroshi Okada. Biochemical Effects of Fatty Acid and its Derivatives on l-G lutamic Acid Fermentation. *Agricultural and Biological Chemistry*, 29(4):351–359, 4 1965.

[87] Erkki Oura and Heikki Suomalainen. BIOTIN-ACTIVE COMPOUNDS, THEIR EXISTENCE IN NATURE AND THE BIOTIN REQUIREMENTS OF YEASTS. *Journal of the Institute of Brewing*, 88(5):299–308, 9 1982.

[88] Jingbai Wen, Yanqiu Xiao, Ting Liu, Qiuqiang Gao, and Jie Bao. Rich biotin content in lignocellulose biomass plays the key role in determining cellulosic glutamic acid accumulation by Corynebacterium glutamicum. *Biotechnology for Biofuels*, 11(1):132, 12 2018.

[89] Xushen Han, Li Li, and Jie Bao. Microbial extraction of biotin from lignocellulose biomass and its application on glutamic acid production. *Bioresource Technology*, 288(May):121523, 9 2019.

[90] C. Keilhauer, L. Eggeling, and H. Sahm. Isoleucine synthesis in Corynebacterium glutamicum: molecular analysis of the ilvB-ilvN-ilvC operon. *Journal of Bacteriology*, 175(17):5595–5603, 9 1993.

[91] Jens Schneider, Petra Peters-Wendisch, K. Corinna Stansen, Susanne Götker, Stanislav Maximow, Reinhard Krämer, and Volker F. Wendisch. Characterization of the biotin uptake system encoded by the biotin-inducible bioYMN operon of Corynebacterium glutamicum. *BMC Microbiology*, 12(1):6, 12 2012.

[92] Matthew D. Rolfe, Christopher J. Rice, Sacha Lucchini, Carmen Pin, Arthur Thompson, Andrew D.S. Cameron, Mark Alston, Michael F. Stringer, Roy P. Betts, József Baranyi, Michael W. Peck, and Jay C.D. Hinton. Lag phase is a distinct growth phase that prepares bacteria for exponential growth and involves transient metal accumulation. *Journal of Bacteriology*, 194(3):686–701, 2012.

[93] Robert L. Bertranda. Lag phase is a dynamic, organized, adaptive, and evolvable period that prepares bacteria for cell division. *Journal of Bacteriology*, 201(7):1–21, 2019.

[94] N. B. Pamment and R. J. Hall. Absence of External Causes of Lag in Saccharomyces cerevisiae. *Journal of General Microbiology*, 105(2):297–304, 4 1978.

[95] G. Duffy, J.J. Sheridan, R.L. Buchanan, D.A. McDowell, and I.S. Blair. The effect of aeration, initial inoculum and meat microflora on the growth kinetics of Listeria monocytogenes in selective enrichment broths. *Food Microbiology*, 11(5):429–438, 10 1994.

[96] A. C. Jason. A deterministic model for monophasic growth of batch cultures of bacteria. *Antonie van Leeuwenhoek*, 49(6):513–536, 1983.

[97] Maxime Ardré, Guilhem Doulcier, Naama Brenner, and Paul B. Rainey. Interaction among bacterial cells triggers exit from lag phase. *bioRxiv*, page 2022.01.24.477561, 2022.

[98] TOSHIRO SHIDA, KAZUO KOMAGATA, and KOJI MITSUGI. REDUCTION OF LAG TIME IN BACTERIAL GROWTH. *The Journal of General and Applied Microbiology*, 21(5):293–303, 1975.

[99] Jean Christophe Augustin, Agness Brouillaud-Delattre, Laurent Rosso, and Vincent Carlier. Significance of inoculum size in the lag time of Listeria monocytogenes. *Applied and Environmental Microbiology*, 66(4):1706–1710, 2000.

[100] Tobin P. Robinson, Olosimbo O. Aboaba, Anu Kaloti, Maria J. Ocio, Jozsef Baranyi, and Bernard M. Mackey. The effect of inoculum size on the lag phase of Listeria monocytogenes. *International Journal of Food Microbiology*, 70(1-2):163–173, 2001.

[101] Shinsuke Sakai, Yoshiki Tsuchida, Shohei Okino, Osamu Ichihashi, Hideo Kawaguchi, Takashi Watanabe, Masayuki Inui, and Hideaki Yukawa. Effect of lignocellulose-derived inhibitors on growth of and ethanol production by growth-arrested Corynebacterium glutamicum R. *Applied and Environmental Microbiology*, 73(7):2349–2353, 2007.

[102] Yota Tsuge, Motonori Kudou, Hideo Kawaguchi, Jun Ishii, Tomohisa Hasunuma, and Akihiko Kondo. FudC, a protein primarily responsible for furfural detoxification in Corynebacterium glutamicum. *Applied Microbiology and Biotechnology*, 100(6):2685–2692, 2016.

[103] Pingping Zhou, Imrana Khushk, Qiuqiang Gao, and Jie Bao. Tolerance and transcriptional analysis of Corynebacterium glutamicum on biotransformation of toxic furaldehyde and benzaldehyde inhibitory compounds. *Journal of Industrial Microbiology and Biotechnology*, 46(7):951–963, 2019.

[104] Shohei Okino, Masayuki Inui, and Hideaki Yukawa. Production of organic acids by Corynebacterium glutamicum under oxygen deprivation. *Applied Microbiology and Biotechnology*, 68(4):475–480, 2005.

[105] Masayuki Inui, Shikiko Murakami, Shohei Okino, Hideo Kawaguchi, Alain A. Vertès, and Hideaki Yukawa. Metabolic analysis of Corynebacterium glutamicum during lactate and succinate productions under oxygen deprivation conditions. *Journal of Molecular Microbiology and Biotechnology*, 7(4):182–196, 2004.

[106] H. L.T. Mobley and R. P. Hausinger. Microbial ureases: Significance, regulation, and molecular characterization. *Microbiological Reviews*, 53(1):85–108, 1989.

[107] Andreas Burkovski. Ammonium assimilation and nitrogen control in Corynebacterium glutamicum and its relatives: An example for new regulatory mechanisms in actinomycetes. *FEMS Microbiology Reviews*, 27(5):617–628, 2003.

[108] Ruth M. Siewe, Brita Weil, Andreas Burkovski, Lothar Eggeling, Reinhard Krämer, and Thomas Jahns. Urea uptake and urease activity in Corynebacterium glutamicum. *Archives of Microbiology*, 169(5):411–416, 4 1998.

[109] Gabriele Beckers, Anne K. Bendt, Reinhard Krämer, and Andreas Burkovski. Molecular identification of the urea uptake system and transcriptional analysis of urea transporter- and urease-encoding genes in Corynebacterium glutamicum. *Journal of Bacteriology*, 186(22):7645–7652, 2004.

[110] Andreas Burkovski, Marc Jakoby, Ruth Siewe, Jana Meier-Wagner, Reinhard Krämer, and Lars Nolden. Multiplicity of ammonium uptake systems in Corynebacterium glutamicum: role of Amt and AmtB. *Microbiology*, 147(1):135–143, 1 2001.

[111] H.-B. Pan and B. W. Darvell. Calcium Phosphate Solubility: The Need for Re-Evaluation. *Crystal Growth & Design*, 9(2):639–645, 2 2009.

[112] Shuichi Aiba and Hisamoto Furuse. Some comments on respiratory quotient (RQ) determination from the analysis of exit gas from a fermentor. *Biotechnology and Bioengineering*, 36(5):534–538, 8 1990.

[113] Benedikt Heyman, Hannah Tulke, Sastia Prama Putri, Eiichiro Fukusaki, and Jochen Büchs. Online monitoring of the respiratory quotient reveals metabolic phases during microaerobic 2,3-butanediol production with Bacillus licheniformis. *Engineering in Life Sciences*, 20(3-4):133–144, 3 2020.

[114] Luc De Vuyst, Raf Callewaert, and Kurt Crabbé. Primary metabolite kinetics of bacteriocin biosynthesis by Lactobacillus amylovorus and evidence for stimulation of bacteriocin production under unfavourable growth conditions. *Microbiology*, 142(4):817–827, 4 1996.

[115] S. Anastasiadou, M. Papagianni, G. Filiousis, I. Ambrosiadis, and P. Koidis. Growth and metabolism of a meat isolated strain of Pediococcus pentosaceus in submerged fermentation. *Enzyme and Microbial Technology*, 43(6):448–454, 11 2008.

[116] Sofia Anastasiadou, Maria Papagianni, George Filiousis, Ioannis Ambrosiadis, and Pavlos Koidis. Pediocin SA-1, an antimicrobial peptide from Pediococcus acidilactici NRRL B5627: Production conditions, purification and characterization. *Bioresource Technology*, 99(13):5384–5390, 9 2008.

[117] Nelson P. Guerra and Lorenzo Pastrana. Modelling the influence of pH on the kinetics of both nisin and pediocin production and characterization of their functional properties. *Process Biochemistry*, 37(9):1005–1015, 4 2002.

[118] Alain A. Vertès. Protein Secretion Systems of Corynebacterium glutamicum. In *Corynebacterium glutamicum Biology and Biotechnology*, pages 351–389. 2013.

[119] Carlos F. Gonzalez and Blair S. Kunka. Plasmid-Associated Bacteriocin Production and Sucrose Fermentation in Pediococcus acidilactici. *Applied and Environmental Microbiology*, 53(10):2534–2538, 10 1987.

[120] Line Johnsen, Gunnar Fimland, Vincent Eijsink, and Jon Nissen-Meyer. Engineering Increased Stability in the Antimicrobial Peptide Pediocin PA-1. *Applied and Environmental Microbiology*, 66(11):4798–4802, 11 2000.

[121] Jing Guo, Zhenping Ma, Jinshan Gao, Jinhua Zhao, Liang Wei, Jun Liu, and Ning Xu. Recent advances of pH homeostasis mechanisms in Corynebacterium glutamicum. *World Journal of Microbiology and Biotechnology*, 35(12):192, 12 2019.

[122] Kinga Jakob, Peter Satorhelyi, Christian Lange, Volker F. Wendisch, Barbara Silakowski, Siegfried Scherer, and Klaus Neuhaus. Gene Expression Analysis of Corynebacterium glutamicum Subjected to Long-Term Lactic Acid Adaptation. *Journal of Bacteriology*, 189(15):5582–5590, 8 2007.

[123] Sarah Täuber, Luisa Blöbaum, Volker F. Wendisch, and Alexander Grünberger. Growth Response and Recovery of Corynebacterium glutamicum Colonies on Single-Cell Level Upon Defined pH Stress Pulses. *Frontiers in Microbiology*, 12(October):1–13, 10 2021.

[124] H.E. Lundager Madsen and G. Thorvardarson. Precipitation of calcium phosphate from moderately acid solution. *Journal of Crystal Growth*, 66(2):369–376, 3 1984.

[125] Omar Mekmene, Sophie Quillard, Thierry Rouillon, Jean Michel Bouler, Michel Piot, and Frédéric Gaucheron. Effects of pH and Ca/P molar ratio on the quantity and crystalline structure of calcium phosphates obtained from aqueous solutions. *Dairy Science and Technology*, 89(3-4):301–316, 2009.

[126] Handially Santos Vilela, Marcela Charantola Rodrigues, Bruna Marin Fronza, Rafael Bergamo Trinca, Flávio Maron Vichi, and Roberto Ruggiero Braga. Effect of Temperature and pH on Calcium Phosphate Precipitation. *Crystal Research and Technology*, 56(12), 12 2021.

[127] H. Newesely. Changes in crystal types of low solubility calcium phosphates in the presence of accompanying ions. *Archives of Oral Biology*, 6(C):174–180, 1961.

[128] J. A. M. Van Der Houwen and E. Valsami-Jones. The Application of Calcium Phosphate Precipitation Chemistry to Phosphorus Recovery: The Influence of Organic Ligands. *Environmental Technology*, 22(11):1325–1335, 11 2001.

[129] G. H. Nancollas, M. Lore, L. Perez, C. Richardson, and S. J. Zawacki. Mineral phases of calcium phosphate. *The Anatomical Record*, 224(2):234–241, 6 1989.

[130] Sergey V. Dorozhkin. Amorphous calcium (ortho)phosphates. *Acta Biomaterialia*, 6(12):4457–4475, 12 2010.

[131] A. Yu Malysheva and B. I. Beletskii. The state of water in tricalcium phosphate obtained by precipitation from a solution. *Glass and Ceramics (English translation of Steklo i Keramika)*, 58(3-4):147–149, 2001.

[132] A. Destainville, E. Champion, D. Bernache-Assollant, and E. Laborde. Synthesis, characterization and thermal behavior of apatitic tricalcium phosphate. *Materials Chemistry and Physics*, 80(1):269–277, 4 2003.

[133] Peter Sinner, Marlene Stiegler, Oliver Goldbeck, Gerd M. Seibold, Christoph Herwig, and Julian Kager. Online estimation of changing metabolic capacities in continuous Corynebacterium glutamicum cultivations growing on a complex sugar mixture. *Biotechnology and Bioengineering*, 119(2):575–590, 2022.

[134] J. H. T. Luong. Generalization of monod kinetics for analysis of growth data with substrate inhibition. *Biotechnology and Bioengineering*, 29(2):242–248, 2 1987.

[135] Noor Salam Khan, Indra Mani Mishra, R. P. Singh, and Basheshwer Prasad. Modeling the growth of Corynebacterium glutamicum under product inhibition in L-glutamic acid fermentation. *Biochemical Engineering Journal*, 25(2):173–178, 2005.

[136] Dirk Kiefer, Manuel Merkel, Lars Lilge, Rudolf Hausmann, and Marius Henkel. High cell density cultivation of Corynebacterium glutamicum on bio-based lignocellulosic acetate using pH-coupled online feeding control. *Bioresource Technology*, 340(July):125666, 2021.

[137] M. L. Cabo, M. A. Murado, Ma P. González, and L. Pastoriza. Effects of aeration and pH gradient on nisin production. A mathematical model. *Enzyme and Microbial Technology*, 29(4-5):264–273, 2001.

[138] Subbi Rami Reddy Tadi, Sandipan Mukherjee, Sandhya Sekhar, Aiyagari Ramesh, and Senthilkumar Sivaprakasam. Valorization and Kinetic Modelling of Pediocin Production from Agro and Dairy Industrial Residues by Pediococcus pentosaceus CRA51. *Waste and Biomass Valorization*, (0123456789), 2023.

[139] Farah Fadwa Ben Belgasem and Hamzah Mohd Salleh. Characterization of Recombinant Enzymes. In Azura Amid, editor, *Recombinant Enzymes - From Basic Science to Commercialization*, pages 41–60. Springer International Publishing, Cham, 2015.

[140] Jianqiang Lin, Sang Mok Lee, Ho Joon Lee, and Yoon Mo Koo. Modeling of typical microbial cell growth in batch culture. *Biotechnology and Bioprocess Engineering*, 5(5):382–385, 2000.

[141] Can Li, Jianqun Lin, Ling Gao, Huibin Lin, and Jianqiang Lin. Modeling and simulation of enzymatic gluconic acid production using immobilized enzyme and CSTR–PFTR circulation reaction system. *Biotechnology Letters*, 40(4):649–657, 4 2018.

[142] Han Min Woo, Stephan Noack, Gerd M. Seibold, Sabine Willbold, Bernhard J. Eikmanns, and Michael Bott. Link between Phosphate Starvation and Glycogen Metabolism in Corynebacterium glutamicum, Revealed by Metabolomics. *Applied and Environmental Microbiology*, 76(20):6910–6919, 2010.

[143] Ulrike Sorger-Herrmann, Hironori Taniguchi, and Volker F. Wendisch. Regulation of the pstSCAB operon in Corynebacterium glutamicum by the regulator of acetate metabolism RamB Microbial biochemistry, physiology and metabolism. *BMC Microbiology*, 15(1):1–13, 2015.

[144] Yuhuan Chen, Richard D. Ludescher, and Thomas J. Montville. Electrostatic interactions, but not the YGNGV consensus motif, govern the binding of pediocin PA-1 and its fragments to phospholipid vesicles. *Applied and Environmental Microbiology*, 63(12):4770–4777, 1997.

[145] A. K. Bhunia, M. C. Johnson, B. Ray, and N. Kalchayanand. Mode of action of pediocin AcH from Pediococcus acidilactici H on sensitive bacterial strains. *Journal of Applied Bacteriology*, 70(1):25–33, 1991.

[146] S. Anastasiadou, M. Papagianni, I. Ambrosiadis, and P. Koidis. Rapid quantifiable assessment of nutritional parameters influencing pediocin production by Pediococcus acidilactici NRRL B5627. *Bioresource Technology*, 99(14):6646–6650, 9 2008.

List of Figures

List of Tables